CONTRIBUTIONS OF LAND SURFACE FORCED MESOSCALE CIRCULATIONS TO THE TOTAL HEAT, MOISTURE AND MOMENTUM BUDGETS OVER BOREAS

Pier Luigi Vidale

Roger A. Pielke, Adviser
NASA Grant No. NAG-5-2302
EPA Grant No. R824993-01-0
CAPES Fellowship No. 1154/92-2

Colorado State University

DEPARTMENT OF ATMOSPHERIC SCIENCE

PAPER NO. 660

CONTRIBUTIONS OF LAND SURFACE FORCED MESOSCALE CIRCULATIONS TO THE TOTAL HEAT, MOISTURE AND MOMENTUM BUDGETS OVER BOREAS

Pier Luigi Vidale

Department of Atmospheric Science
Colorado State University
Fort Collins, Colorado
Spring 1998

Atmospheric Science Paper No. 660

ABSTRACT

CONTRIBUTIONS OF LAND SURFACE FORCED MESOSCALE CIRCULATIONS TO THE TOTAL HEAT, MOISTURE AND MOMENTUM BUDGETS OVER BOREAS

As one of the Aircraft Flux Measurements team for NASA's BOREAS field experiment, we were made responsible for the integration of surface turbulent fluxes of heat and moisture measured by aircraft over portions of the BOREAS domain. We approached this task by integrating data analysis, analytical modeling and numerical modeling. Results from aircraft and surface observations provided evidence for the existence of significant mesoscale circulations over the BOREAS domain, mainly associated with lake-forest surface heating gradients. Linear analytical modeling for this region indicated a good potential for the development of mesoscale circulations and of associated vertical mesoscale heat fluxes, which display a different vertical distribution from the turbulent ones. With lower predominant wind speed magnitudes, mesoscale sensible heat fluxes can be comparable to turbulent fluxes within the Convective Boundary Layer, warming its lower part and cooling its upper part; with high predominant winds, the mesoscale fluxes can influence the whole troposphere, usually resulting in a net negative flux of momentum and heat. Using RAMS, forced at its lower boundary with a vegetation classification derived from AVHRR data, we have successfully simulated and validated the surface flux heterogeneity observed in BOREAS over three case studies. We have found that there are significant contributions to the total budgets of heat over the BOREAS domain, generated by mesoscale circulations. While further analysis is warranted to document this effect, the existence of mesoscale flow is not surprising, since it is related to the presence of landscape patches, including lakes, which are of a size on the order of the local Rossby radius and which have spatial differences in

average diurnal surface sensible heat flux of over 300 W m^{-2}. We have also analyzed the vertical temperature profile simulated in our case study as well as high resolution soundings from Candle Lake, and we have found vertical profiles of diurnal temperature change, also above the boundary layer height, which we attribute in part to mesoscale contributions. Our conclusion is that, in regions with organized landscapes, such as BOREAS, even with relatively strong synoptic winds, dynamical scaling criteria should be used to integrate the surface flux measurements to a regional scale. From the numerical modeling point of view we have verified the usefulness of our coupled model (RAMS-LEAF-2), when used in conjunction with the BOREAS AVHRR regional vegetation classification, in correctly forcing the local circulations we have studied. This classification is only complete if used with its biophysical ancillary data sets and with other high resolution physiographical data sets (soils, topography), collected for the experiment.

Pier Luigi Vidale
Department of Atmospheric Science
Colorado State University
Fort Collins, Colorado 80523
Spring 1998

ACKNOWLEDGEMENTS

I would like to thank Roger Pielke, who not only served as adviser, but provided unlimited support, giving trust, responsibility and independence. This allowed me to fully experience being a BOREAS investigator and to interact with other excellent scientists worldwide. I am also very grateful for his continuous encouragement and for his unfailing optimism.

My committee members at CSU, R. Johnson, M. Montgomery and W. Parton, were also helpful and open, and provided excellent guidance and resources to tackle the numerous problems I encountered along the project.

Louis Steyaert of the EROS Data Center/NASA GSFC, introduced me to GIS modeling, taught me how to set up my own GIS modeling framework, and proved to be an incredible source of information, advice, and practical help in most aspects of my data needs for BOREAS.

Ron Dobosy, Tim Crawford and Dennis Baldocchi, of NOAA/ATDD, provided flux data from the LongEZ flights, and helped with data analysis and software tools. R. Dobosy was also an invaluable source of advice and information about aircraft data processing.

TABLE OF CONTENTS

LIST OF FIGURES

LIST OF TABLES

Glossary and List of Abbreviations

AES: Atmospheric Environmental Services.

AFM: Airborne Flux Measurements.

Allometry: the measurement of the relative growth of a part in relation to an entire organism or to a standard.

AMS: Automated Meteorological Stations.

AM88 Avissar-Mahrer 1988 SVATS: RAMS surface sub-model previous to LEAF.

AVHRR: Advanced Very High Resolution Radiometer.

BATS: Biosphere - Atmosphere Transfer Scheme.

BL: Boundary Layer.

BOREAS: Boreal Ecosystem Atmosphere Study.

BORIS: BOREAS Information System.

CAPE: Convective Available Potential Energy.

CBL: Convective Boundary Layer.

DEM: Digital Elevation Model.

ECMWF: European Center for Middle-range Weather Forecasting.

Ecotone: a transition area between two adjacent ecological communities.

EOS: Earth Observing System.

FIFE: First ISLSCP Field Experiment.

FPAR: Fraction of Photosynthetically Available Radiation (PAR, 0.4-0.7 μm). Portion of PAR absorbed by the green vegetation canopy.

GCM: Global Circulation Model.

GIS: Geographic Information System.

Golden Day: a measurement campaign day with very low atmospheric optical thickness, ideal for radiative transfer work.

HWM: Heat, Water and Momentum.

HWMC: Heat, Water, Momentum and Carbon.

IFC (IFC1, IFC2, and IFC3): Intensive Field Campaign.

IGBP: International Geosphere-Biosphere Program.

ISLSCP: International Satellite Land Surface and Cloud Project.

LAI: Leaf Area Index.

LEAF, LEAF-2: Land Ecosystem - Atmosphere Feedback.

LES: Large Eddy Simulation.

LSP: Land Surface Parameterization.

LUT: Look-Up Table.

MAPE: Mesoscale Available Potential Energy.

ML: Mixed Layer.

MODIS: Moderate Resolution Imaging Spectroradiometer.

MTPE: Mission to Planet Earth.

NASA: National Aeronautics and Space Administration.

NCEP: National Center for Environmental Prediction.

NDVI: Normalized Difference Vegetation Index.

NOAA: National Ocean and Atmosphere Administration.

NSA: Northern Study Area.

NWP: Numerical Weather Prediction.

OJP: Old Jack Pine.

Pedology: soil science.

Phenology: periodic biological phenomena that are correlated with climatic conditions (e.g. the greening and wilting of leaves over the growing season).

PILPS: Project for Intercomparison of Landsurface Parameterization Schemes.

RAMS: Regional Atmospheric Modeling System.

RS: Remote Sensing.

SiB: Simple Biosphere Model.

SR: Simple Ratio.

SSA: Southern Study Area.

SVATS: Soil - Vegetation - Atmosphere Transfer Scheme.

SVI: Spectral Vegetation Index.

TM: Thematic Mapper.

USGS: United States Geological Service.

Chapter 1

INTRODUCTION

1.1 Motivation of This Study

This work gives continuation to efforts in our research group that go back more than a decade, trying to characterize and understand mesoscale processes associated with landscape heterogeneity and their impact on the atmosphere. The expertise in our group lies specifically in the mesoscale modeling area, but the research focus has spanned across atmospheric scales and included analysis of data from many campaign efforts that support, motivate and make possible the modeling exercise.

Since 1993, within our NASA BOREAS (Boreal Ecosystem Atmosphere Study) research project, we have been made responsible, as part of one of the Airborne Flux Measurements (AFM) teams, for the integration of measurements from a variety of land, airborne and space platforms over the BOREAS domain, in an 'upscaling' exercise that required the development and use of multiple modeling and data management skills. In particular, we were responsible for the integration of measurements from aircraft, in order to produce two-dimensional maps of the surface fluxes of heat and moisture over the boreal landscape.

A mesoscale numerical model such as RAMS (Regional Atmospheric Modeling System) is an ideal tool for this kind of undertaking, especially after it was successfully used in support of other field campaigns. BOREAS promised to be, and was, a much more interesting test bed for some of the mesoscale ideas that have been raised in our past research.

This dissertation reports on the challenges we met, the lessons we learned and the testing of our hypotheses on the mesoscale as a result of our BOREAS mission.

1.2 Objectives of This Study

With this study we intend to give continuity to past studies in the modeling of Soil-Vegetation-Atmosphere-Transfer (SVAT) processes, to address the issue of the upscaling of surface fluxes of heat and moisture, to study possible conditions for the generation of mesoscale circulations, and to characterize potential impacts of those circulations on the large-scale atmosphere.

In order to accomplish these objectives we have formulated several working hypotheses.

1.3 Hypotheses

1.3.1 Main Hypothesis

Under weak to moderate synoptic wind conditions, contributions from mesoscale circulations caused by landscape heterogeneity need to be included in the calculation of the total terrestrial heat, moisture and momentum budgets.

1.3.2 Sub-Hypothesis 1

Sub-grid (in Global Circulation Model, GCM, and synoptic model terms) heat, moisture and momentum budgets over a heterogeneous domain can be linearly scaled up to spatial sizes of hundreds of kilometers or more on a side.

1.3.3 Sub-Hypothesis 2

The high Bowen ratios in the BOREAS region, due to slowly transpiring vegetation (controlled by low soil temperatures, especially in spring) result in enhanced mesoscale circulation effects over the BOREAS domain.

We therefore intend to assess the relative importance of turbulent and mesoscale fluxes of heat, water and momentum (HWM) within the lower part of the atmosphere using a mixed approach of modeling and data analysis. Specifically, we would like to better understand if and how heated and moistened air (from heating, transpiration and evaporation from the surface) eventually reaches the free atmosphere above the convective boundary layer (CBL).

1.4 Relevance of This Work

GCM, synoptic and regional climate modelers, because of computational restraints, are limited in their ability to explicitly resolve mesoscale phenomena. Should the main hypothesis be rejected, it would make sense to continue the work in this area as is classically done, linearly averaging surface fluxes over each grid cell. Should the hypothesis fail to be rejected, however, this work would suggest that sub-grid interactions due to mesoscale circulations need to be parameterized, as is done, for instance, for cumulus cloud precipitation.

1.4.1 Terrestrial Ecosystem Processes and Improvements in Numerical Weather Prediction

Betts et al. (1993, 1996, 1997a, 1998) reported on substantial improvements in the quality of NWP (later transferred to climate models) achieved by a better representation of land surface processes in such models. Most of the improvements have come from results of large scale experiments such as BOREAS. For example, until very recently, most NWP models overestimated evaporation rates over the BOREAS domain in the summer (causing very frequent rainfall forecasts that did not verify), and specified unrealistic values for the winter albedo over the conifer forest, causing unrealistic heating rates at the surface which resulted in forecast error (Sellers et al. 1995a and Betts and Ball 1997).

1.4.2 Applicability of the Scaling Debate

The relevance of the scaling debate lies in the fact that the community needs to verify whether linear scaling is universally applicable, as it heavily influences the planning of field campaigns, the interpretation of measurements and the planning of numerical simulations. Current campaign strategies employ point surface measurement platforms that are deployed with the purpose of finding representative sites for each land surface class, so that their measurements can be upscaled by using relative abundance information derived from remote sensing (see Chapter 2 for an expanded discussion).

Should significant mesoscale circulations affect the environment in the proximity of the 'representative' measurement sites, that is, should landscape patches interact with

each other and not just with the atmosphere above them, the significance of the point measurements will need to be re-interpreted.

Chapter 2

LITERATURE REVIEW: LAND SURFACE PROCESSES AND MESOSCALE CIRCULATIONS INDUCED BY THEM

2.1 The Scaling Debate

Point field measurements, taken at tower footprint scales (at most a few km) in order to describe the functioning of each land surface patch, need to be scaled up to larger spatial scales in order to be useful in the understanding of biosphere-atmosphere interactions. There are many ways to perform this upscaling, but the issue is whether these different ways are equivalent and how much should be allocated in terms of computational resources in order to accurately calculate this upscaling.

2.1.1 Linear Scaling and Applications

In linear scaling (see also Fig. 2.8 and Fig. 4.1) point measurements are scaled up according to the relative abundance, in a given area, of the type of physiographical class associated with each representative measurement site. The problem is, of course, to be able to identify 'typical' or representative sites, so that the integrated (or averaged) HWM fluxes will be accurate for the region. Usually the upscaling calculation is performed by using survey data (from remote sensing or ground measurements) that will do at least some of the following.

1. Assign a basic pixel size and then aggregate the land surface by predominant element or other, more sophisticated technique.

2. Break down the patches into distinct classes through some kind of supervised or unsupervised criteria, based on morphological characteristics (e.g. trees versus grasses), physiological characteristics (e.g. C_3 versus C_4 grasses), sometimes also including

information about habitat and climate (e.g. tall grasses in marshy regions or tall grasses in steppe). In more complete approaches, surface surveys and remote sensing products are also used to specify fields of biophysical characteristics to be associated with each class.

3. Account for the abundance of each class over the region to which we want to upscale.

4. Calculate the surface fluxes as area weighted contributions from each class.

Examples of experimental campaign strategies in support of this approach are given in Sellers et al. (1992, 1995b, 1997).

Within numerical models, especially large-scale ones, the upscaling is not only linear, but usually accomplished by coupling a land surface model and ancillary data sets originally developed for the simulation of one specific site (usually a tower site). A predominant class is then assigned to an entire grid cell. The modeling problem then lies in assigning typical biophysical characteristics to each one of these classes, so that, once a land surface classification is used over a certain domain, quantities such as albedo, roughness length, Leaf Area Index (LAI), fractional coverage and all the stomatal control internal parameters will produce a reasonable response of the land surface to the model's large-scale atmospheric forcings.

In order to address the aggregation problem, a very large number of classes and sub-classes are at times utilized, incorporating a wide range of ancillary information, so that most possible combinations of biophysical characteristics are covered. Mosaic approaches (assigning multiple classes to each grid point) are also at times applied to the calculation of fluxes over each grid cell in order to try and address the sub-grid heterogeneity in a statistical fashion (Avissar 1995).

Examples of global classifications efforts are the International Satellite Land Surface and Cloud Project (ISLSCP, Meeson et al. 1995; Sellers et al. 1995c) products (multi-classification over the globe at 1 degree), the Global Ecosystems (Olson and Watts 1982, 94 classes at 1 km) and the Biosphere-Atmosphere Transfer Scheme (BATS, Dickinson et al. 1986; 18 classes at 1 km), typically used in GCM applications. Among regional

classifications are the U.S. Geological Survey Land Use/Land Cover System (Anderson et al. 1976, 167 classes) and a hierarchy of International Geosphere-Biosphere Program (IGBP) classifications at 1 km (Belward and Loveland 1995), typically used in NWP/research models. Unfortunately, biophysical parameters tables for use in land surface modeling exist but for a few of these classifications at resolutions under one degree.

Remote Sensing Techniques

Another approach, used for instance in the latest SiB2 model versions (Sellers et al. 1996) relies heavily on remote sensing, consisting in the definition of a very small number of classes, (typically six to nine) based strictly on physiological/morphological criteria, and using remote sensing products called Spectral Vegetation Indices (SVIs, such as Normalized Difference Vegetation Index, NDVI, Simple Ratio, SR), derived from the Advanced Very High Resolution Radiometer (AVHRR) sensor mounted on the National Ocean and Atmosphere Administration (NOAA) series of polar orbiting satellites, to define the phenology (most importantly, a time and space field of LAI for the model domain). Sellers et al. (1992) showed how the relationship between SVI and the Fraction of Photosynthetically Available Radiation (FPAR) and between FPAR and canopy conductance (g_c) and photosynthesis (A_C) are linear or near-linear, providing a basis for the estimation of area averages of FPAR, A_C and g_c from SVIs. The usefulness of SVIs is based on the large difference between the visible and near-infrared reflectances of green leaves as compared to the relatively uniform spectra of soil and rock surfaces. The RS product interacts with minimal information about the land surface to create continuous fields of the biophysical parameters, which are then used within the model for HWM flux calculation.

These techniques allow for intra-class variability of biophysical parameters, although they still rely on aggregation rules for the basic land surface classification, which determines an a-priori embedded scaling in the flux calculation over a target region. This approach, while very attractive for its generality and practicality, also suffers from some technical limitations. For instance, NDVI data is very much dependent on aerosol corrections, so that it will be feasible operationally only after the launching of the Moderate Resolution Imaging Spectroradiometer (MODIS). Also, for NDVI products, the NDVI-LAI relationship

is ill posed for classes such as conifers, so that it is not generally applicable (Hall et al. 1995).

2.1.2 Critique of Linear Scaling Universality

The problem with linear scaling lies in the assumption that there exist representative measurement sites and representative measurement footprints. The typical up-scaling that is applied in large field experiments takes the measurement data from stand scale to the larger scale directly, ignoring the mesoscale completely.

Examples of when this technique might fail are given in Sun et al. (1997a,b), Taylor et al. (1998), Vidale et al. (1997) and Wang et al. (1998) (see also the flux enhancement discussion in Chapter 4). If a local circulation, such as a lake breeze or a slope circulation, is present and influences the environment around a measurement site (both in terms of wind speed and of temperature / moisture content of the air) the flux measurement from that site will not be linearly scalable, but will instead need to be embedded in a fine-scale model, used as a physical interpolator, so that effects from local circulations will be taken into account. Figure 2.1 summarizes the conceptual model for the Candle Lake breeze during the daytime (Sun et al. 1997a). All the fluxes shown in the figure can be enhanced by the lake breeze circulation. For instance, lake air (cooler, moister and richer in CO_2) advected over the forest will cause an increase in the Bowen ratio because the stomata will be able to assimilate CO_2 with less aperture (and less moisture loss), thus enhancing the vertical sensible heat flux and reducing the latent heat flux.

2.2 Soil – Vegetation – Atmosphere Transfer Scheme Techniques

SVATS techniques are abundant in the literature and the multiple combinations of coupling between atmospheric models, land surface models, soil models, hydrology models etc. are too many to be listed here, but a few general comments will help later interpretation.

2.2.1 Structural Strategies

From the point of view of the structural description of land surface processes, solutions range from not including them at all, using for instance analytical functions that simulate

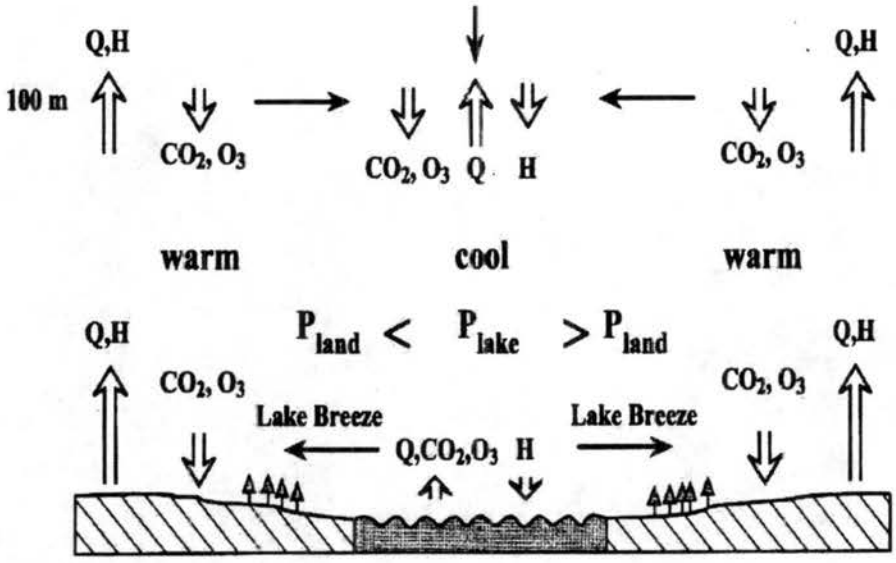

Figure 2.1: The Candle Lake breeze conceptual model for daytime, by Sun et al. (1997a). Candle Lake is at the center, the induced wind patterns are represented by black arrows, the fluxes by open arrows. H is the sensible heat flux, Q is the latent heat flux, CO_2 and O_3 represent carbon and ozone fluxes, respectively. P symbolizes pressure.

the diurnal heating oscillation at the surface, to very complex, multi-tiered models that take into account the multiple interactions of radiation with the canopy and the different leaf orientations.

Hierarchically (and historically) land surface models can be listed as:

- Bucket Models (Manabe 1969), in which water from precipitation is stored into reservoirs of different capacity depending on soil depth;
- Pennman-Monteith Equation (Monteith 1965), in which a first attempt at including control on the Bowen ratio by the biosphere is made;
- Big Leaf Models (e.g. BATS, Dickinson et al. 1986; Avissar and Mahrer 1988, AM88), in which part of a grid cell is covered by a vegetated 'carpet' which has separate biophysical parameters from the soil fraction;
- Canopy Models (e.g. Land Ecosystem - Atmosphere Feedback, LEAF, Lee 1992, Walko et al. 1998; Simple Biosphere Model, SiB, Sellers et al. 1996), in which

the vegetated canopy has a completely separate heat and moisture budget from the surface and in which canopy air buffers the exchanges between the land surface underlying the vegetation and the atmosphere above it.

2.2.2 Representation of Biophysical Processes

In terms of the mechanics which control the HWM fluxes by living matter, strategies range in complexity from very bulk representations to solutions that attempt to catch the actual processes within the photosynthesis machinery:

- Two parameters: using an 'effective LAI' and leaf water potential (e.g. the IAGL model of De Ridder and Schayes 1997);
- Multi-parameter (Jarvis 1976): these models include separate parameterizations for the effects of different environmental conditions (temperature, canopy air moisture and CO_2 content, radiation, wind speed, water in the root layer) in order to represent the vegetation response in terms of stomatal control (hence Bowen ratio), see Fig. 2.2 and Fig. 2.3;
- Multi-parameter (e.g., Farquhar et al. 1980, von Caemmerer and Farquhar 1985 assimilation models and Ball-Berry, Ball 1980, stomatal resistance models): these models include detailed descriptions of the carbon-water stomatal exchanges as controlled by the photosynthesis processes, under the assumption that the vegetation will try to maximize its appropriation of CO_2 while trying to maintain its moisture, thus regulating its stomatal aperture, while constrained by environmental factors and by nutrient availability, see Fig. 2.4.

2.2.3 The Project for Intercomparison of Landsurface Parameterization Schemes Program and its Results

The PILPS program (Henderson-Sellers 1995; Qu et al. 1998; Timbal et al. 1998) attempts to address the issue of the proliferation of land surface schemes, devising methods for cross comparison and clear quality assessment criteria. Its purpose is manifestly to improve the accuracy of SVATS used in a variety of numerical models. This program has

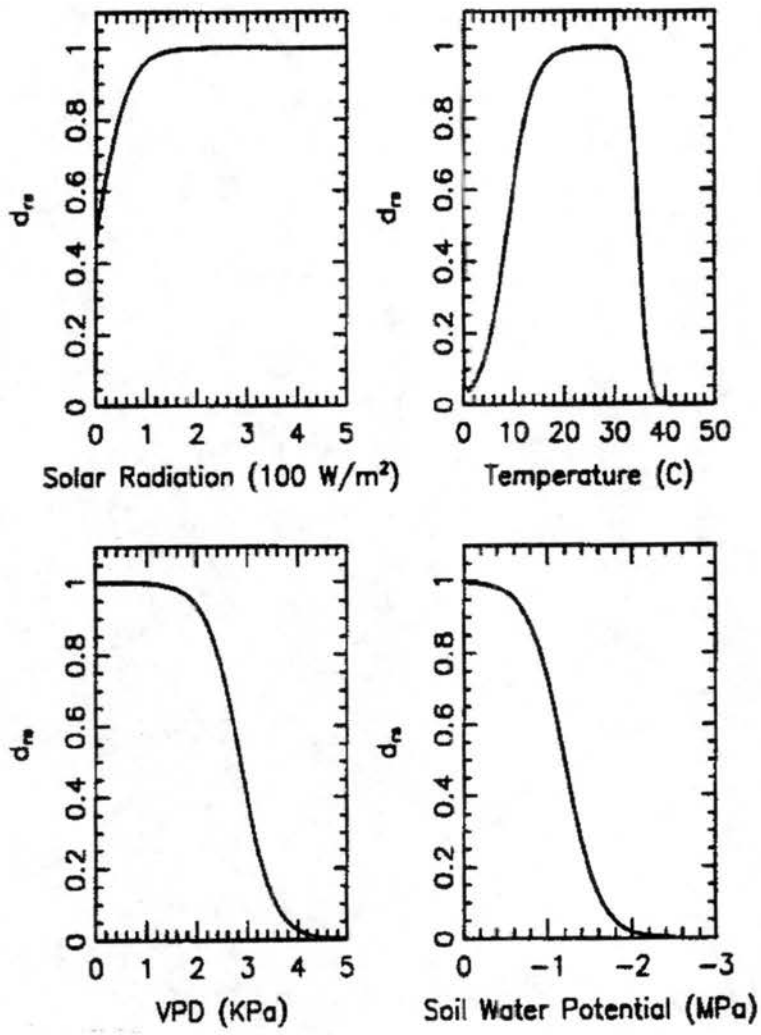

Figure 2.2: The Jarvis stomatal conductance parameterization contained in the AM88 and LEAF-2 SVATS, represented as multiplicative factors to a maximum potential stomatal conductance: a) dependence on PAR; b) dependence on air temperature; c) dependence on vapor pressure deficit; d) dependence on soil water potential.

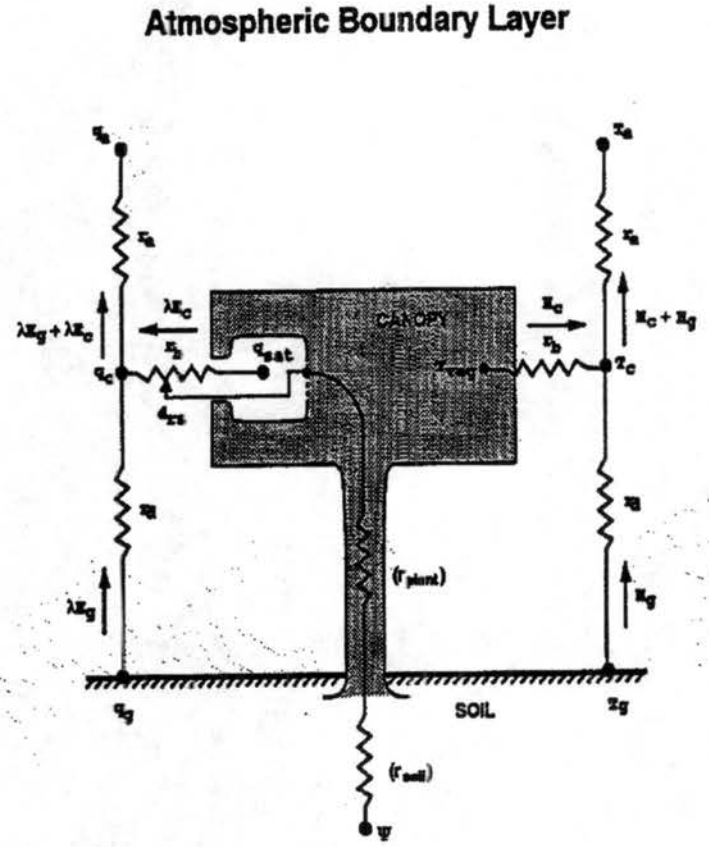

Figure 2.3: The LEAF SVATS structural diagram. The pathways on the left represent exchanges of latent heat from the soil and the stomata, as a set of parallel resistors; the symbols on the right represent exchanges of sensible heat. T is temperature, q is specific humidity, λ is the latent heat of vaporization, r are resistances, subscripts 'veg' refer to vegetation, 'c' to canopy air, 'a' to surface layer air (first model level), 'g' to ground (adapted from Lee 1992).

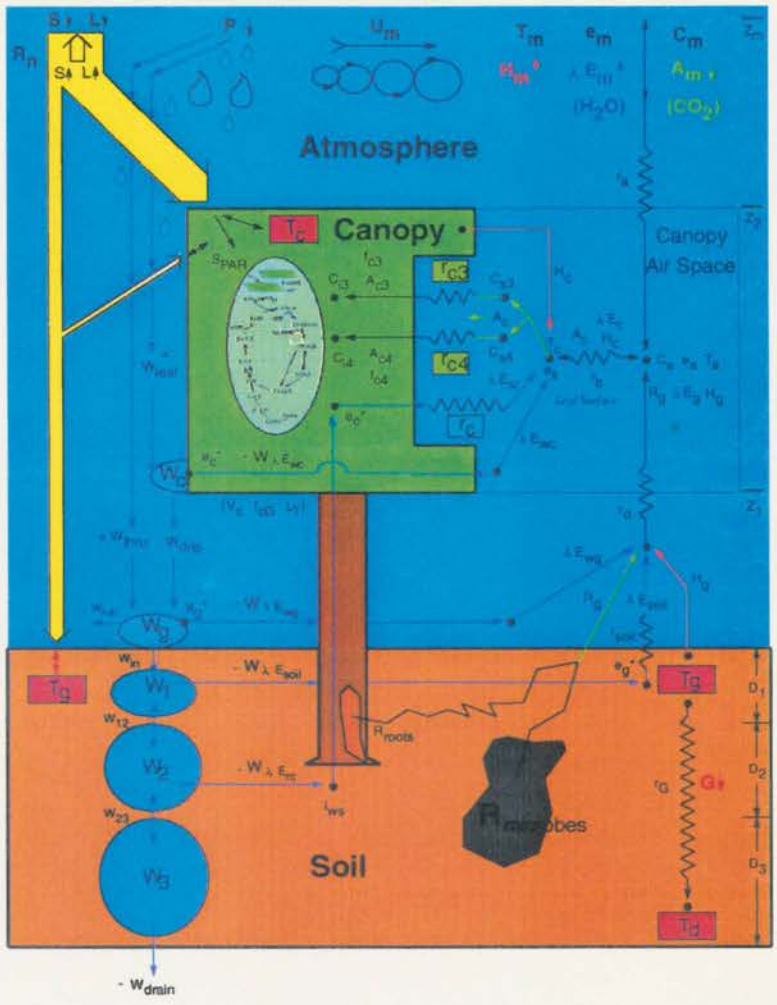

Figure 2.4: The SiB2 structural diagram, with a depiction of the photosynthetic processes that define stomatal conductance (courtesy: S.A. Denning and J. Berry).

helped point out errors in parameterizations, in the physics and/or in the data sets for different types of applications over the globe and over the course of a yearly cycle. The principal findings from this program are:

- Despite the complexity introduced by coupling a SVATS to an atmospheric model, it affords substantial improvement in the representation of HWM fluxes as compared to the use of a bucket-type model in off-line runs;
- The correct specification of land surface biophysical parameters is crucial for the calculation of realistic surface fluxes;
- The range of energy partitioning by land surface schemes ranged in PILPS phase 2 (off line models) within about 25 W m^{-2}, or 2 K in surface radiative temperature range, due mainly to the surface moisture budget;
- The on-line runs showed even more disagreement than the phase 2 experiments, due to differences in the atmospheric forcings of the host models.

Since the PILPS program is still underway, a clear understanding of the accuracy achieved by the different coupling solutions is not yet available.

2.3 Work in Land Surface Effects Within our Research Group

The issue of the influence of mesoscale phenomena on the atmosphere has been addressed within our research group with focus on both modeling and data analysis. A summary of the research results organized by approach strategy is provided below.

2.3.1 Analytic Tools

Linear analytical tools allow for rigorous testing of hypotheses and offer a computationally economical alternative to complex numerical tools, from which it is very hard to separate cause and effect. They also work quite effectively as scaling test beds. Dalu et al. (1996) and Ye and Pielke (1995) used the linear analysis tool originally developed by Dalu and Pielke (1993), and extended its capabilities to include non-zero large-scale winds and a periodic distribution of surface patchiness.

Among their major conclusions are:

1. With little or no synoptic wind over sufficiently large heterogeneously heated landscape patches, the mesoscale (resolved) vertical velocity is in phase with the CBL temperature perturbations and the mesoscale heat flux is positive and of the same order as the diabatic (turbulent) heat flux within the CBL. Above the CBL, the mesoscale heat flux is negative and penetrates into the free atmosphere through a height comparable to the depth of the CBL.

2. In the presence of synoptic flow, the mesoscale perturbation is in the form of propagating waves that penetrate deeply into the free atmosphere. As a result, there is a net downward flux of momentum, which is dissipated within the CBL by turbulence. Mixing with the environment of the air particles displaced by the waves results in a net negative mesoscale heat flux, which contributes to the weakening of the stability of the free atmosphere (troposphere; see Fig. 2.5).

3. Strong synoptic advection can significantly reduce the mesoscale-induced horizontal temperature gradients in the CBL, thereby weakening the intensity of the mesoscale flow. Turbulent diffusion also weakens the temperature gradients and the intensity of the mesoscale flow when the horizontal wavelength of the surface heat patches is comparable to the CBL depth or smaller.

4. When the synoptic wind is very strong, the mesoscale perturbation is very weak and vertically trapped.

2.3.2 Numerical Tools

In order to include nonlinear effects, and more realistic feedbacks between the land surface and the atmosphere, numerical modeling techniques must be applied. The research work in our group mainly utilizes RAMS (Pielke et al. 1992, Nicholls et al. 1995) to perform numerical analysis.

Papers by Pielke et al. (1997, 1998), Walko et al. (1995) and Zeng and Pielke (1995a and 1995b) list, among their conclusions:

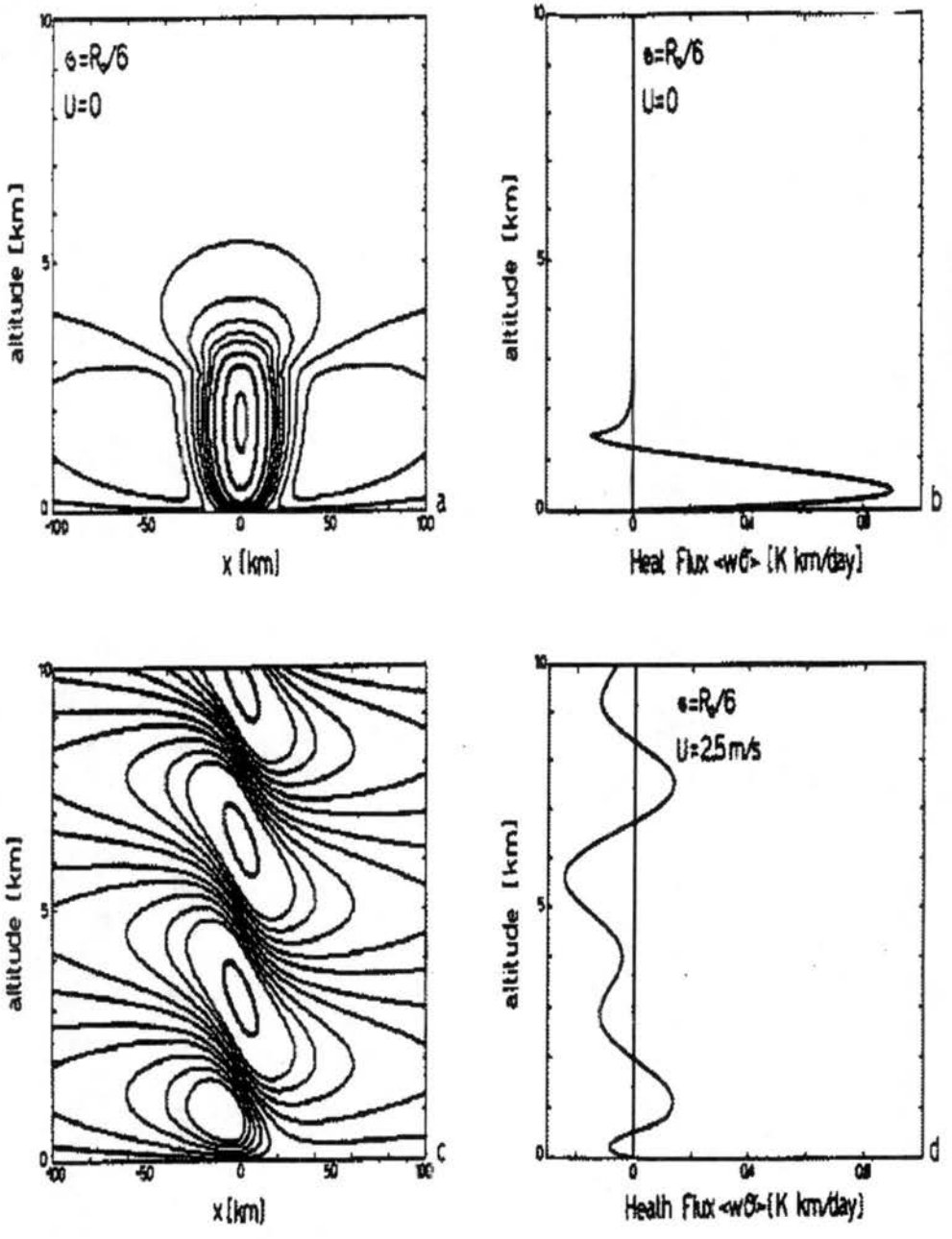

Figure 2.5: a) Vertical velocity isolines, w, over an isolated diabatic heat source, for zero predominant winds; b) the mesoscale heat flux associated with case a); c) vertical velocity isolines, w, over an isolated diabatic heat source, for a 2.5 m s^{-1} predominant winds; b) the mesoscale heat flux associated with case c). Adapted from Dalu et al. 1996.

1. The important controls on mesoscale fluxes resulting from land surface heterogeneities include boundary layer depth, horizontal size of the surface heat patches, the potential temperature difference between the patches, the surface sensible, moisture, and momentum fluxes, and the height above the surface (Zeng and Pielke 1995b).

2. Knowledge of the details of the landscape (including soil moisture, landscape type, and fractional coverage) are essential for accurate simulations of mesoscale and cumulus processes over land during the summer. Figure 2.6 perhaps most succinctly demonstrates the importance of landscape on deep cumulonimbus convection. Using identical lateral boundary conditions and the same initial conditions, RAMS was integrated for 15 May 1991 with the 1991 landscape (top result for 1400 LST) and the natural landscape (bottom result for 1400 LST). The differences are dramatic. The additional Convective Available Potential Energy (CAPE) provided by the greater vegetation coverage in the current landscape (where there is agriculture and shrubland as contrasted with the natural landscape, which was a short grass prairie) produced the area of thunderstorms shown in the top figure. The simulated meteorology was realistically represented on this date by RAMS (Shaw 1995, Shaw et al. 1997). The storm shown in Fig. 2.6 (top) in the real world spawned a tornado which has been simulated in a 6-nested grid run by Grasso (1996). In contrast, when a short grass prairie is assumed as the lower boundary condition, only shallow cumulus developed.

2.3.3 Observational Analysis

Modeling of atmospheric features is seriously incomplete without validation of the results. While there is no way we can validate the natural landscape results, our research premise is that if we can validate the model to a quantitatively defined level of skill for the current landscape, we have confidence that we are demonstrating a real sensitivity of the atmosphere to the landscape structure.

Papers that deal with model-data intercomparisons with focus on the landscape influence include Eastman et al. (1998), Lee at al. (1995), Moran and Pielke (1996a, b), Mukabana and Pielke (1996), Segal et al. 1989, Shaw et al. (1997), Taylor et al. (1998), Vidale et al. (1997), Walko and Pielke (1994), and Ziegler et al. (1995; 1997).

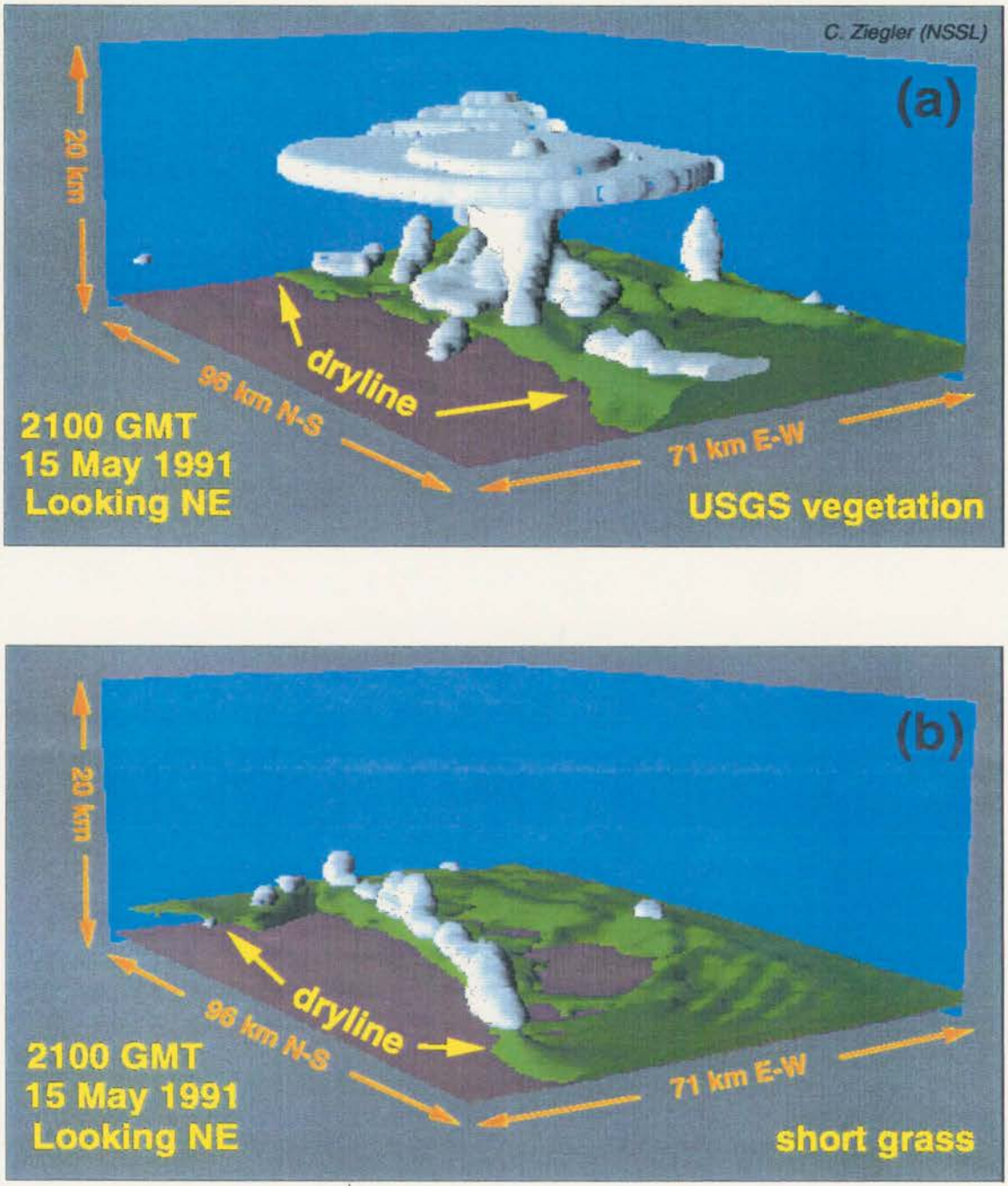

Figure 2.6: RAMS model output cloud and water vapor mixing ratio fields at 21 GMT on 15 May 1991. A 4-nested RAMS integration was utilized for this experiment with the coarsest outer grid covering most of the western United States. The clouds are depicted by white surfaces with $q_c = 0.01$ g/kg, with the sun illuminating the clouds from the west. The vapor mixing ratio in the planetary boundary layer is depicted by the green surface with $q_v = 8$ g/kg. The tan surface is the ground. Areas formed by the intersection of clouds or the vapor field with lateral boundaries are flat surfaces, and visible ground implies $q_v < 8$ g/kg. The vertical axis is height, and the blue backplanes are the north and east sides of the grid domain (from Pielke et al. 1997).

Among their conclusions are:

1. There are significant spatial variations in surface heat and moisture fluxes due to landscape variations. These variations in the middle of a summer or spring day are often hundreds of W m^{-2}.

2. Organized land cover patchiness has been shown observationally to induce horizontal diabatic heating gradients that are as intense as the ones present in a sea breeze case (e.g. Segal et al. 1989, for irrigated regions in Colorado).

3. Even in situations that linear theory would have as less favorable, such as in the case of the snow-covered lakes in boreal winter, the measurements of Taylor et al. (1998) for Namekus Lake (3 km in diameter) show that significant mesoscale circulations are made possible by a combination of surface forcings;

4. Flux variations are evident above the surface as well; however, we still do not have definitive observational evidence of mesoscale fluxes due to landscape variations.

2.3.4 Latest Results from BOREAS and Other Field Programs in Support of Landscape Effects

We have recently completed a fine-scale model run for a relatively strong winds BOREAS case study day (Vidale et al. 1997). Despite the strong winds, we did find evidence of mesoscale fluxes due to lakes within the boreal forest and strong surface flux heterogeneity associated with the different landscape types in both the model and observations.

These results have also been confirmed for other days during BOREAS and their generality was confirmed by Sun et al. (1997a), who analyzed data from three aircraft and found the Candle Lake breeze to be active on most BOREAS campaign days.

More results from BOREAS will be discussed in Chapter 4.

2.3.5 Related Landscape Work by Other Investigators

As described in the previous summary, there is strong theoretical, numerical modeling, and observational evidence of the importance of heterogeneous landscapes on boundary

layer and mesoscale atmospheric processes. Examples of research work on this topic by other investigators are described in the following summary.

Procedures to represent landscape heterogeneity within a larger-scale area, such as a GCM or NWP grid cell, have focused on a summation of surface fluxes within that area, proportionally weighted by the fluxes from each land surface type. Examples of this approach are reported in Avissar (1995), Avissar and Pielke (1989), Bonan et al. (1993), Clark and Arritt (1995), Collins and Avissar (1994), Dickinson (1995), Giorgi (1997a,b), Henderson-Sellers et al. (1993), Kosta and Suarez (1992), Li and Avissar (1994), Miller (1993), Pitman (1994), Pleim and Xiu (1995), and Sun and Mahrt (1995).

Evidence exists, however, that mesoscale fluxes that result from landscape heterogeneity in flat terrain can often be as large as, and larger than, turbulent fluxes, as well as have a different vertical distribution than the turbulent fluxes averaged over the scale of a GCM or NWP grid increment. Examples of studies that document the modification of atmospheric boundary layer structure, and/or the development of mesoscale flow due to land surface inhomogeneity are reported in André et al. (1989a), Avissar and Chen (1993), Chen and Avissar (1994), Guo and Schuepp (1994), Manqian and Jinjun (1993), Raupach (1991), Segal and Arritt (1992), and Zhong and Doran (1995). A number of these papers are summarized in Cotton and Pielke (1995) and Avissar (1995).

Observations have also documented the importance of heterogeneous landscape in influencing boundary layer structures and mesoscale fluxes (Balling 1988, Beljaars and Holtslag 1991, Doran et al. 1992, 1995, Mahrt and Ek 1993, Mahrt et al. 1994a,b, Segal et al. 1988, 1989, and Smith et al. 1992) and in affecting such related properties as soil water infiltration (Wood et al. 1992).

Figure 2.7 reproduced from Banta and McNider (1997), illustrates that CBL depth associated with adjacent unstably stratified boundary layers does vary spatially. They found variations in depth of 400-500 meters in mid-July 1995 between an urban area and an adjacent rural area (the CBL was shallower in the region northwest of the city; the synoptic flow was very light over the Nashville, Tennessee area). Such a variation in CBL depth would be expected to generate a solenoidal mesoscale circulation.

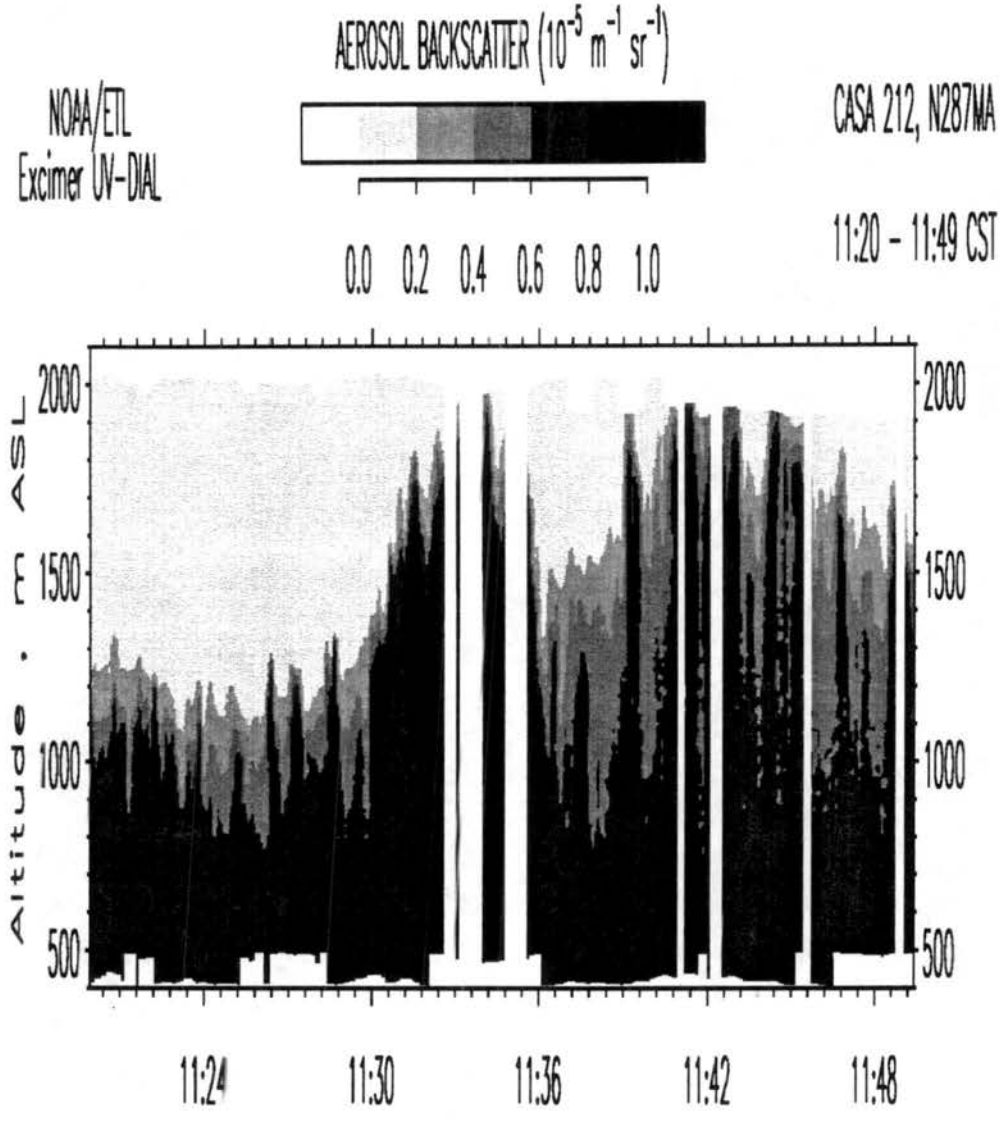

Figure 2.7: Aerosol and O_3 data from a NW-SE flight leg with Nashville, Tennessee near the center (1 min = 4 km) of one of 2 legs that formed an X over Nashville. These measurements clearly showed variability of the CBL over this region, with highest values over the city, high values outside the city in most directions, but distinctly lower values by 400-500 m to the northwest of Nashville (left side of figure). The CBL estimate from profiler data similarly showed suppressed mixing heights to the NW as compared with the other directions. and measurements of surface thermal properties showed that this region was cooler than the other regions around and within Nashville, reflecting differences in surface characteristics and soil moisture (from Banta and McNider 1997).

Doran and Zhong (1995) showed that variability of mixed-layer depths over a heterogeneous landscape can be significant and lead to errors in flux parameterizations, when ignored.

In the horizontal. Ogunjemiyo et al. (1998) have shown for BOREAS how a region of relatively homogeneous land cover (mainly black spruce) is capable of creating and sustaining significant surface sensible heat flux gradients over a period of many days.

By using a three dimensional, nonlinear numerical model, Wang et al. (1998) gave an evaluation of the mesoscale flow for a stochastic distribution of thermal inhomogeneities, showing how the impact of synoptic wind on mesoscale circulations is relatively weak, although mesoscale heat fluxes were found to be smaller on days with sustained winds than on days with weak winds. They also proposed that the impact of the thermally-induced mesoscale circulations can represent a significant heat transport mechanism, extending up to about five kilometers when the atmosphere is neutral, although it can become suppressed when the atmosphere is stable. Mesoscale momentum fluxes, on the other hand, were found to be comparable to turbulent momentum fluxes even in a stable atmosphere.

Field programs which focus on land surface-atmosphere interactions provide an observational data base associated with landscape effects on weather: FIFE (Sellers et al. 1992 and Betts and Beljaars 1993) in Kansas, U.S.A.; BOREAS (Sellers et al. 1995b, 1997) in Saskatchewan and Manitoba, Canada; LOTREX (Schädler et al., 1990) in Hildesheimer Börde, Germany; EFEDA (Bolle et al. 1993) in Spain; HAPEX-MOBILHY (André et al. 1989b; Noilhan et al. 1991) in France; HAPEX-NIGER92 (e.g., Gash et al. 1991) in Niger; SEBEX (Wallace et al. 1991) in the Sahel of Africa; and in the Amazon region (e.g., Shuttleworth 1985; Wright et al. 1992; Gash and Shuttleworth 1991).

A recent compilation of work on these topics can be found in the AMS Preprint Volume of the Symposium on the Boundary Layers and Turbulence (Land-Surface) held 2-7 February 1997 in Long Beach.

2.3.6 Critique of the Importance of Mesoscale Effects Generated by Surface Heterogeneity

While there is considerable evidence, as summarized in these papers, that mesoscale effects are important over heterogeneous landscapes, this conclusion has not been univer-

sally accepted. Indeed, as an example, Doran et al. (1997) present a thought-provoking paper where, using RAMS, they show that, when real-world data are used, mesoscale fluxes in clear sky conditions from landscape heterogeneity are relatively unimportant.

Other studies, such as Sellers et al. (1992) and Sellers et al. (1995d, 1997), suggested that a weighted summation of surface fluxes (weighted by landscape types) will give essentially identical results as when a domain-averaged condition is used to compute the fluxes. The conclusion from this study was that, at least for the FIFE study area, mesoscale fluxes are unimportant. However, the FIFE domain covered a relatively homogeneously vegetated region of 15 by 15 km and the 1995 study only examined heterogeneity over a strip of land of 15 by 2 km (Figure 2.8), which, according to linear analysis, is insufficient to generate mesoscale circulations even under moderate winds, especially for low surface sensible heat gradients.

Furthermore, the "Golden Days" used to investigate these issues in FIFE were predominantly windy days (see Table 2.1 reproduced from Eastman et al. 1998). Except for the 11 October 1987 case, the remaining days used for much of the intensive FIFE analyses were strong synoptic wind days. As shown in Dalu et al. (1996), we expect mesoscale fluxes to be less important under strong winds.

It is also important to point out that the Sellers et al. (1992, 1995d) work investigated *surface fluxes*. While mesoscale fluxes can feedback and influence the surface fluxes, the work of Dalu et al. (1996) suggests that the most important (relative to turbulent fluxes) effect of mesoscale fluxes is to influence atmospheric structure *above* the surface layer. In the Dalu et al. (1996) paper the turbulent (diabatic) heat flux and mesoscale flux are contrasted in a linear model for several sized heat patches, intensity of horizontal mixing, and synoptic wind speed. For the light synoptic wind speeds, the mesoscale cooling effect above the CBL (due to adiabatic lifting), is substantial.

The Doran et al. (1997) study also made their conclusion only for situations free of cumulus clouds. For situations in which cumulus clouds develop, however, a positive feedback between mesoscale focusing of this convection and subsequent cumulus convective growth can be important.

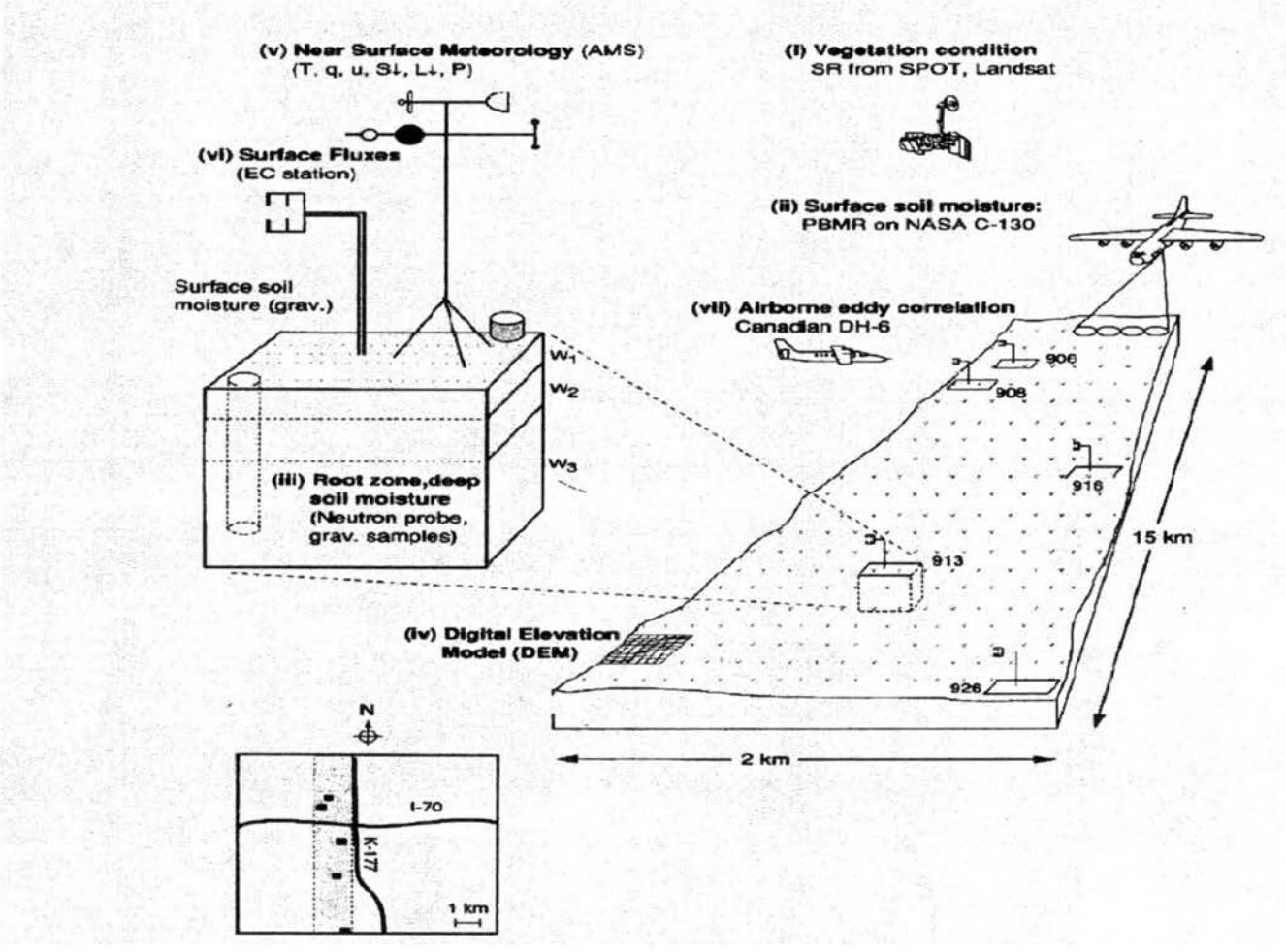

Figure 2.8: The Kansas FIFE flux measurement strategy and the domain of the landscape heterogeneity study.

Table 2.1: Average wind speeds for five "golden days" taken from the FIFE AMS data. (Averaged from 15 GMT through 21 GMT using all available stations; from Eastman et al. 1998.)

Date	$\|\vec{u}\|$ m s^{-1}
6 June 1987	9.3
11 July 1987	8.2
15 August 1987	8.0
11 October 1987	1.3
4 August 1989	6.7

In a preliminary study in the FIFE area, Eastman et al. (1998) showed differences in fluxes when RAMS is integrated in a Large Eddy Simulation (LES) mode with and without the phase change of water permitted. When shallow cumulus clouds are permitted to develop, the landscape patchiness focuses the cumulus and results in a different vertical turbulent flux profile than when no landscape variations are permitted.

2.4 Summary

Work in the representation of processes ranging from the land surface to turbulence and to mesoscale circulations, with distinct spatial and temporal scales, points to the importance of their correct representation for NWP and climate simulation experiments. Less work has been done in quantifying the different impacts of mesoscale processes and on testing and developing strategies for their representation.

Chapter 3

METHODS

3.1 Basic Strategy

The basic strategy of this work consists of linking observational evidence, analytical modeling and numerical modeling to the highest possible extent, making use of data from the BOREAS field campaigns.

3.2 Analytical Modeling

We first introduce some methodology that was derived from the studies by Dalu et al. (1996, 1998). This scaling tool was used to plan the numerical simulations with the RAMS model, especially in terms of grid deployment and averaging rules.

3.2.1 Governing Equations

The two-dimensional and Boussinesq primitive equations, in linear form, used in the model of Dalu et al. (1996) are:

$$\left(\frac{\partial}{\partial t}+\lambda\right) u + U\frac{\partial u}{\partial x} - fv + \frac{\partial \phi}{\partial x} = K\left(\frac{\partial^2}{\partial x^2}+\frac{\partial^2}{\partial z^2}\right) u \tag{3.1}$$

$$\left(\frac{\partial}{\partial t}+\lambda\right) v + U\frac{\partial v}{\partial x} + fu = K\left(\frac{\partial^2}{\partial x^2}+\frac{\partial^2}{\partial z^2}\right) v \tag{3.2}$$

$$\left(\frac{\partial}{\partial t}+\lambda\right) w + U\frac{\partial w}{\partial x} + \frac{\partial \phi}{\partial z} - b = K\left(\frac{\partial^2}{\partial x^2}+\frac{\partial^2}{\partial z^2}\right) w \tag{3.3}$$

$$\left(\frac{\partial}{\partial t}+\lambda\right) b + U\frac{\partial b}{\partial x} + N_0^2 w = Q + K\left(\frac{\partial^2}{\partial x^2}+\frac{\partial^2}{\partial z^2}\right) b \tag{3.4}$$

$$\frac{\partial u}{\partial x}+\frac{\partial w}{\partial z}=0. \tag{3.5}$$

In these equations u, v, w are the wind components, U is the large-scale flow intensity in the middle of the CBL (here taken as 850 hPa), b is the buoyancy force, f is the Coriolis parameter, N_0 is the Brunt-Väisälä frequency, Q is the diabatic buoyancy source related to the vertical divergence of the sensible heat flux in the CBL, and ϕ is the geopotential as in Rotunno (1983). λ is the Rayleigh friction, usually taken as 10^{-4} s^{-1} as in Haurwitz (1947), who empirically determined its value: a λ of the order of the Coriolis parameter induces a phase lag in the hodograph of the horizontal wind vector of the same order as the one observed in different sea breeze cases. λ (whose inverse is of the order of the lifetime of the mesoscale flow) can be thought of as a bulk parameter which represents frictional losses by low wavenumbers; diffusion (K) acts instead on high wavenumbers. Typical values for all parameters, as were applied for BOREAS, will be given in Chapter 5. As a lower boundary condition we assume that the vertical momentum component vanishes at the ground, $w(x, z=0, t)=0$.

This model can be used to study the impact of the mesoscale flow on the *large-scale* atmospheric parameters, when the mesoscale flows persist for few days during weak large-scale flow conditions.

By considering flow in the $x-z$ plane only, the mesoscale flow is driven by the horizontal gradient of the vertical divergence of the diabatic source, Q in Eq.(3.4):

$$Q = Q_0\, q(t)\, r(x,z); \tag{3.6}$$

$q(t)$ is its time behavior, and $r(x,z)$ its spatial distribution. Also, the primitive equations (3.1 - 3.5) can be reduced to an equation for the streamfunction ψ (see also Dalu et al. 1998), by assuming $U=0$ and including vertical diffusion:

$$\left[\left(\frac{\partial}{\partial t}+\lambda-K\nabla^2\right)^2+f^2\right]\frac{\partial^2\psi}{\partial z^2}+\left[\left(\frac{\partial}{\partial t}+\lambda-K\nabla^2\right)^2+N^2\right]\frac{\partial^2\psi}{\partial x^2}=-\frac{\partial Q}{\partial x} \qquad (3.7)$$

$$\frac{\partial\psi}{\partial z}=u \quad \text{and} \quad \frac{\partial\psi}{\partial x}=-w.$$

This equation can then be solved by Laplace transformations in time and Fourier transformations in space. We typically integrated the model over a domain of 1024 km (256 points in x) by 5.012 km (256 points in z).

3.3 RAMS

RAMS (Pielke et al. 1992; Nicholls et al. 1995) is a primitive equation model that includes several optional physical packages (parameterizations) for radiation, turbulence, moist processes, surface, soil and hydrological processes (i.e. a SVATS).

Since we chose days without convection or cloud cover (because of the data collection strategy decided by the BOREAS operational group), the only physical packages of relevance are the SVATS, the turbulence and the radiation (described later as most were modified from the standard RAMS options). We used RAMS in its quasi-compressible (Boussinesq approximation), nonhydrostatic mode, with a hybrid scheme in time and a second order advection in space.

Numerical simulations were performed with RAMS using a two-way, interacting nested grids configuration (i.e. the communication between grids allows the finer grids to influence the parent grid and vice-versa) which allowed us to focus on the study areas with increasing resolution. The horizontal grids are described in Chapter 4. The vertical grid increment was initiated at 30 m above ground level (so that the first atmospheric level corresponded, as nearly as possible, to that of most aircraft measurements) and was then telescoped upwards through 28 levels.

3.4 Short Description of LEAF-2

The Surface-Atmosphere Vegetation Transfer Scheme (SVATS) used in RAMS is the LEAF-2 sub-model (Lee 1992; Walko et al. 1998), which is a one-level canopy model capable

of representing the surface energy balance as mediated by surface aerodynamics (Louis et al. 1982), parameterized canopy conductance (Jarvis 1976), and multi-level dynamic soil processes (Tremback and Kessler 1985). Within each LEAF-2 grid cell, a number of surface cover patches co-exist, with a minimum number of two (one water body and one vegetation type) and a maximum number limited by computer resources. Quantities which are averaged linearly by patch fractional area are the actual surface fluxes, and not the patch biophysical characteristics, in agreement with the discussion of Sun and Mahrt (1995) and Mahrt et al. (1997) on the computation of fractional contributions to surface fluxes.

3.4.1 Principal Components and Structural Diagram

LEAF-2 contains a set of equations which represent the storage and exchange of heat and moisture associated with the atmosphere-terrestrial landscape interface. Its formulation involves the following physical components:

1. Soil
2. Temporary surface water (e.g. snowcover)
3. Permanent water bodies
4. Vegetation
5. Canopy air
6. The free atmosphere (lowest level)

The soil component is subdivided into several vertical levels to represent vertical variability. Each layer is normally 4 to 20 centimeters thick, so that the soil is typically represented to a depth of a meter or more. The internal energy and moisture content are prognosed in each soil layer (Tremback and Kessler 1985). Temporary surface water is included as precipitation which has reached the ground and has not yet percolated into the ground or run off into a permanent water body (oceans, lakes and permanent rivers). It includes snowcover, snow melt, rainwater, and temporary streams and ponds. If in the form of snowcover, temporary surface water may also be divided into several vertical layers,

depending on the depth of snow present. The mass and thermal energy are also prognosed for each temporary surface water layer.

Vegetation is represented by a single prognostic temperature and surface moisture (dew or intercepted rainfall). This does not imply that vegetation itself is assumed to consist of a single layer; the large surface area of leaves exposed to air (canopy air) is accounted for in evaluating turbulent exchange of heat and moisture. Canopy air is defined as air in close proximity to and influenced by vegetation and is also represented by a single prognostic value of temperature and moisture (water vapor mixing ratio). It serves as the medium in direct communication, via turbulent fluxes, with the soil or snowcover, vegetation, and the free atmosphere, allowing the latter components to influence each other indirectly.

The temperatures of permanent water bodies are not currently prognosed but are specified as temporally constant or seasonally varying. Water surface temperature and diagnosed water vapor pressure are used in computing sensible heat and vapor fluxes with the air.

Prognoses of all the above heat and moisture variables are governed by conservation equations which include storage terms and various fluxes between components of the system represented in LEAF-2. These components (except for permanent water bodies), and the flux pathways between them, are illustrated in Fig. 3.1.

This example contains two patches beneath the same atmospheric column (A), where both Patch 1 and Patch 2 have partial vegetation cover, and only Patch 2 has snowcover. Snowcover (S) and soil (G) are each divided into two layers, which is the minimum number to illustrate internal snowcover and soil fluxes. These layers are indexed from bottom layer up so that in the case of snowcover, snow layers can be added or removed from the top during accumulation or melt.

Fluxes are denoted by terms of the form F_{hgs}, where F stands for flux (although for clarity the F is not included in Fig. 3.1), the first subscript (w, h, or r) indicates whether the flux is water transfer, heat transfer (by turbulent exchange, conduction, or precipitation) or longwave radiative transfer, and the second and third subscripts denote the source and receptor, respectively, of the fluxed quantity (g for ground, s for snow, v for

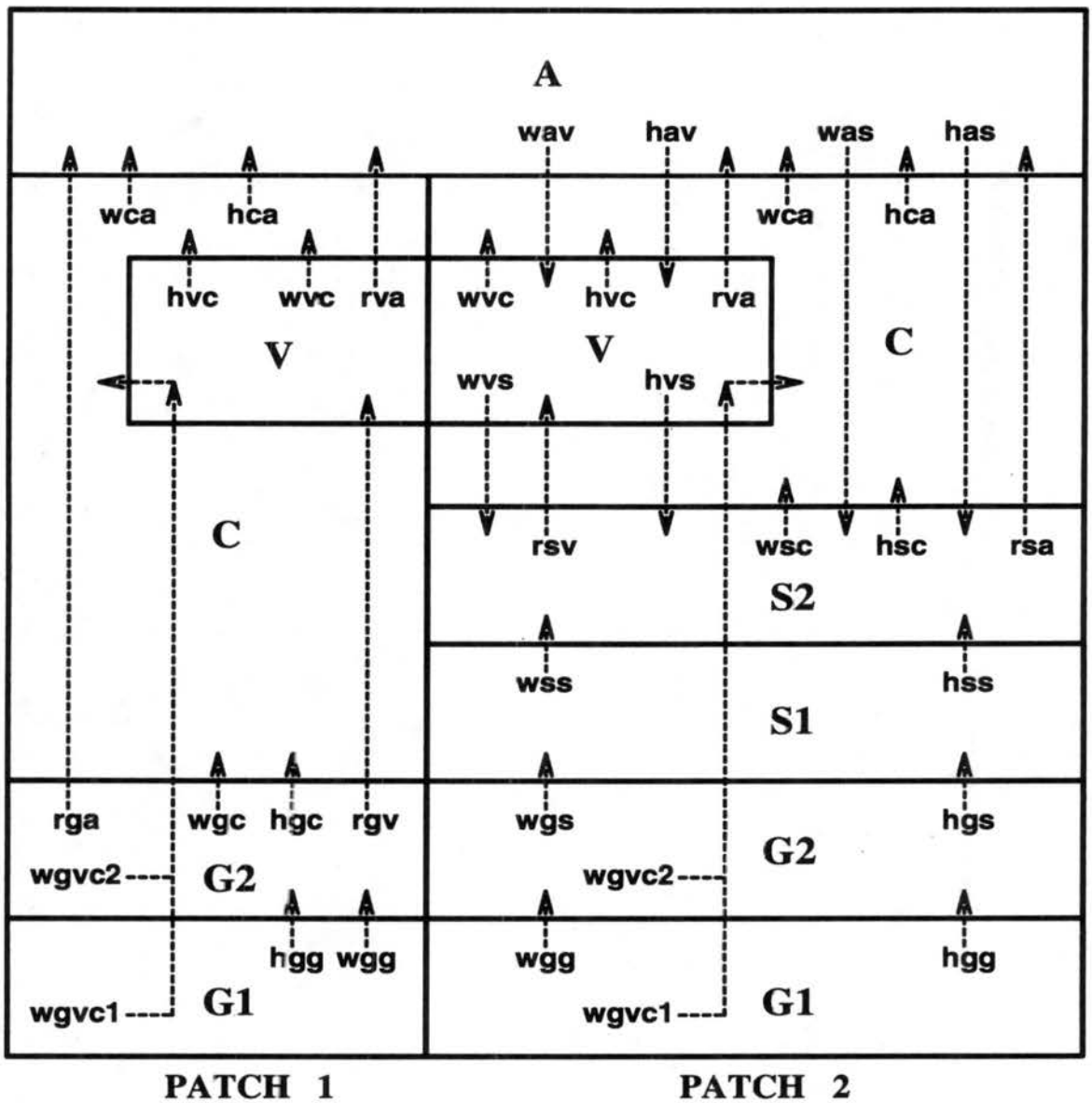

Figure 3.1: The LEAF-2 structural diagram: example for two patches from Walko et al. (1998). Symbols are explained in the text.

vegetation, c for canopy air, and a for free atmosphere). The one exception in notation is F_{wgvc} which denotes a flux of water from the soil to the canopy air via the vegetation in the form of transpiration. This is distinguished from the flux F_{wvc} which is a flux of water by means of evaporation from surface vegetation moisture, such as dew or intercepted rain, to the canopy air. Fluxes are defined as positive in the direction of the arrows; negative values imply transport in the opposite sense. Shortwave radiative transfer (not illustrated in Fig. 3.1) is denoted as a net amount S received by each component of the system under the combined influence of all others, rather than as fluxes exchanged between the components. Subscripts (g, s, and v) attached to S denote reception by the ground, snowcover, and vegetation, respectively. Numbered subscripts (1 and 2) are added to S_s and F_{wgvc} to denote reception by a specific snowcover or soil layer.

3.4.2 Advantages of the LEAF-2 SVATS Over the AM88 Formulation

Advantages in using LEAF-2 over the older SVATS in RAMS (Avissar and Mahrer 1988) are multiple:

- the existence of a canopy and canopy air, so that a true, independent budget for the vegetation can be calculated;
- mosaic capabilities (for surface physiography, hydrology and for multi-layer soils and multi-layer snow);
- assimilation of 3-D soil type information (previously 2-D);
- easier assimilation of remotely-sensed fields of biophysical parameters for the specification of surface biophysical characteristics;
- new surface layer parameterization (Louis et al. 1982), used at the European Center for Middle-range Weather Forecasting (ECMWF) from the early 1980s until the mid 1990s;
- frozen precipitation accumulation and frozen soil processes, for BOREAS winter work;
- availability of the TOPMODEL (Beven 1982; 1984; Beven and Kirkby 1979) hydrology package (although not used in this short time scale study).

3.4.3 Other Physical Packages Added to RAMS-LEAF-2

During the testing and development of the RAMS-LEAF-2 coupling, we also found it necessary to add a newer, simpler mixing length parameterization and we opted for the one by Lüpkes and Schlünzen (1996), which is a Richardson number based parameterization and was developed and used for similar applications. This package was also used in the study by Taylor et al. (1998) for winter work in BOREAS.

We use the following equations:

$$K_M = \begin{cases} l_n^2 \left|\frac{\partial v}{\partial z}\right| (1 - 5Ri)^2 & 0 \leq Ri \leq 0.2 \\ l_n^2 \left|\frac{\partial v}{\partial z}\right| (1 - 16Ri)^{1/2} & -5 \leq Ri \leq 0 \end{cases} \tag{3.8}$$

and

$$K_H = \begin{cases} K_M & 0 \leq Ri \leq 0.2 \\ K_M(1 - 16Ri)^{1/4}, & -5 \leq Ri \leq 0 \end{cases} \tag{3.9}$$

where K_H and K_M are the eddy diffusivities for heat and momentum, l_n is the mixing length for neutral stratification, which is specified according to Blackadar (1962) as

$$l_n = \frac{\kappa z}{1 + \frac{\kappa z}{\lambda_a}}. \tag{3.10}$$

Ri is the gradient Richardson number:

$$Ri = \frac{\frac{g}{\theta_v}\frac{\partial \overline{\theta_v}}{\partial z}}{\left[\left(\frac{\partial \overline{U}}{\partial z}\right)^2 + \left(\frac{\partial \overline{V}}{\partial z}\right)^2\right]} \tag{3.11}$$

κ is the Von Karman constant (0.4), the asymptotic mixing length λ_a is taken as

$$\lambda_a = 0.007\frac{u_\star}{f}, \tag{3.12}$$

where $u_\star$ is the friction velocity.

We also added an extra stomatal control term that describes the root uptake dependence on soil temperature by level (W. Parton, personal communication), which was necessary given the extremely low soil temperatures in the region. This control is coded as an extra resistance term that couples in series with the other resistance factors that influence stomatal control.

3.4.4 Model Surface Boundary Conditions: The Predominant Pixel and the Mosaic Modes

The surface vegetation characteristics were defined using the AVHRR vegetation classification discussed in the next chapter (Fig. 4.5a) which has nominal resolution at 1 km, and actual useful resolution at 2-3 km. Grid 3 was designed, therefore, to be able to resolve the finest scales defined by this product and to obey the scale separation criteria established in Chapter 5 (i.e. modeled turbulent processes have scales under one CBL depth and mesoscale processes have scales of at least twice the CBL depth). Grids 1 and 2 were initialized, for separate model runs, by the use of a predominant pixel or by a mosaic technique (Avissar and Pielke 1989). When the model is initialized in predominant pixel mode, the surface physiography information is transferred to each grid point by interpolation so that only two patches exist, one of water and one of land, with water-land relative abundances calculated from the area each covers in the original data set. When a mosaic run is initiated, a number N of patches is assigned to each grid cell, with relative abundances calculated by area coverage and stored in a Look Up Table (LUT), together with individual biophysical characteristics. With this technique, contrary to the other mode, no information about the location of pixels inside each grid point is available, just the knowledge of how many there are. The statistics and parameters are then used in the surface layer flux calculations: first fluxes of momentum, sensible and latent heat are calculated separately for each patch, then they are summed according to the relative area of each patch over the grid point, so that the first atmospheric layer receives the grid average fluxes. The mosaic mode is usually applied over large domains, for long-term calculations, while the predominant pixel mode is usually applied in fine-scale, short-term runs, where more resolution can be afforded. Figure 3.2 shows in practice what happens in applying either mode around the Candle Lake (Saskatchewan) region, over a domain of approximately 27 by 27 km.

3.4.5 Model Initialization

The initial meteorological conditions and the hourly grid 1 boundary conditions (outer five points) were derived from the United States ETA model analysis (Black 1994) at 00 and 12 UTC, using the Davies (1983) technique. Surface water temperature was defined

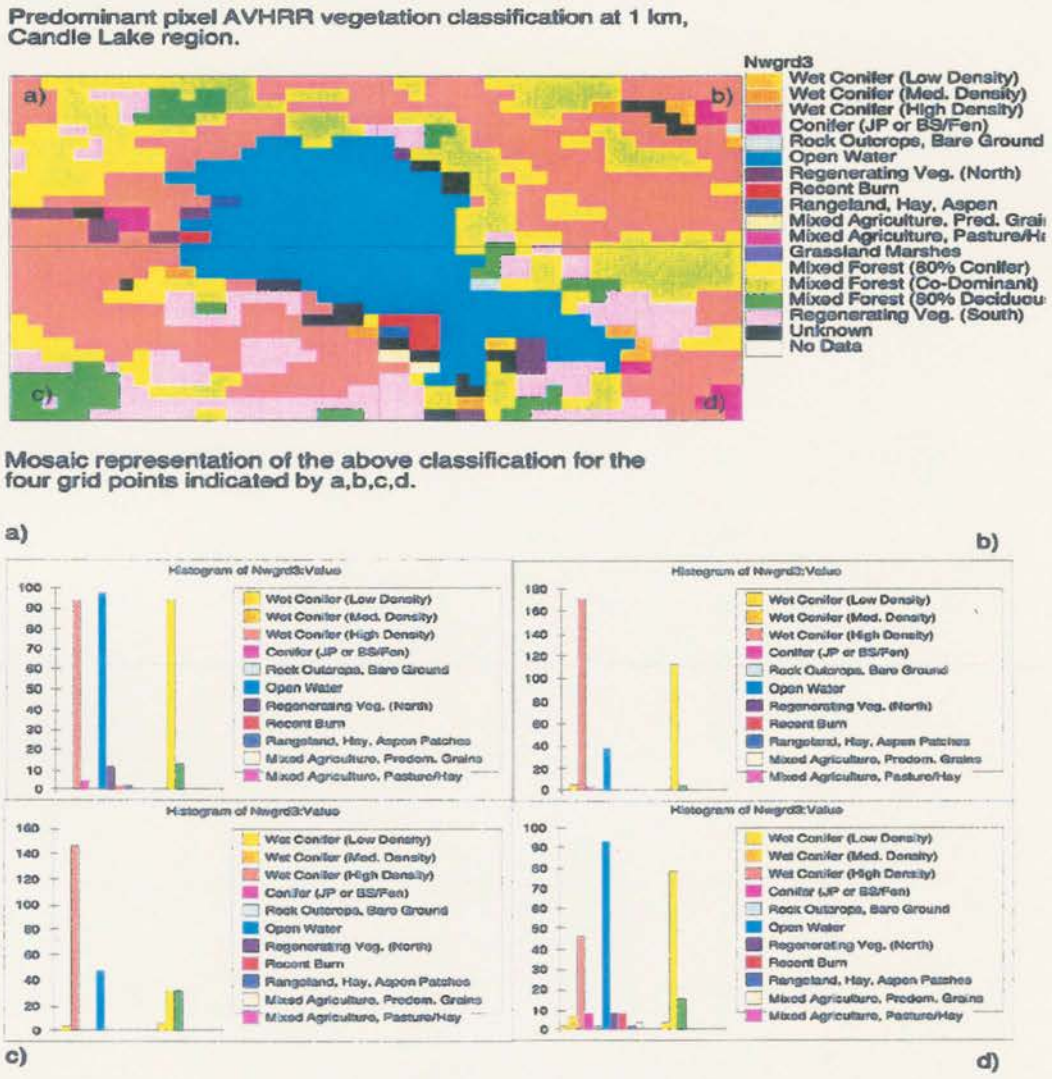

Figure 3.2: The predominant pixel and the mosaic modes available in LEAF-2. Top: the Candle Lake region as represented in a fine-scale run, with a predominant pixel classification. Bottom: the same region, for a coarse-scale run (four grid points, represented by the boxes in the top map), with a mosaic (statistical) representation of the surface physiography.

using aircraft measurements (Sun et al. 1997a). Extensive use of the BORIS (BOREAS Information Service) data sets allowed us to refine the model initialization locally with all available information from observations, especially in the case of soils data (e.g. profiles of initial soil water content and soil temperature, which were locally distributed according to vegetation type). After doing this, the model was allowed to run for more than a full diurnal cycle (two nights and one day) before using its output for analysis. This was to permit the soil heat and moisture component of the model to adjust to the atmospheric forcing.

3.5 Geographic Information System Modeling

In order to be able to assimilate the remote sensing data provided by other BOREAS teams, we decided to acquire a GIS package (ArcInfo) and to process the RS information locally. This allowed us to test various aggregation techniques and to be able to target our analysis of surface heterogeneity to specific modeling needs, apart from being able to incorporate data sets from different sources.

3.6 The Use of BOREAS Data Sets and Their Uniqueness

BOREAS provided unique opportunities to test our mesoscale ideas by concentrating the efforts of an unusually large number of observational teams and a great variety of observational platforms, deployed over a large, very heterogeneous area. The specifics of the BOREAS project and some of the main findings to this date will be discussed in the Chapter 5.

3.7 Summary

In order to be able to effectively address the science issues to which we were assigned as part of our BOREAS research, we created a set of tools (analytical and numerical) and a vast data base that are capable of working synergetically. Methods to link these tools depend on scaling analysis; this will be discussed in the next chapter.

Chapter 4

THE BOREAL ECOSYSTEM-ATMOSPHERE STUDY

4.1 Overview of the BOREAS Project

BOREAS is a large-scale, international investigation focused on improving our understanding of the exchanges of radiative energy, sensible heat, water, CO_2 and trace gases between the boreal forest and the lower atmosphere. A primary objective of BOREAS is to collect the data needed to improve models which can simulate the important processes controlling these exchanges, so that scientists can anticipate the potential effects of global change, principally altered temperature and precipitation patterns, on the biome. [1]

The scientific issues at stake are as follows:

- sensitivity of the boreal forest biome to changes in the physical climate system;
- the carbon cycle and biogeochemistry in the boreal forest;
- biophysical feedbacks on the physical climate system.

These scientific issues provided the motivation for the design and execution of a cooperative field experiment involving elements of land surface climatology, biogeochemistry and terrestrial ecology with remote sensing playing a strong integrating role. A coordinated multidisciplinary approach to the design of BOREAS was adopted from the outset to ensure the maximum benefit from each discipline's participation. The experimental phase of BOREAS ran over three years, 1993-1996; the long-term, climatological data collection will run for a few more years at selected sites.

---

[1] The following discussion is an edited version of information provided by BORIS and contained in several BOREAS white papers, of which we were contributors.

4.1.1 Objectives of the BOREAS Experiment in the Context of our Research

More specific objectives, for the purposes of this dissertation are:

1. improve the process models which describe the exchanges of radiative energy, water, heat, carbon and trace constituents between the boreal forest and the atmosphere;

2. develop methods for applying the process models over large spatial scales, using remote sensing and other integrative modeling techniques.

4.1.2 The Design of the BOREAS Experiment

The principal objectives of BOREAS relate to two different spatial scales that must be reconciled within the experiment design. The primary focus of Objective 1 is best addressed by local-scale (a few centimeters to a few kilometers) process studies which involve detailed coordinated in-situ observations; e.g., leaf and soil plot scale, CO_2 and water flux measurements and tower-mounted eddy correlation. These local-scale studies must be connected to the larger-scale measurement and analysis tools associated with Objective 2 which is directed toward defining regional-scale (10 to 1000 kilometers) fluxes and states. In BOREAS, as in previous field experiments such as FIFE (Sellers et al. 1992) and HAPEX-Sahel (Goutorbe et al. 1994), the science team adopted a nested multiscale measurement strategy to integrate observations and process models over a defined range of spatial scales (see Fig. 4.1). At the regional scale, satellite remote sensing, meteorological observations and modeling, and airborne flux measurements provide a large-scale picture of the important processes governing the exchanges of energy, water and carbon between the atmosphere and the land surface. Embedded within the region, data collected from the tower flux sites and process/auxiliary sites are used for point validation while studies carried out at intermediate scales (study area and modeling sub-area scales, see below) are being used to test different integration approaches.

4.1.3 The BOREAS Study Region

The BOREAS Project was set on the northern and southern edges of the Canadian boreal forest in a 1000 x 1000 km region covering most of Saskatche-wan and Manitoba, Canada.

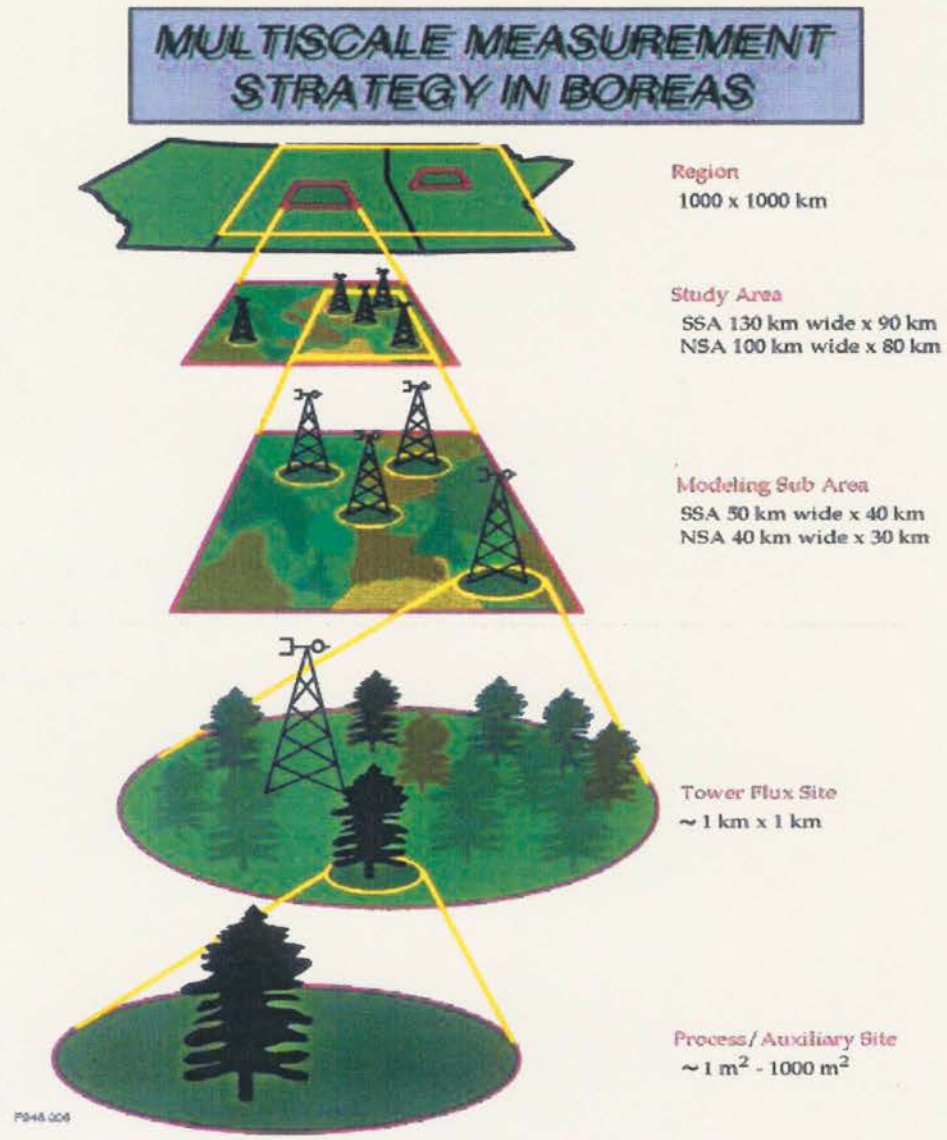

Figure 4.1: Multi-scale measurements in BOREAS.

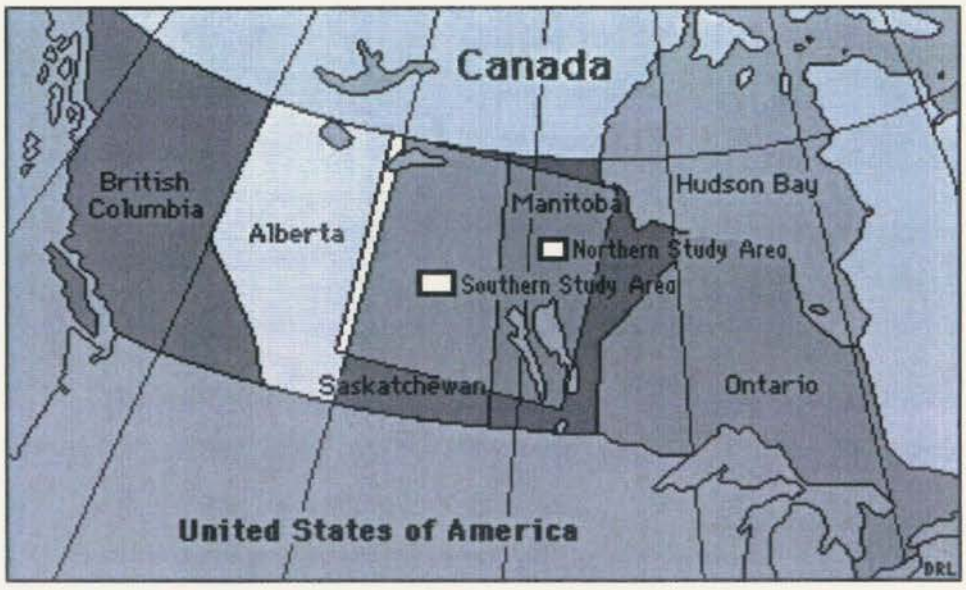

Figure 4.2: The BOREAS domain and the study areas.

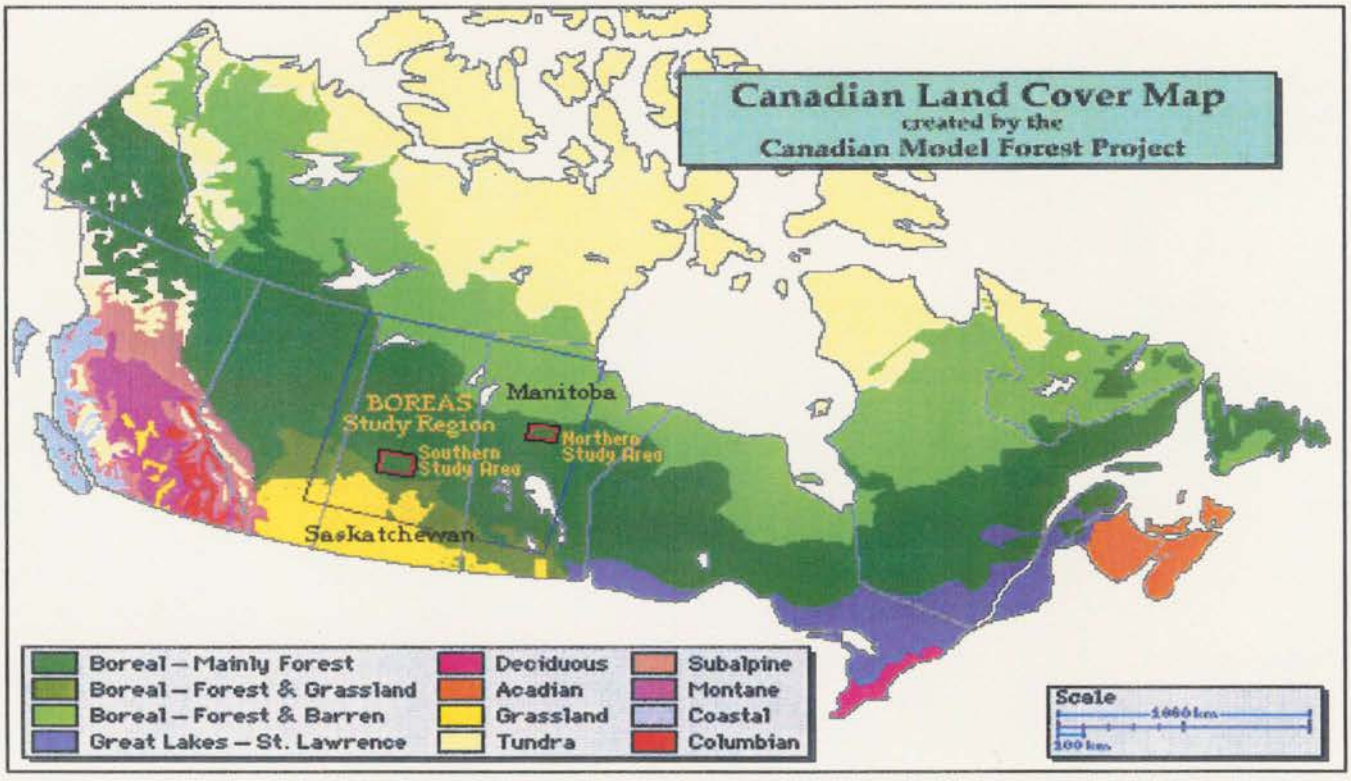

Figure 4.3: Land cover map of Canada showing the BOREAS Study Region and the Northern and Southern Study Areas.

The northern ecotone of the forest is delineated by temperature (growing degree days) while the southern boundary is determined by moisture stress and fire frequency in central and western Canada, and by ecological competition with temperate deciduous forest to the east of the Great Lakes. A minimum of two intensive study areas is therefore desirable as this would allow the observation of processes associated with at least two of the controlling factors (temperature in the north, moisture in the south). Each study area covers a domain big enough to allow the acquisition of useful airborne flux measurements and satellite observations but small enough to permit reasonable coverage with surface instruments. The definition and allocation of the auxiliary/process study sites is directed at defining the variability of surface states and processes and associated remote sensing signatures within and between the main sites. Almost all of the land surface climatology, nutrient cycling and tropospheric chemistry process studies (i.e. flux towers and other flux measurement efforts) and most of the remote sensing validation work is being conducted within these areas (see Fig. 4.3 and Fig.4.4). The distance between the two study areas is large enough to resolve the ecological gradient but small enough to permit the ferrying of research aircraft and specialized equipment.

- Region: An area of roughly 1000 km by 1000 km covering a large portion of Saskatchewan and Manitoba. This was the domain of meteorological and satellite data acquisition and large-scale modeling.

- Study Areas: These two areas were embedded within the region and were the focus of satellite and airborne remote sensing studies, airborne flux measurement and mesoscale modeling. The Southern Study Area (SSA, 11,170 square km) was located north of Prince Albert, Saskatchewan, and the Northern Study Area (NSA, 8,000 square km) lied west of Thompson, Manitoba.

- Transect: This is the area connecting and including the NSA and SSA, running from Thompson, Manitoba to Prince Albert National Park (PANP), Saskatchewan. It is approximately 800 km long. It was mainly flown by aircraft, but there were some ground instruments positioned at meteorological sites along the way.

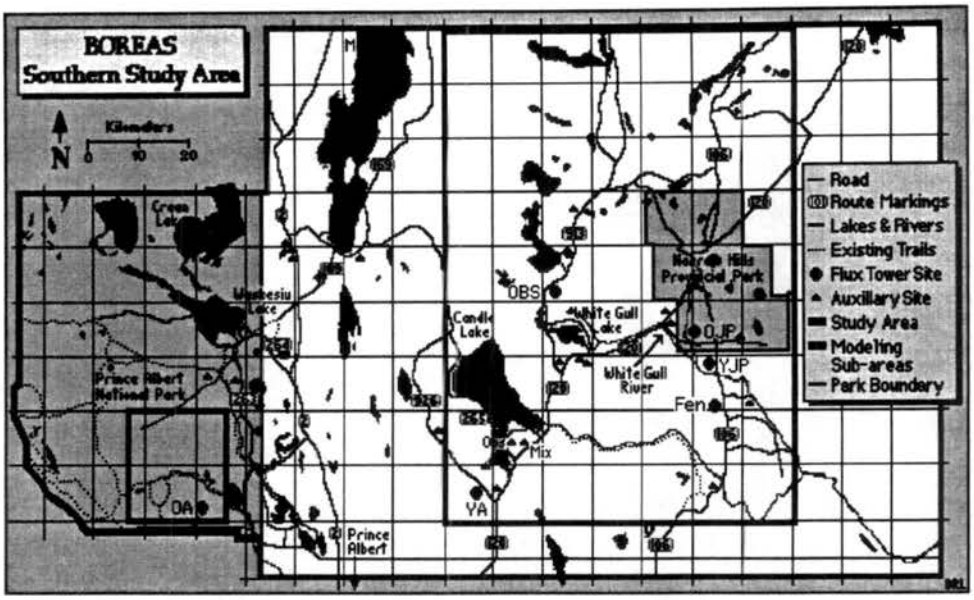

Figure 4.4: The BOREAS Southern Study Area and the measurements sites around Candle Lake.

- Modeling Sub-Areas: These were the test areas for modeling activities and gridded data products; they have the highest priority for airborne remote sensing studies and low-level airborne flux measurements. These sub-areas are located within the study areas.

- Tower Flux (TF) Sites: These are sites within the study areas where flux measurement towers (TF sites) operate. The TF sites are located in the center of areas of around 1 square km of relatively homogeneous vegetation cover, and are expected to measure fluxes representative of these vegetation types. Ten TF sites operated during the field campaigns.

- Auxiliary and Process Study Sites: Approximately 80 auxiliary and process study sites, some located within the TF sites, most of the others elsewhere within the study areas, were used for investigator studies or correlative targets for remote sensing investigations. A few of these sites were foci for carbon cycle studies which incorporated measurements of leaf physiology, litterfall and soil CO_2 flux. The majority of the sites serve as remote sensing targets and were visited by teams during the field year (1994) who collected a common set of biometric measurements: leaf area index,

crown closure, stem area density, etc. These data will be used to improve our ability to interpret satellite and airborne remote sensing data into biophysical and ecological parameters.

4.1.4 The BOREAS Intensive Field Campaigns (IFCs)

Most BOREAS measurements took place during IFCs meant to cover the onset, peak and end of the growing season, in order to accompany the evolution of the phenology. IFC1 ran therefore between 24 May and 16 June 1994, IFC2 between 19 July and 10 August, and IFC3 between 30 August and 19 September. Within each IFC, very clear days in which most measurement platforms were successfully deployed were labeled "Golden Days".

Table 4.1: The BOREAS golden days for the 1994 IFCs.

IFC	SSA Golden Days	NSA Golden Days
FFC-W	Feb 5 - Feb 9 1994	Feb 5 - Feb 9 1994
FFC-T	April 17, April 19 1994	April 17, April 20 1994
IFC-1	June 5 - June 9 1994	June 7 - June 12 1994
IFC-2	July 21 - July 25 1994	Aug 3 - Aug 8 1994
IFC-3	Sept 10 - Sept 17 1994	Sept 5 - Sept 10, Sept 17 1994

4.1.5 The BOREAS Science Groups

In 1992, 85 science teams were selected out of over 240 proposals to take part in BOREAS. These were organized into six disciplinary groups for easier organization during the field phase and for data classification:

- Airborne Fluxes and Meteorology (AFM), of which we are AFM-12
- Hydrology (HYD)

- Remote Sensing Science (RSS)
- Staff Science
- Terrestrial Ecology (TE)
- Tower Fluxes (TF)
- Trace Gas Biogeochemistry (TGB)

Data from each team was made available (as soon as Principal Investigator, P.I., certified) on the BORIS system, so that a high degree of remote interaction between team investigators was made possible throughout the project. Within this team framework, which also reflects the multi-scaling approach, we were responsible for the upscaling of the aircraft flux measurements to a regional scale. The tower to aircraft upscaling and comparisons were therefore the responsibility of other teams and we are relying on the aircraft flux validation for the comparisons discussed in Chapter 6. In 1994, however, as part of the BOREAS modeling exercise, we did address the issue of long-term validation of our SVATS against tower data. The results of that validation effort are contained in a NASA report entitled "Preliminary results from the terrestrial modeling exercise for the BOREAS Experiment" (Coughlan 1994).

4.1.6 Summary of Results From BOREAS

- The photosynthetic machinery of the boreal forest has considerably less capacity than that of the temperate forests to the south. This is reflected in low photosynthetic and carbon drawdown rates which are associated with low transpiration rates.
- The coniferous vegetation in particular follows a very conservative water use strategy. The vegetation transpiration stream is drastically reduced by stomatal closure when the foliage is exposed to dry air, even if soil moisture is freely available. This feedback mechanism acts to keep the surface transpiration rate at a steady and surprisingly low level (less than 2 mm/day over the season).

- The low evaporation and transpiration rates coupled with a high available energy during the growing season (the albedos are among the lowest observed over vegetated regions) can lead to high sensible heat fluxes and the development of deep planetary boundary layers, particularly during the spring and early summer. These planetary boundary layers are often characterized by intense mechanical and sensible heat-driven turbulence.

- As far as we know, all current climate and numerical weather prediction models grossly overestimate evaporation and transpiration from the region.

4.2 Description of the RAMS Physiography Data used in our BOREAS Modeling

4.2.1 The AVHRR Vegetation Classification of Steyaert et. al. (1997)

Most of the field campaigns mentioned in the previous section focused attention on the problem of scaling up surface fluxes from leaf-stand scale to GCM grid scales (Fig. 4.1). In FIFE, given the small study region (15 by 15 km) and the relatively homogeneous land cover, this was achieved with considerable success.

Unlike FIFE, the BOREAS project covered a regional scale (approximately 10^6 km^2), over very heterogeneous terrain and land cover. Figures 4.5a and 4.5b were produced using a land cover classification derived from the NOAA AVHRR data (Steyaert et al. 1997). Figure 4.5a covers most of the BOREAS domain; Fig. 4.5b is a subset of Fig. 4.5a, corresponding to the blue rectangle in Fig. 4.5a.

We have included various types of ancillary information in these two figures to help identify items mentioned in this paper. The vegetation cover data set, originally in the Albers Equal Area projection, was re-mapped to geographic coordinates, for assimilation by our atmospheric model. The latitude-longitude reference lines and the provincial boundaries are indicated in black.

The RAMS grid number 1, corresponding to the domain of Fig. 4.5a, comprised both the NSA and the SSA, approximately covering the region from 52.09 to 56.60 degrees north and 107.63 to 96.38 degrees west (about 700 by 500 km), with a horizontal grid separation

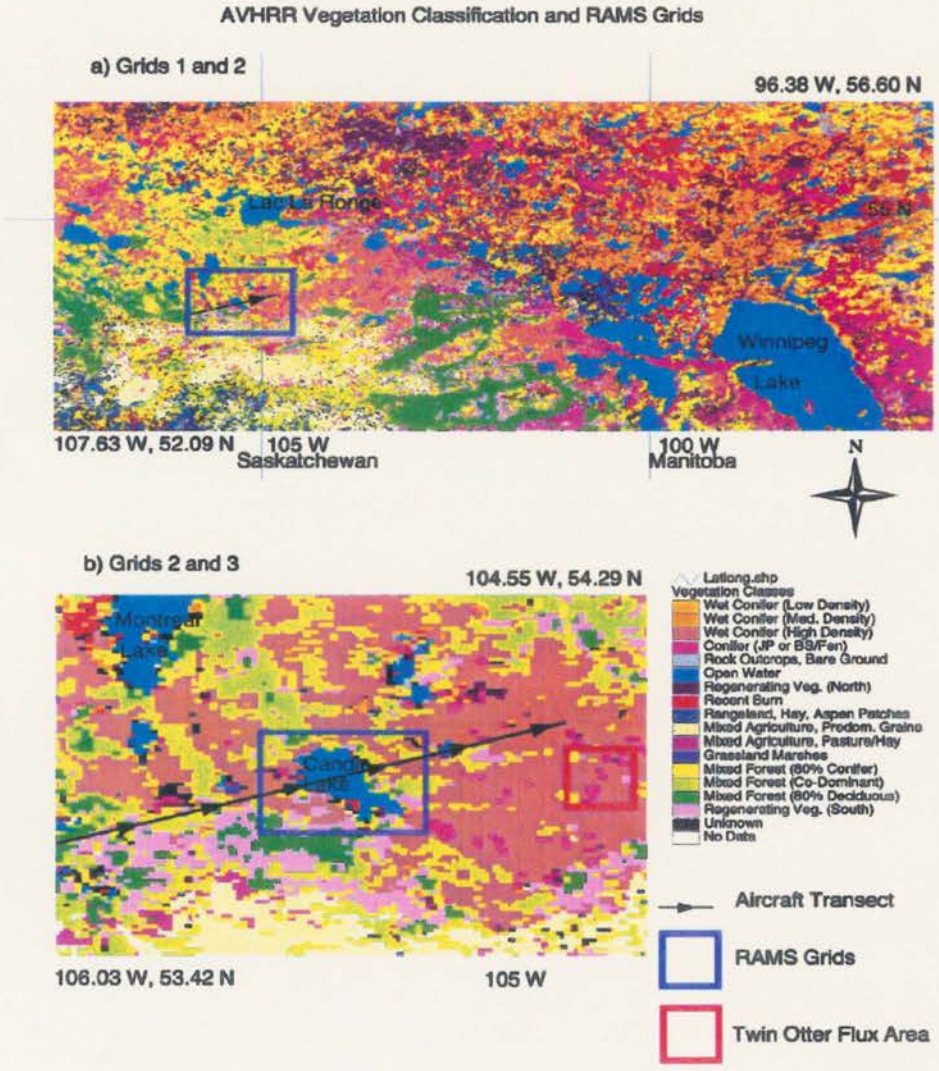

Figure 4.5: a): The AVHRR 1 km BOREAS regional land cover classification. Dark lines and letters indicate latitudes and longitudes with an interval of 5 degrees. The map corresponds to RAMS Grid 1 (52.09 to 56.60 degrees north and 107.6 to 96.38 degrees west); and b): The AVHRR 1 km BOREAS regional land cover classification for RAMS grid number 2. Dark lines indicate latitudes and longitudes in degrees with an interval of 0.5 degrees. The map limits are 53.42 to 54.29 degrees north and 106.0 to 104.6 degrees west. The red rectangle corresponds to the Twin Otter integrated flux region. Other symbols are explained in the legend.

of 10 km. Grid 2 covered most of the SSA, from 53.42 to 54.29 degrees north and 106.03 to 104.55 degrees west (about 95 by 95 km), with a horizontal grid increment of 2.5 km. Grid 3 was designed to cover the region around Candle Lake, for comparison with aircraft observations, and comprised the region from 53.72 to 53.96 degrees north and 105.5 to 105.1 degrees west (about 27 by 27 km), with a grid separation of 625 m.

Within the study region (Fig. 4.5a) there are numerous lakes (13% of the coverage by area), variable topography, several forest types and large areas of burned vegetation in various stages of regeneration.

The boreal forest, as depicted in Fig. 4.5a, is oriented diagonally from NW to SE and some important gradients in biophysical parameters aligned with a SW-NE transect through the forest. From a larger-scale perspective (i.e. also encompassing BOREAS bordering regions), for instance, LAI has a maximum over the forest, with minima further south (agriculture, pasture) and further north (tundra).

Over the southern BOREAS region, for the growing season, we identified at least five large groupings of land cover type that determine the surface fluxes:

- Forests: including wet conifers (with albedos of about 10%); mixed forests (dominated by conifers); and deciduous trees (albedos of about 20%). All have high fractional vegetation coverage, high LAI, high roughness length, generally dry conditions (in terms of canopy-atmosphere exchanges, although the soils are predominantly wet).

- Recent Burns: recently burned regions, in some cases with dark albedos, comparable to water.

- Regeneration: with low LAI, low roughness length for recent stages of regeneration; higher LAI, high roughness length for older regeneration stages.

- Agriculture: with high albedo, low roughness length.

- Lakes: with low albedo, zero LAI, low roughness length.

Over the northern BOREAS region we can expect influences on surface fluxes to depend on the distribution of:

- Forests: with low albedo, medium LAI, high roughness length, generally drier and colder conditions, as compared to the southern BOREAS region.
- Recent Burns: some of which are 40-50 km in extent, with very low albedo.
- Regeneration: with variable vegetation composition and age, depending on the date of the last burn.
- Rock outcrops: with high albedo, low LAI, low roughness length, typically associated with burn scars.
- Lakes: with low albedo, zero LAI, low roughness length.

The landscape patchiness discussed above displays a non-random area frequency distribution, as shown by Fig. 4.6, where patch area intervals are plotted versus area frequencies. While it is clear in this figure how the base AVHRR pixel size of 1 by 1 km dominates the distribution (also rendering the size distribution artificially discrete), hundreds of patches with areas of multiple hundred km^2 are present in the domain. The issue of the minimal patch size required for mesoscale atmospheric circulations to be forced by this patchiness will be discussed in the next section.

Biophysical characteristics are also quite heterogeneous within each class in Figs. 4.5a and 4.5b, and gradients in LAI, fractional vegetation coverage, and vegetation height are quite pronounced. Furthermore, LAI and albedo display pronounced time variability within the growing season (see for instance the LAI product of Chen and Cilhar 1996). The method of classification employed in building the BOREAS AVHRR land cover map attempted to address this problem by breaking classes into sub-classes which included some degree of information about location and prevailing environmental conditions (e.g. Regeneration North versus Regeneration South; or High Density Conifer versus Low Density Conifer versus Upland Dry Conifer).

These elements of surface patchiness (which in our atmospheric model control the surface-atmosphere feedbacks), create horizontal gradients in surface and Boundary Layer (BL) heat fluxes, due to differential solar radiation absorption, evaporation, transpiration and aerodynamic transfer, which may in turn generate mesoscale circulations.

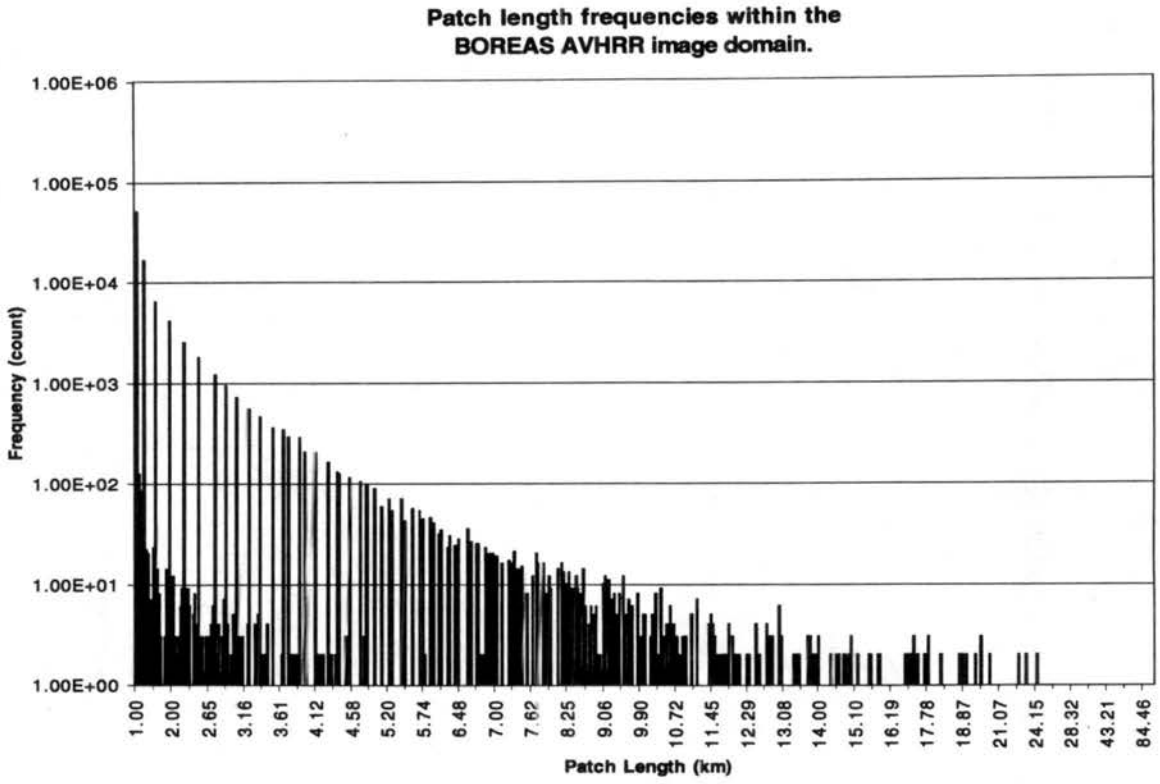

Figure 4.6: The patch size frequency for the BOREAS AVHRR classification.

An example of the resulting heterogeneity in fluxes measured during BOREAS is found in Ogunjemiyo et al. (1998), who derived maps of average sensible and latent heat fluxes for the two study areas for each Intensive Field Campaign (IFC) from the Twin Otter flights. A portion of the SSA, depicted as a red square on the right-hand side of Fig. 4.5b, corresponds to the region over which the Twin Otter measurements were averaged to obtain mean IFC representation of diurnal fluxes of heat. Figure 6 in that paper (see Ogunjemiyo et al. 1998) illustrates the existence of mean diurnal gradients, with maximum sensible heat flux near the dense conifer forest, measuring about 150 W m^{-2} over 10 km. These gradients are sustained both over the IFC time scale and over the whole growing season and their value is sizable even though the surface heterogeneity (as characterized by the AVHRR product) over that area is not as pronounced as over other parts of the domain. The spatial patterns obtained by averaging over all IFCs exhibit the strongest gradient for the all-IFC average along a SW-NE transect, co-located with the local topography gradient (Fig. 4.7).

Another important element of surface heterogeneity is represented by the orographic features (Fig. 4.7), which, although not very pronounced, are sufficient to induce horizontal gradients in the surface sensible heat flux, which in turn can generate mountain-valley flows.

4.2.2 Topography

The BOREAS regional topography (BORIS, Staff Science) slopes from east to west and some hills are located within the SSA. Two other terrain features are present on the southern boundary of Fig. 4.7; by comparison with Fig. 4.5a, it interesting to observe how these local gradients in orography correspond to sharp changes in vegetation cover. Montreal Lake (SSA), Candle Lake (SSA, at the center of RAMS Grid 3) and Lake Winnipeg (large lake in the south-eastern region) are positioned near hilly terrain, as defined by the 1 km DEM data set. The potential impact of orography over local circulations will be explored in Chapter 6 by analyzing the wind fields produced by our numerical model.

4.2.3 Pedology

We have also obtained a regional soils classification (BORIS, Staff Science; see Fig. '4.8), which helped define the soil types within the model domain. This data set is two-dimensional and we have therefore made the assumption that the vertical soil profile is homogeneous at each grid point, although we have made use of the 3-D capability in LEAF-2 in some experiments with an organic soil-top layer. Those experiments are not included here because of the difficulty in obtaining biophysical parameters for the organic layers.

4.3 BOREAS Data Sets in Support of the Existence of Mesoscale Circulations

4.3.1 Synoptic-Scale Boundary Layer Winds During BOREAS

Data from the National Center for Environmental Prediction (NCEP) reanalysis project, analyzed for the period from May to October 1994, is presented in Fig. 4.9. The relevant wind to be considered for the maintenance of differences between two adjacent boundary layers is the wind at the center of the BL, which could potentially mix them and eliminate the contrast that would force a mesoscale circulation. We have therefore analyzed the wind speed at 850 hPa for the NCEP grid point nearest the BOREAS SSA, representative at

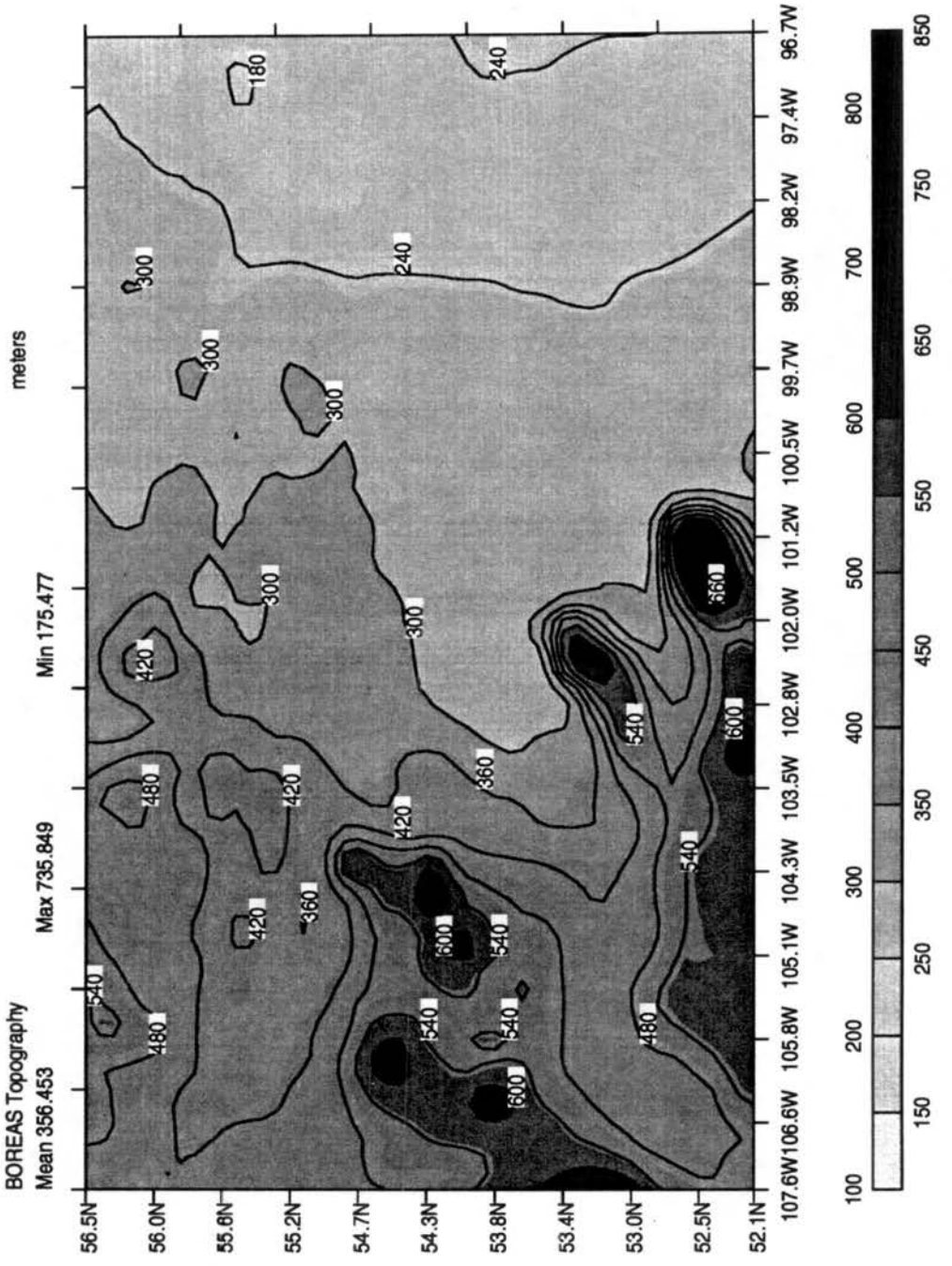

Figure 4.7: The BOREAS regional topography (m) for the RAMS simulations.

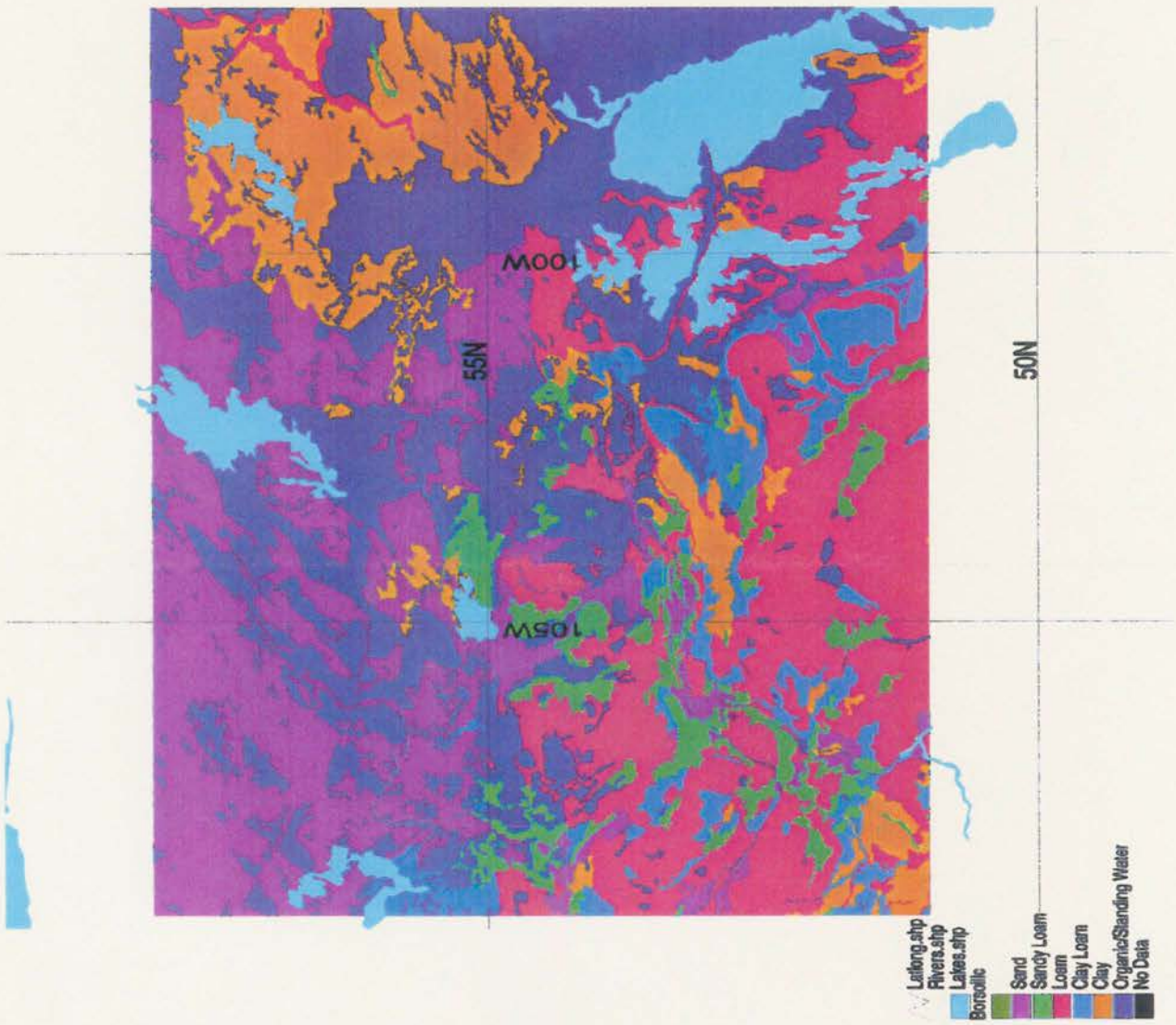

Figure 4.8: The BOREAS regional soils classification for the RAMS simulations.

the NCEP analysis scale of 2.5 by 2.5 degrees (thus a large scale). The histogram in Fig. 4.9 shows how the occurrence of moderate winds is not unusual for the SSA region. What remains to be answered is what linear theory means by 'light to moderate winds'. By comparing this information with table 5.1, and with Fig. 4.9 from Vidale et al. (1997), illustrating patch scale distribution, it is possible to expect a significant occurrence of days during which mesoscale circulations are active.

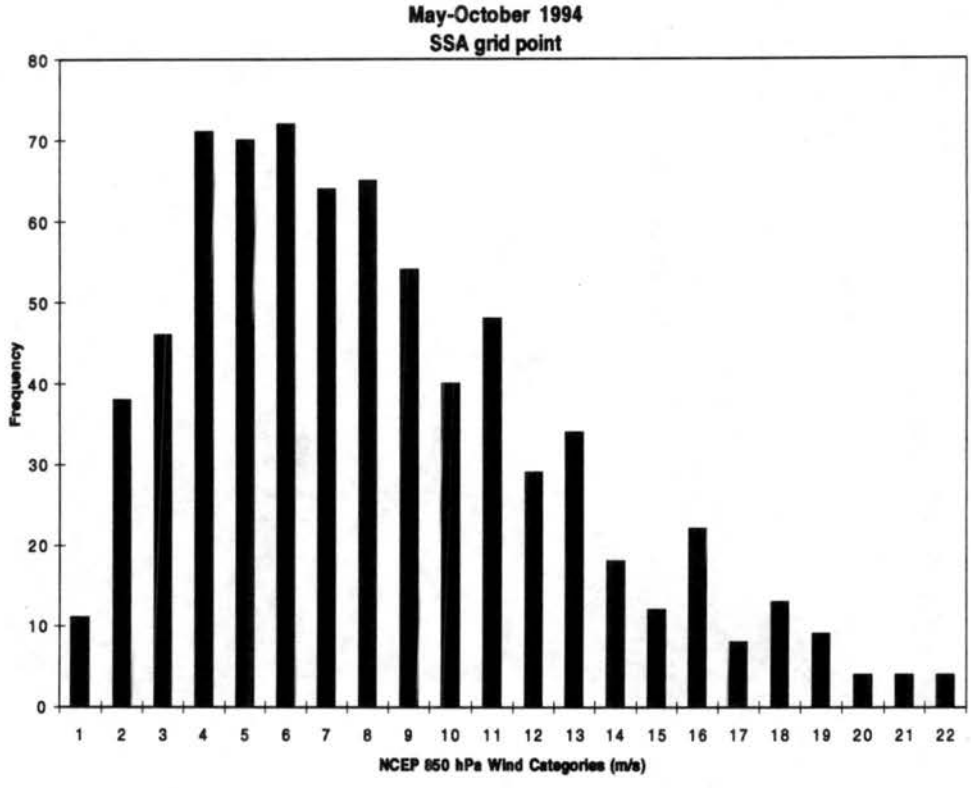

Figure 4.9: The NCEP reanalysis wind speeds (m s^{-1}, at six hours intervals) for the grid point nearest the BOREAS SSA. The horizontal grid spacing is of 2.5 by 2.5 degrees. Winds are separated in 1 m s^{-1} bins by magnitude, and the frequency of occurrence of each bin is plotted on the y axis.

4.3.2 Aircraft Data

The aircraft data campaigns in BOREAS were part of the upscaling exercise: transects covering the SSA in checkboard fashion were flown at altitudes as low as 30m, while higher altitude, linear transects were flown across the boreal forest from the SW to the NE. Within the SSA, most of the flights included Candle Lake transects, because this water body was

meant to provide biogenically clean and stable air for sensor calibration. This choice relied on the assumption that the lake did not interact with its surroundings.

However, Dr. Dobosy, of NOAA/ATDD, has in the past approached us with examples of days in which coherent circulations seem to be identifiable from the LongEZ aircraft data sets for those Candle Lake transects. Coherent circulations appear in the form of heat, water, momentum and carbon (HWMC) fluxes that have spatial and time scales beyond those normally thought of as atmospheric turbulence (Fig. 4.10) and appear closely associated with strong heat fluxes into lakes and out of forests. Other such examples appear in Dobosy et al. (1997).

The aircraft data shown here (and later in Chapter 6) to which we (and the LongEZ PIs) refer as 'turbulent' reflect time averages of 60s which correspond to a maximum spatial footprint of 3 km. The mesoscale base state defined by the LongEZ PIs corresponds instead to a 400s average, hence a footprint of 20km. The two are shown in Fig. 4.10.

The case of 26 May 1994, which is one of several possible examples, illustrates some of the issues that need to be explored in order to understand how to extrapolate the local budgets of HWMC for the region. On this day the wind was from the south, so it had a component across the aircraft transect (WSW to ENE) with intensities in the region of up to 7.5 m s^{-1} near the surface. The first two figures represent transects through Candle Lake (105.4W to 105.3W) over multiple legs, clearly showing the evolution of the diurnal heating as time elapses. By looking at Fig. 4.10a, depicting base state potential temperature (defined as 400 s, or 20 km averages) the evolution of the heating on the E side of Candle Lake is quite different from the evolution on the W bank. The smoothness of the heating gradient and the local maximum reached at the end of the day (possibly due to a convergence zone) are indicative of scales larger than the turbulent scale. The base state moisture content, in Fig. 4.10b shows a zonal gradient with a scale which is again much larger than a turbulent scale.

Maps of departure (from base state) CO_2 content (Fig. 4.10c) and potential temperature (Fig. 4.10d), as well as moisture (not shown), based on multiple legs, display maxima around the lake boundaries, decaying over a distance comparable to the lake size,

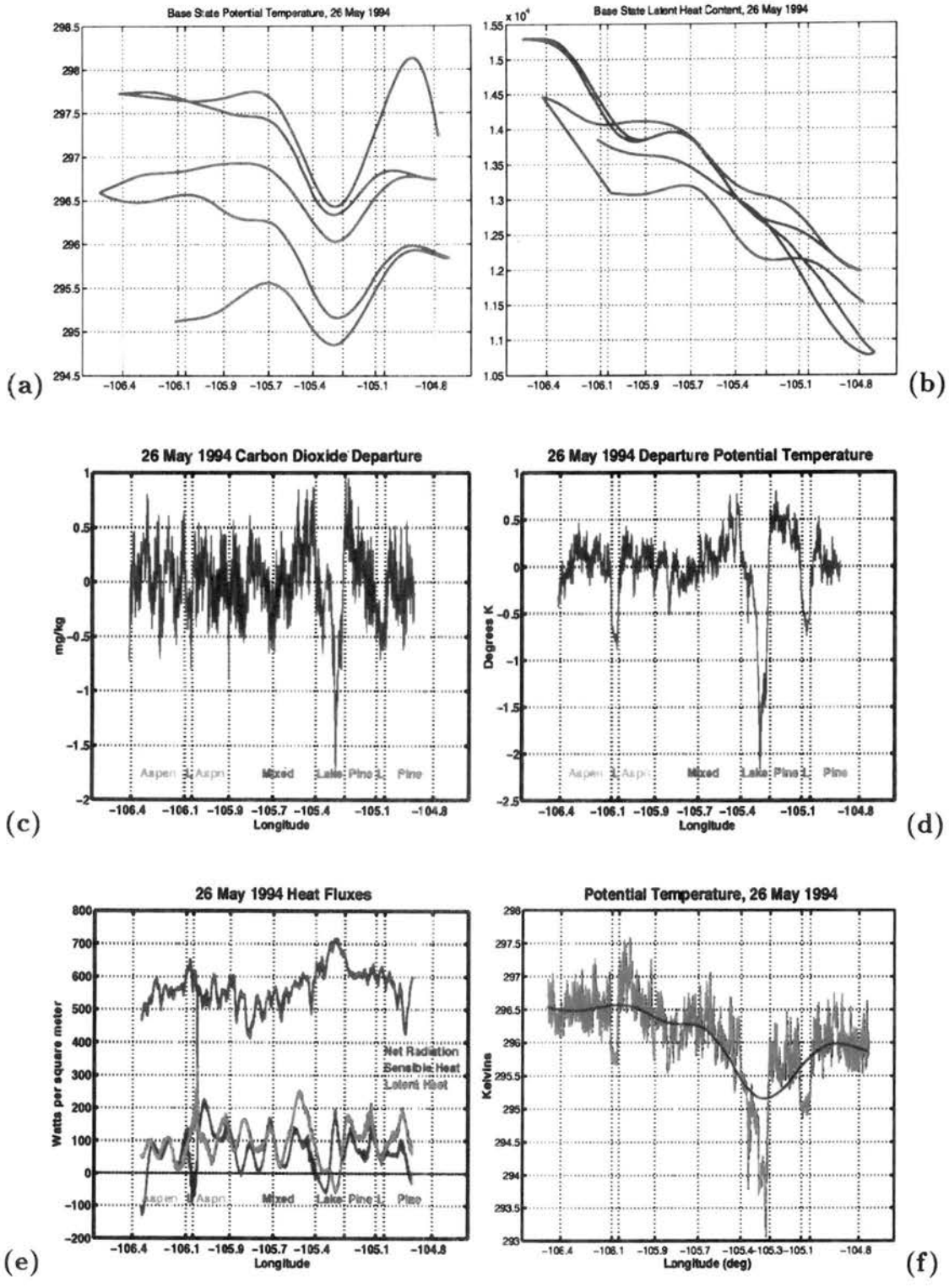

Figure 4.10: LongEZ data for the Candle lake transect for 26 May 1996. a) Base potential temperature; b) base moisture; c) departure CO_2; d) departure potential temperature; e) 30 m heat fluxes; f) Potential temperature (1 leg). Courtesy: Ron Dobosy, NOAA/ATDD.

illustrating possible flux enhancement mechanisms by advection due to the lake breeze. These figures also raise a question about the formation and influence region of an internal boundary layer, especially on the downwind side of the lake.

A map of the near surface sensible and latent heat fluxes (Fig. 4.10e) shows a sensible heat flux maximum over the eastern portion of Candle Lake, probably indicative of downward transport of cold moist air (confirmed by the latent heat minimum and by negative vertical velocity, not shown), and very probably a lake breeze signature.

Fig. 4.10f, shows potential temperature data from one leg and the reduction to a base state by averaging. The red curve is suggestive of the fact that there is in fact no real scale separation, and also better illustrates the asymmetry in the lake cooling influence, due to a combination of prevailing wind speed and of a lake breeze cell on the east side of Candle Lake.

The relevance of this data analysis is that, by defining averaging rules that are in agreement with atmospheric dynamics principles, and that are compatible with the measurements, we can explore the question of the existence and the areal extent of coherent circulations associated with regions of large horizontal surface sensible heating gradients.

4.4 Open Issues

Among the research problems that still need to be tackled in BOREAS are:

1. Aircraft-tower intercomparisons: the representativeness of each instrument and their footprints. Scaling rules and their testing are needed in order to interpret the data.

2. Long-term effects of mesoscale circulations: are local mesoscale circulations (such as the ever-present lake breezes; Sun et al. 1997a, Vidale et al. 1997, Taylor et al. 1998) important in determining the heat, water, momentum, and carbon (HWMC) fluxes over the entire growing season and over multiple years?

3. Impact of vegetation classifications from remote sensing and of their resolution: how useful are regional vegetation classifications ?

4. Horizontal (and intra-class) variability in biophysical parameters and of their inter-annual variability: can they significantly alter the BOREAS budgets of HWMC?

5. Long-term fire patterns and connection between fire patterns and thunderstorm recurrence at a location; can convection be phase-locked by local solenoidal circulations generated by the vegetation patchiness?

6. CO_2 "chimneys" (the hypothesis of Sun et al. 1997b): when and where do they occur? How much can they affect the measurements of CO_2 flux at night ?

4.5 Summary

BOREAS provided a unique opportunity to test hypotheses about the formation of mesoscale circulations induced by complex distributions of surface physiographical elements. Data from the IFCs helped us to understand the scaling of coherent circulations in the region and to plan our investigation. Evidence of mesoscale circulations associated with the presence of lakes, even under moderate winds, is present in the aircraft data analysis of Sun et al. (1997) and Dobosy et al. (1997).

Chapter 5

RELEVANCE OF MESOSCALE PROCESSES FOR BOREAS: EVIDENCE FROM ANALYTICAL MODELING

Given the past studies mentioned in Chapter 3, we wished to assess the relevance of the possible formation of mesoscale circulations for our numerical modeling in support of BOREAS. Specifically, we wanted to establish some basic scaling rules to apply to the numerical domain.

5.1 Questions Posed to Linear Theory

1. What is meant by 'light to moderate winds' for a given patch length and a given heating gradient ?

2. What is the effect of the mesoscale circulations on the tropospheric basic state ?

3. Within which horizontal distance are the mesoscale circulations active and their effects significant ?

4. What is the vertical distribution of the 'mesoscale signatures' ?

5. What is the typical magnitude of the mesoscale flux contributions under different environmental conditions ?

6. What are the 'dynamic rules' for including or excluding contributions from mesoscale circulations ?

5.2 Scaling Rules from Linear Theory

Dalu et al. (1996) have partially addressed item 1, by detailing the relationship between patch size and wind speed in terms of a Mesoscale Available Potential Energy (MAPE, i.e. the potential energy created by mesoscale circulations that will be available after those circulations end their life cycle). We have re-formulated their work here in order to derive scaling estimates that would be directly applicable to our BOREAS effort.

We recognized four types of surface heterogeneity in BOREAS that could be responsible for the generation of mesoscale circulations:

- land-water contrasts (i.e. a stable versus a mixed or unstable BL);
- deeper to shallower CBL (as in Fig. 2.7);
- hilly terrain (e.g. around Candle Lake);
- roughness discontinuity (rough to smooth forest)

We have calculated MAPE for each one of these conditions, using typical BOREAS conditions and measured parameters, for periodic distributions of patches of different wavelengths (represented by a horizontal wavenumber, k). We have then assumed that all the MAPE is converted into kinetic energy, so that an induced wind speed could be calculated. We have defined a significant mesoscale circulation to be one that has at least a 1 m s^{-1} induced wind speed. Among the controlling parameters, we have imposed a linear diffusion coefficient of 100 m^2 s^{-2}, a dissipation coefficient of 10^{-4} s^{-1}, and a thermal stability of 3 K per km. Sensitivity to these parameters will be discussed later in this chapter. The details of each derivation are given in Appendix A.

5.2.1 Water-Land Distribution

For this case, we hypothesized the growth of a periodic distribution (with wave number k) of convective boundary layers next to stable layers, so that mesoscale circulations are initiated. Using the definition of MAPE from Dalu et al. (1996; Eq. 2.2.16 and Appendix A), with an asymptotic inversion height (h_0) of 2 km,

$$MAPE = \int_{-R_0}^{R_0}\int_0^h \left(\frac{gz\theta_i}{\Theta}\right) dzdx - \int_{-R_0}^{R_0}\int_0^{h_0/2} \left(\frac{gz\theta_f}{\Theta}\right) dzdx = \frac{g\Theta_z}{\Theta}\frac{h_0^3}{24}3a^2\left[R_0 - \frac{1}{2k}\sin(2kR_0)\right]$$

(symbols are defined in the appendix).

A plot for the dependence of MAPE on synoptic- wind speed and wave number is available in Dalu et al. (1996). Basically, this equations shows how MAPE will be larger for a larger asymptotic CBL height, and will peak at a specific wave number (patch size on the order of R_0).

5.2.2 Land-Land Distribution

MAPE in this case was calculated by supposing that the differential heating between two land patches will cause a differential inversion height of 500m (between h_{0_1} and h_{0_1}), as for instance was shown in Fig. 2.7.

$$MAPE = g\frac{\Theta_z}{\Theta}\frac{h_{0_1}^3}{24}3a^2\left[R_0 - \frac{1}{4k}\sin(2kR_0)\right] - g\frac{\Theta_z}{\Theta}\frac{h_{0_2}^3}{24}\left\{3a^2\left[R_0 + \frac{1}{4k}\sin(2kR_0)\right.\right.$$

$$\left.\left. +3a\sin\frac{(kR_0)}{k}a^3\left[\frac{\sin(kR_0)}{k} - \frac{1}{3k}\sin^3(kR_0)\right]\right\}\right.$$

5.2.3 Mountain-Valley Distributions

Just as in the previous cases, a periodic mountain-valley distribution will cause the generation of MAPE through induced vertical velocity. The maximum hill height (H) is 200m.

$$MAPE = g\frac{\Theta_z}{\lambda\Theta}(kUH)\left[\frac{2}{k}\sin kR_0\frac{1}{\mu^2}\left(1-\cos\mu\frac{h_0}{2}\right) - \frac{h_0}{\mu}\left[R_0 - \frac{1}{4k}\sin(2kR_0)\right]\right]$$

5.2.4 Rough-Smooth Forest Distributions

This calculation, using a differential roughness length of 1 m, never produced MAPE of significant magnitude, therefore it is not included in the table.

Table 5.1 summarizes the results from these MAPE calculations.

Table 5.1: Minimal patch size for a mesoscale circulation to occur.

	Minimal Required Patch Size for Significant Mesoscale Circulation to Occur (km)		
Predominant Wind Speed	Lake-Forest	Forest-Forest	Hills
1	7.5	10.5	$O(R_0)$
2	12.5	19.5	$O(R_0)$
4	22.5	39.5	$O(R_0)$
6	32.5	58.5	$O(R_0)$
8	42.5	72.5	42.5
10	52.5	90.5	8.5

[1]This analysis does not include, however, pressure drag interactions with the heating gradient which would occur in moderate and strong wind. We will include that effect in a planned BOREAS follow-on research.

Clearly, the necessary patch size for a significant mesoscale circulation to occur is directly proportional to the wind speed and proportional to the heating magnitude. The effect is similar for the two adjacent CBLs, although smaller, since the MAPE is also smaller. The hilly terrain case has the opposite dependence to prevailing wind speed: with more winds, a smaller patch is sufficient to generate a mesoscale circulation.

These numbers suggest that the potential for the generation of mesoscale circulations over BOREAS exists (compare with Fig. 4.9, with thermal effects prevailing under lower predominant wind speeds and mechanical effects prevailing under higher winds. Of course in reality these effects can be combined and act synergetically if the individual contributions are in phase with each other. It is left to numerical modeling to verify if this type of relationship holds true. In the context of the fully coupled model, surface heterogeneity at the mesoscale comprises biophysical characteristics associated with the vegetation (albedo, roughness length, LAI, percent coverage of vegetation and soil), together with soil type, soil moisture content and snow cover.

5.2.5 Transition From a Closed Circulation to a Wavy Regime

Dalu et al. (1996) also discuss how at small horizontal wavenumbers the mesoscale circulation is trapped and the penetration depth of the mesoscale flow into the free atmosphere above the CBL is on the order of the inverse of the vertical wavenumber. At

large horizontal wavenumbers the mesoscale perturbation is made of propagating waves, which penetrate deeply into the free atmosphere. The latter condition is verified when the vertical wavenumber in that model is negative:

$$\mu = \sqrt{(l^2 - k^2)/(k^2 + k_0^2)} \tag{5.1}$$

where $k_0 = \frac{f}{U}$ is the inertial wavenumber and $l = \frac{N_0}{U}$ is the Scorer parameter.

Table 5.2: Patch size for wavy regime to initiate.

	Minimal Required Patch Wavenumber for transition to wavy regime (km)		
Predominant Wind Speed	k_0 (km^{-1})	l (km)	k (km^{-1})
20	50	0.5	5
10	100	1	10
5	200	2	20
2.5	400	4	40
1	1000	10	100

Again this points to the need for the construction of a relationship between patch size, wind speed and CBL heating gradient intensity, from observations and from fully coupled case studies.

5.3 Time and Spatial Scales: Analytical Guidance for Numerical Modeling

Many authors have given definitions of atmospheric scales, some based on spatial and time categories (e.g. Orlanski 1975); others using dynamical approaches (e.g. Ooyama 1980). Here we make use of dynamical definitions.

The mesoscale fluxes have different time scales than the turbulent HWM fluxes, also tending to reach peak magnitude later in the diurnal cycle. The characteristic time scale of a forced mesoscale flow in the presence of friction, λ (and the flow reaches full maturity in a time $4 \cdot T$), is defined in Eq. 5.2:

$$T = \frac{1}{\sqrt{f^2 + \lambda^2}} \tag{5.2}$$

where f is the local Coriolis parameter (here 10^{-4} s^{-1}) and λ corresponds to a linearized friction term (here a value of $\lambda \tilde{<} 10^{-4}$ s^{-1} is used as in Haurwitz 1947).

In terms of cell dimensions, these studies suggested that the asymptotic ($t >> T$) horizontal extension of the circulation cells is on the order of the local Rossby radius (defined as Eq. 5.3), while the vertical extent is on the order of the depth of the CBL. They also pointed out that these scales define lower and upper limits for the existence of these circulations in terms of the spatial scale of the forcing (i.e., the size of the landscape inhomogeneities).

From linear theory applied to the BOREAS region, the local Rossby radius (R_0) is on the order of 100 km or smaller, calculated from:

$$R_0 = \frac{N_0 \cdot z_i}{\sqrt{f^2 + \lambda^2}} \tag{5.3}$$

where N is the Brunt-Väisälä frequency, (depending on the stability, a value of $N = 5 \cdot 10^{-3}$ s^{-1} will give $R_0 \simeq 70$ km, a value of $N = 1 \cdot 10^{-2}$ s^{-1}, close to climatology, will give $R_0 \simeq 140$ km), z_i is the CBL depth (here assumed 2000 m).

Dalu and Pielke (1993) showed how a typical sea breeze can be expected to advance inland by a distance that scales with R_0 over the diurnal cycle of the breeze formation. The observational results of Simpson (1994) confirm the validity of this scaling.

Theoretical results from Dalu et al. (1996) showed that the strongest mesoscale flows occur when the horizontal wavelength of the inhomogeneities (i.e. one land patch and one water patch) are on the order of two local Rossby radii, and become negligible when this wavelength is on the order of twice the depth of the CBL.

5.3.1 Scale Separation in RAMS as Suggested from Linear Work

Turbulent processes are defined therefore, in the context of our specific BOREAS case study, as being intermittent and having time scales much smaller than the diurnal time scale, with spatial scales under 4 km. Mesoscale forcings are defined as having time scales comparable to the diurnal time scale and spatial scales between 4 km and 200 km (or patch sizes of between 2 and 100 km), corresponding approximately to Orlanski's meso-γ and meso-β categories. Synoptic forcing refers here to time scales of multiple days and spatial scales above 200 km.

From the point of view of the surface forcing scales acting on atmospheric circulations, it is therefore to be expected from the previous analysis that patches contained within twice the local Rossby radius (but larger than twice the CBL) will influence and be influenced by mesoscale circulations. It is easily seen from the BOREAS vegetation coverage map (Fig. 4.5a) that most of the central and northeastern part of the domain will have overlapping influence regions due to the spatial distribution of the landscape heterogeneities, including lakes.

In the context of this scale separation we also define turbulent HWM fluxes to be sub-grid (and parameterized) processes, while mesoscale HWM fluxes are resolved by the numerical model.

5.4 Analytical Modeling with a Periodic Forcing

After having calculated some of the scaling quantities for potential mesoscale forcings, we also wanted to be able to assess the impact of the induced circulations on the atmosphere. Hence, we exercised a simplified version of the Dalu et al. (1996) model in order to address items 2-4 under typical BOREAS conditions.

5.5 Parameters for the Analytical Model as Representative for BOREAS

We use the following values for N_0, f, K, asymptotic inversion height h_0 and width of the frontal region of the mesoscale flow L:

$$\Theta_z = 3\,[\mathrm{K/km}]; \quad b = g\frac{\theta}{\Theta}\left[\mathrm{s}^{-1}\right]; \quad N_0 = \left(g\frac{\Theta_z}{\Theta}\right)^{\frac{1}{2}}\left[\mathrm{m\ s}^{-2}\right];$$

$$\omega = \frac{2\pi}{\text{day}}\left[\text{s}^{-1}\right]; \quad f = 2\,\omega \sin(54^o)\left[\text{s}^{-1}\right]; \quad h = 3\,[\text{km}];$$

$$\lambda = 2 - 10 \cdot 10^{-5}\ \left[\text{s}^{-1}\right];\ K = 10 - 100\,[\text{m}^2\text{s}^{-1}];\ \text{L} = 30 - 100\ [\text{km}];$$

where θ is the potential temperature perturbation, Θ is the environment potential temperature, and Θ_z is its vertical gradient. λ is a bulk parameter which represents frictional losses effective at low wavenumbers, K is the diffusion coefficient effective, which accounts for the losses at high wave numbers. We present results from a series of twelve numerical experiments in which we have permutated the values of λ, K and L_0 within the range specified above.

5.5.1 The Periodic Problem: Atmospheric Response to a Periodic-in-Time Forcing

Diabatic Periodic Forcing

Here, we assume that the diabatic forcing Q is periodic with a pulsation ω. In a full diurnal cycle the net diabatic input averages to zero:

$$Q = Q_0\ \text{Im}\left[\frac{\exp(j\omega\, t)}{j}\right]\ \frac{1}{2}\left[1 + \tan h\left(\frac{x}{L}\right)\right]\ \left(\frac{h-z}{h}\right)\ He(h-z) \tag{5.4}$$

$$= Q_0 \sin(\omega\, t)\ \frac{1}{2}\left[1 + \tan h\left(\frac{x}{L}\right)\right]\ \left(\frac{h-z}{h}\right)\ He(h-z)$$

$$Q_0 = N_0^2\, h\, \omega;$$

(He is the Heaviside step function).

The Fourier transform of the streamfunction equation (Eq. 3.7), given the periodic in time forcing (Eq. 5.4), is:

$$\left\{\left[j\omega + \lambda + K(k^2+\mu^2)\right]^2 + f^2\right\}\mu^2\tilde{\psi} + \left\{\left[j\omega + \lambda + K(k^2+\mu^2)\right]^2 + N_0^2\right\}k^2\tilde{\psi} = \tilde{Q} \tag{5.5}$$

$$\tilde{Q} = Q_0\ \frac{\frac{\pi}{2}kL}{\sin h\left(\frac{\pi}{2}kL\right)}\ \frac{2}{\mu}\left[1 - \frac{\sin(\mu h)}{\mu h}\right]$$

$\tilde{\psi}$ is the Fourier transformed streamfunction, and k and μ are the horizontal and the vertical wavenumber, respectively. Solutions to Eq. (5.5), momentum components, particle displacements and temperature perturbations are given in Dalu et al. (1998).

Thermodynamic Imprint of the Mesoscale flow

We have run the analytical model over an x-z domain with an infinite sea next to an infinite land, separated at x=0. We have calculated the streamfunction, the two components of the wind, particles trajectories and thermal fields with different combinations of the parameters λ, k and L, for a total of twelve experiments. Figs. 5.1-5.2 show the results for two of the most interesting cases.

When the forcing is periodic, the net diabatic input averages to zero in a day, which makes evaluation of the net thermodynamic imprint of the mesoscale flow on the free atmosphere easier to compute and clearer to understand.

In a time cycle, each air particle describes a trajectory which is a closed elongated ellipses, Figs. 5.1b-5.2b. The ratio between the minor and the major axis of the ellipses increases as the dissipation increases: the major axis becomes smaller as the minor axis becomes larger. Since the trajectories are closed, the net advected heat averages to zero. However, as the air particles describe their elliptical trajectories, they diffuse and partially mix in the environment, each air particle interacts with the neighboring particles within a distance $r = \sqrt{(2\lambda K/(\lambda^2+\omega^2)}$, in a time $2\lambda/(\lambda^2+\omega^2)$. This diffusion process leaves a thermodynamic imprint with a nonzero average, as shown in Fig. 5.1c-5.2c. This imprint is of the order of tenths of degrees, and may be of climatological significance, when integrated over multiple days over a region with complex surface heterogeneity such as BOREAS.

When the dissipation and diffusion are negligible, the thermodynamic imprint is negligible. The imprint increases with dissipation and diffusion. However, for large values of dissipation, it decreases. The maximum imprint occurs when $\lambda^2 \approx f^2 - \omega^2$, i.e. when λ is close to the value given by Haurwitz and by Grant. The imprint also decreases as the front width (L_0) increases, as the heating gradient is smaller and the circulation is weaker.

The temperature field, Figs. 5.1d-5.2d and the vertical profile of the temperature perturbations, Figs. 5.1e-5.2e are shown when averaged over a cycle at x = 0. In the limit

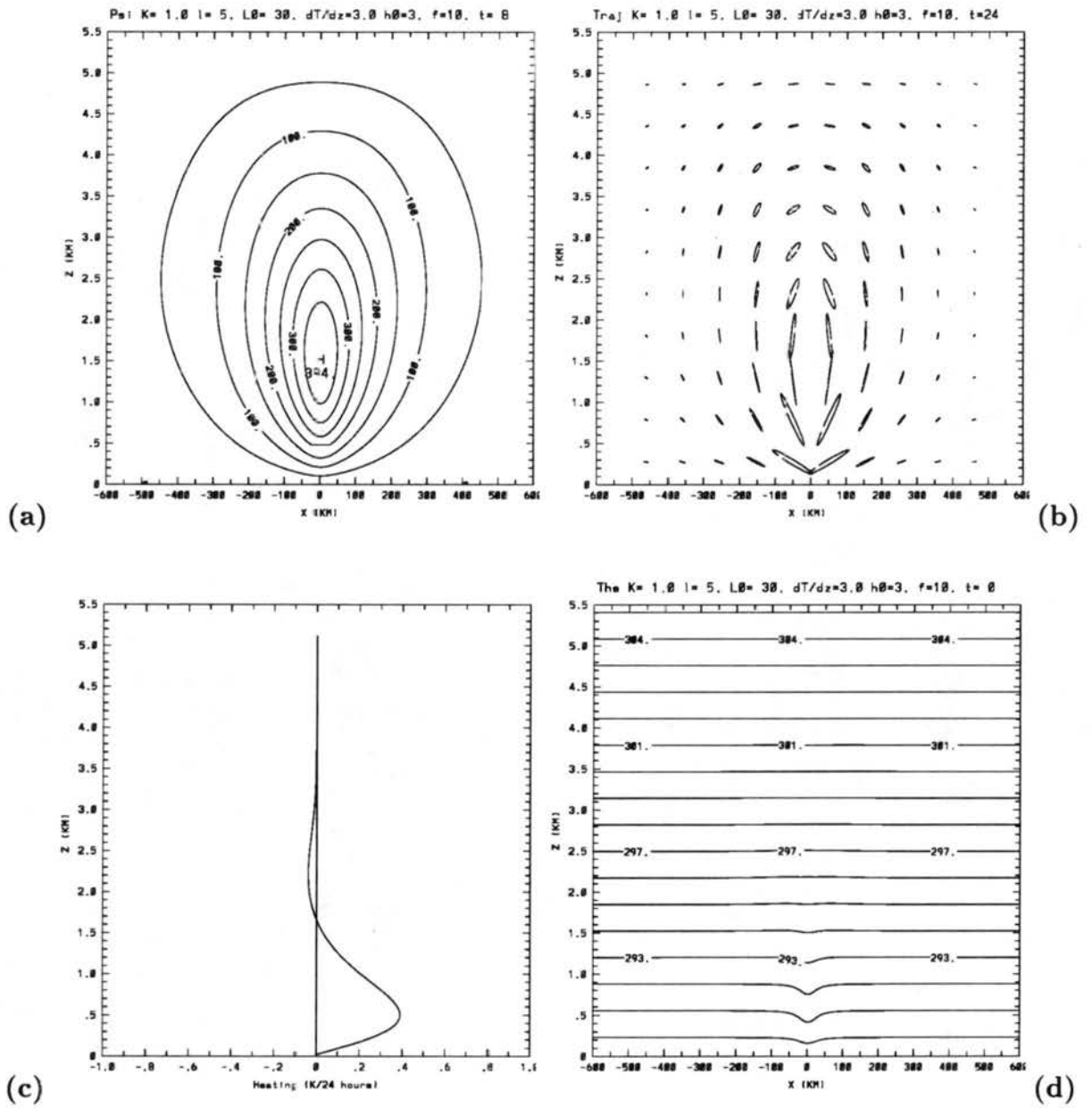

Figure 5.1: Periodic problem results for $\lambda = 5$ day^{-1}, k= 10 m s^{-2} and L=30 km: a) max. daytime streamfunction (*10 m^{2}s^{-1}; b) final trajectories; c) final potential temperature perturbation (K); d) final potential temperature field (K); e) total perturbation thermodynamic imprint at $x = 0$ in 24 hours (K, on the x axis).

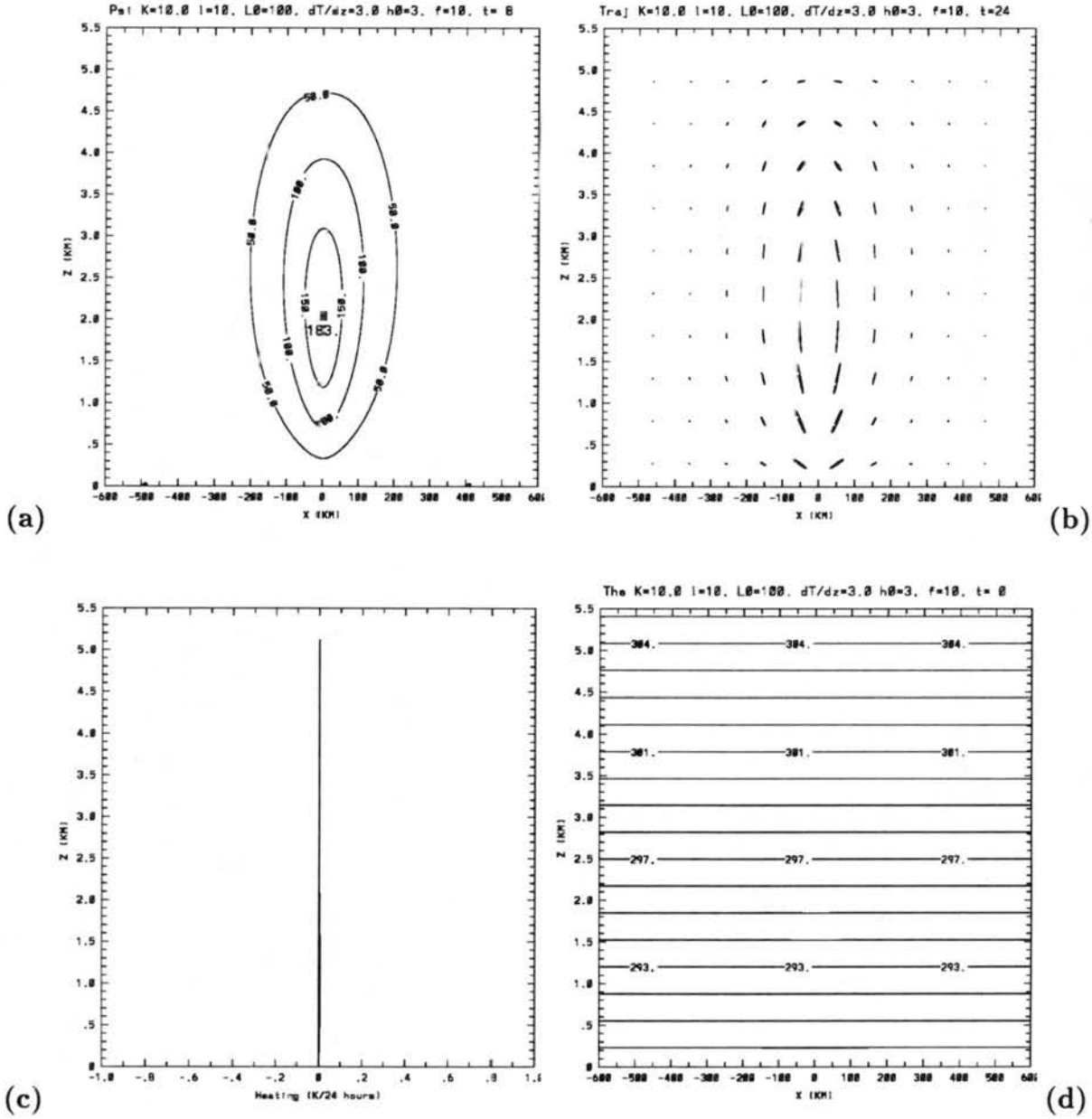

Figure 5.2: Periodic problem results over an $x - z$ domain, for $\lambda = 10$ day$^{-}1$, k= 100 m s^{-2} and L=100 km: a) max. daytime streamfunction (*10 m^{2}s^{-1}; b) final trajectories; c) final potential temperature perturbation (K); d) final potential temperature field (K); e) total perturbation thermodynamic imprint at x=0 in 24 hours (K, on the x axis).

of zero dissipation there is no thermodynamic imprint; the minor axis of the ellipses goes to zero, and the ellipses collapse to a segment which the air particle describes upwards and downwards, without mixing with the environment.

Through these figures it is also possible to see how the imprint scales vertically with the CBL height and horizontally with the Rossby radius.

5.6 Summary: Lessons to be Used for Numerical Modeling Guidance

We have learned in this chapter how to separate turbulent and mesoscale forcings and how to set up numerical grids to represent them. We have defined mesoscale circulations as having spatial scales comparable to R_0 and time scales comparable to T. We have also established a few scaling estimates for BOREAS that will aid in interpretation and in the decisions behind the averaging of quantities, most notably in the averaging necessary for the calculation of mesoscale fluxes.

Chapter 6

EVIDENCE FROM 3-D NUMERICAL MODELING

6.1 Justification

The RAMS numerical experiments have multiple purposes. To begin with, we wanted to establish the capabilities of our coupled model, so that we mainly chose days in which the BOREAS IFCs had been conducted and data for validation were available. Secondly, we intended to test the usefulness of the AVHRR product, since it is the primary upscaling tool for BOREAS, and since similar products are now available for large-scale modeling. We chose to make use of atmospheric forcing data exclusively at the grid 1 boundaries, focusing on the sensitivity to surface boundary conditions and on their impact on the domain, rather than on reproducing observations by the use of calibration or of very specialized data sets, which are not available in operational conditions.

We also chose, whenever possible, BOREAS 'Golden Days', i.e. days in which the optical thickness of the atmosphere was minimal, ideal for radiative transfer work, which were of interest to the rest of the BOREAS community. The problem with golden days is that they are usually rather windy, as was seen in Chapter 2 for FIFE; the same was found in BOREAS. Analytical theory, in the previous chapter, suggested that we should look at days with lighter winds for more substantial (and contained) mesoscale circulations to occur. The other problem with the choice of days was the availability of aircraft data over the SSA: numerous operational issues did not allow for the concurrent presence of all the data platforms that we would wish to have for comparison with the simulations.

We had initially intended to run a suite of case studies during each of the BOREAS Intensive Field Campaigns (IFC1 in the early growing season, IFC2 at the peak of the growing season, with peak LAIs, IFC3 in the late growing season) on days indicated by the

data analysis. Unfortunately, sufficient data was not present at the time of this writing for an IFC3 simulation.

Nonetheless, we have simulated the days of 6-7 June 1994 (very windy), 20-22 June (least windy, with exceptional CBL development) 1994 and 20-22 July 1994 (windy, main validation case) over the whole BOREAS domain, with finer grids over the SSA.

Advantages in using the numerical tool, versus the simple and more economical analytical tool, include the ability to represent non-linear feedbacks between the surface processes and the atmospheric processes, time and space asymmetries in the heating patterns, and the inclusion of realistic atmospheric forcings, especially winds. Having gained some insight from the linear work we should be able to better interpret the numerical results. Therefore, the full 3-D modeling effort had the purpose of producing 3-D depictions of turbulent and mesoscale fluxes, acting in practice as a very sophisticated interpolator that was sensitive to initial and boundary conditions (especially surface physiography). Using this tool we could calculate 3-D fields of turbulent and mesoscale fluxes and construct budgets in order to test the main hypothesis.

The numerical modeling issues at stake were:

- the usefulness and impact of regional physiographical data sets and techniques for their incorporation;
- the conditions for the representation and generation of mesoscale circulations by the local surface heterogeneity;
- the impact of those mesoscale circulations and of their representation on the atmosphere and on BOREAS surface measurements.

6.2 The RAMS Gridding Strategy and the Turbulence/Mesoscale Separation

The analysis stemming from atmospheric dynamics in the previous chapter suggested scaling rules that we have applied directly in our modeling strategy. Thus, for this region, we recognized that patch scales under about 4 km (the typical inversion height was 2 km) would not force mesoscale circulations, and their fractional contributions to HWM fluxes

could be summed linearly. A good example of this fine-scale patching is illustrated by the fen class distribution, which is clearly limited to scales under a few kilometers and is absent from the AVHRR 1 km land cover product (Figs. 4.5a,b). At scales between about 4 km and two local Rossby radii we had to consider non-linear interactions between patches, which dictated lowest resolution needs for the explicit representation of landscape heterogeneity and its feedback to the atmosphere.

Therefore, in the context of our modeling for BOREAS in the summer season, we defined turbulence to be limited to scales under 2 km and the mesoscale forcing to be contained in the 4 km to twice the Rossby radius interval. The scale gap between 1 and 2 CBL depths was handled by the horizontal diffusion scheme, which was set by the grid choice to be most effective at filtering in that interval. It is also important to notice from Fig. 4.6 that there are very few patches in the domain with a scale equal or larger than the Rossby radius, consisting basically of large lakes.

6.2.1 Working Definition of Mesoscale Fluxes

In the context of the simulations in this chapter, we have calculated vertical mesoscale fluxes of scalars by first defining horizontal averaging areas at each model level with a scale equal to the local Rossby radius and by taking the residuals of quantities at each point from this average. Vertical mesoscale fluxes are then defined as correlations of deviations of variables from this base state. For instance, the vertical mesoscale sensible heat flux is the correlation of the vertical velocity perturbation and the potential temperature perturbation from the horizontal base state defined above. We have not included the cross terms (between perturbations and base state terms) because we wanted to be able to compare directly to linear theory and because of the difficulty in defining time averages for the base state, so that our definition of mesoscale fluxes is quite strict and parallel to the typical definition of turbulent fluxes. In practice, we have defined an averaging grid (grid 2) which we used for the calculation of the averages of the principal variables over a region of R_0 by R_0 at each model level. This technique is equivalent to that discussed by Mahrt et al. (1994b) and is consistent with the averaging applied by Dalu et al. (1996).

6.3 The RAMS-LEAF-2 Validation Run: The 21 July 1994 "Platinum Day"

This day was selected because of its relevance to the rest of the BOREAS community; it presented very clear skies, and was ideal for radiative transfer work. Most data platforms were deployed and functioning on this day and the aircrafts were able to fly a very large number of transects over Candle Lake. This was also one of the days with the best data collection in the 1994 campaign, hence the name.

The synoptic situation is depicted in the four panel Fig. 6.1, where geopotential height and winds are shown at 1000 hPa, 850 hPa, 700 hPa and 500 hPa. A weak low pressure system was present over Hudson Bay and a weak high pressure system was present over the SE corner of the domain. Winds in the SSA were from the SE, converging with westerlies to the west of the SSA. The synoptic-scale winds in this case study were still not ideal, with speeds of about 15 m s^{-1} at 850 hPa in the SSA region. The upper air shows a deep trough over the center of the domain, with some acceleration over the SSA. The large-scale (over one R_0) average vertical motion over this region in the 12 hour period, as diagnosed from the ETA model initialization, was about -0.0075 m s^{-1}.

The Candle Lake sounding, Fig. 6.2 at 17.17 UTC (11.17 LT) showed a rather dry atmosphere (again this was a golden day), a CBL with an inversion at 780 hPa, and winds from the west all throughout the troposphere.

The 21 July 1994 case was simulated by initializing the model on 20 July at 00 UTC (19 July 18.00 Local Time) and running RAMS for 60 hours. The temperature of the Candle Lake water (and of every other lake in the domain) for 20-22 July 1994 was set at 283 K, using the surface radiative temperatures reported by Sun et al. (1997). Soil temperature and moisture profiles were initialized using information from the Automated Meteorological Stations (AMS) and the Atmospheric Environmental Services (AES; Betts 1997b) network on 20 July.

6.3.1 Validation and Comparison with Aircraft Observational Evidence

Flux aircraft measurements at various heights (for instance, 30 m for the NOAA LongEZ, 100 m and more for the NCAR Electra) offered additional evidence of the very

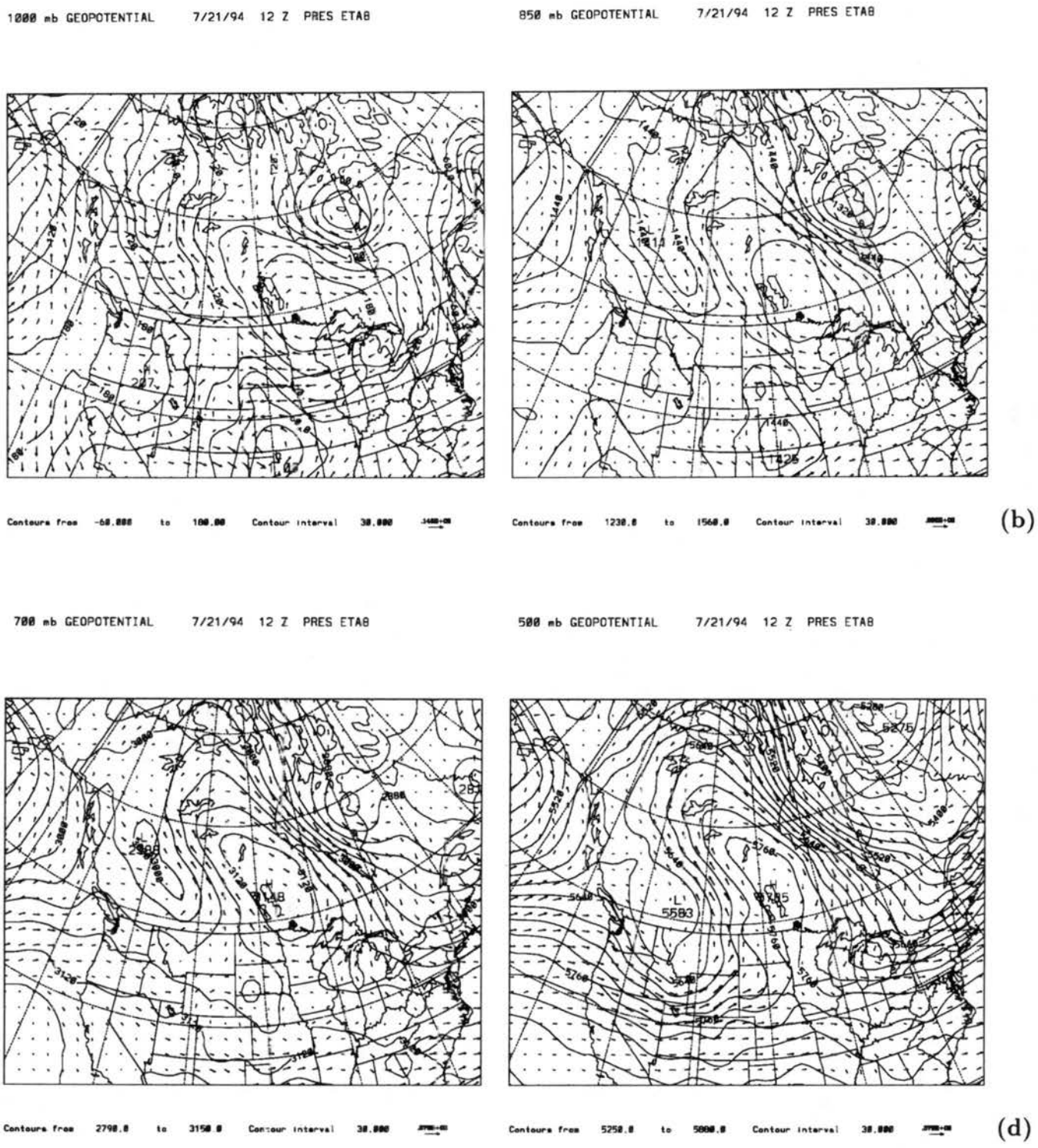

Figure 6.1: The 12 UTC ETA analysis for 21 July 1994: a) 1000 hPa geopotential height (m) and winds (m s^{-1}); b) 850 hPa geopotential height (m) and winds (m s^{-1}); c) 700 hPa geopotential height (m) and winds (m s^{-1}); d) 500 hPa geopotential height (m) and winds (m s^{-1})

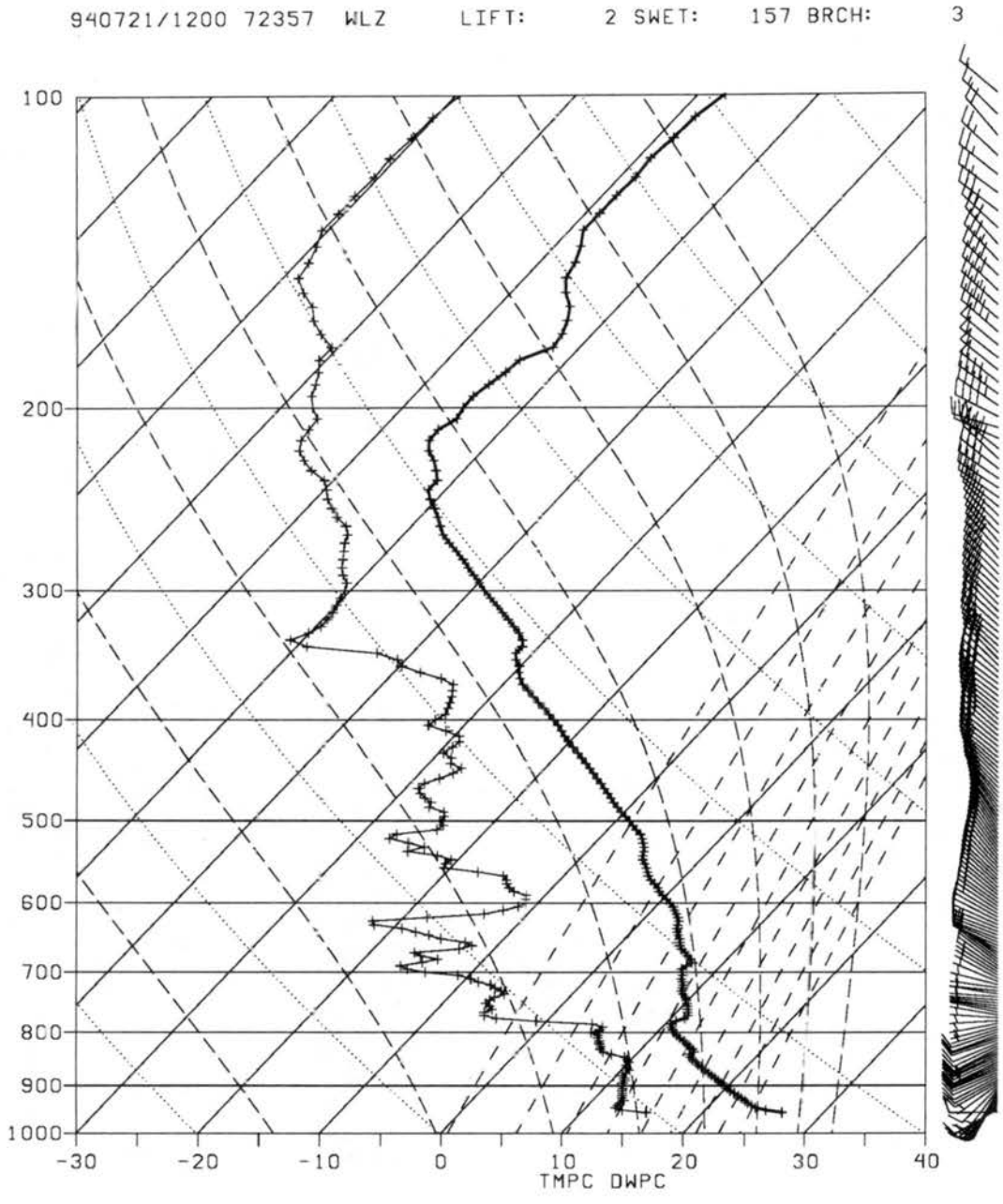

Figure 6.2: The 17 UTC Candle Lake skew-T diagram for 21 July 1994.

heterogeneous horizontal distribution of surface fluxes of HWMC, calculated by eddy correlation techniques. Transects over the Candle Lake region in the SSA comprised regions predominantly covered by deciduous trees (Aspen) in the west, transitioning into a mixed forest cover and, proceeding eastward, into a wet conifer region (Black Spruce, Jack Pine, fens, bogs). Special model slices through grids 2 and 3 were generated, corresponding to aircraft transects. Figure 6.3 (data here reproduced with permission of Crawford and Baldocchi) shows temporally averaged sensible and latent turbulent fluxes, measured by the NOAA LongEZ aircraft over 13 legs between 15.32 and 23.20 UTC on 21 July 1994 (transect indicated on Fig. 4.5b). In particular, the LongEZ measurements of sensible heat over Candle Lake for 21 July 1994 showed a sharp reduction from about 270 W m^{-2} to almost -30 W m^{-2} when moving from the forested regions around the lake to a position directly over the lake. The magnitude of the fluxes and their horizontal gradients over this transect were found to be very similar to others measured during July 1994 by the LongEZ aircraft (not an example of a single day).

Figure 6.3 also shows the turbulent fluxes modeled by the LEAF-2 RAMS coupled model, temporally averaged through the same period for a similar transect over grid 2 (within the grid 3 domain, however, the fluxes are produced by that finer grid, because of the two-way nesting). The model was capable of capturing the spatial pattern of the fluxes quite accurately. The magnitudes of the fluxes were also in reasonable agreement, even without any special tuning of the model parameters that control canopy conductance. For the correct interpretation of the comparison between the two data sets, it is important to remember that the model fluxes are representative of a set of volume averages over grid cells corresponding to the aircraft transect, while the aircraft fluxes are transect and time averages. The aircraft footprint was aggregated up to 3 km by the NOAA/ATDD personnel, the model resolution is 10 km, interpolated to a similar footprint (except within grid 3 there are influences from 2.5 km scales through the 2-way nesting).

Referring to Fig. 6.4, the SW land cover has contributions from the deciduous forest and disturbance classes (higher albedo, lower LAI), while the NE displays lower albedo (conifers) and some patches of drier soils (for the uphill dry conifer). The modeled gradient

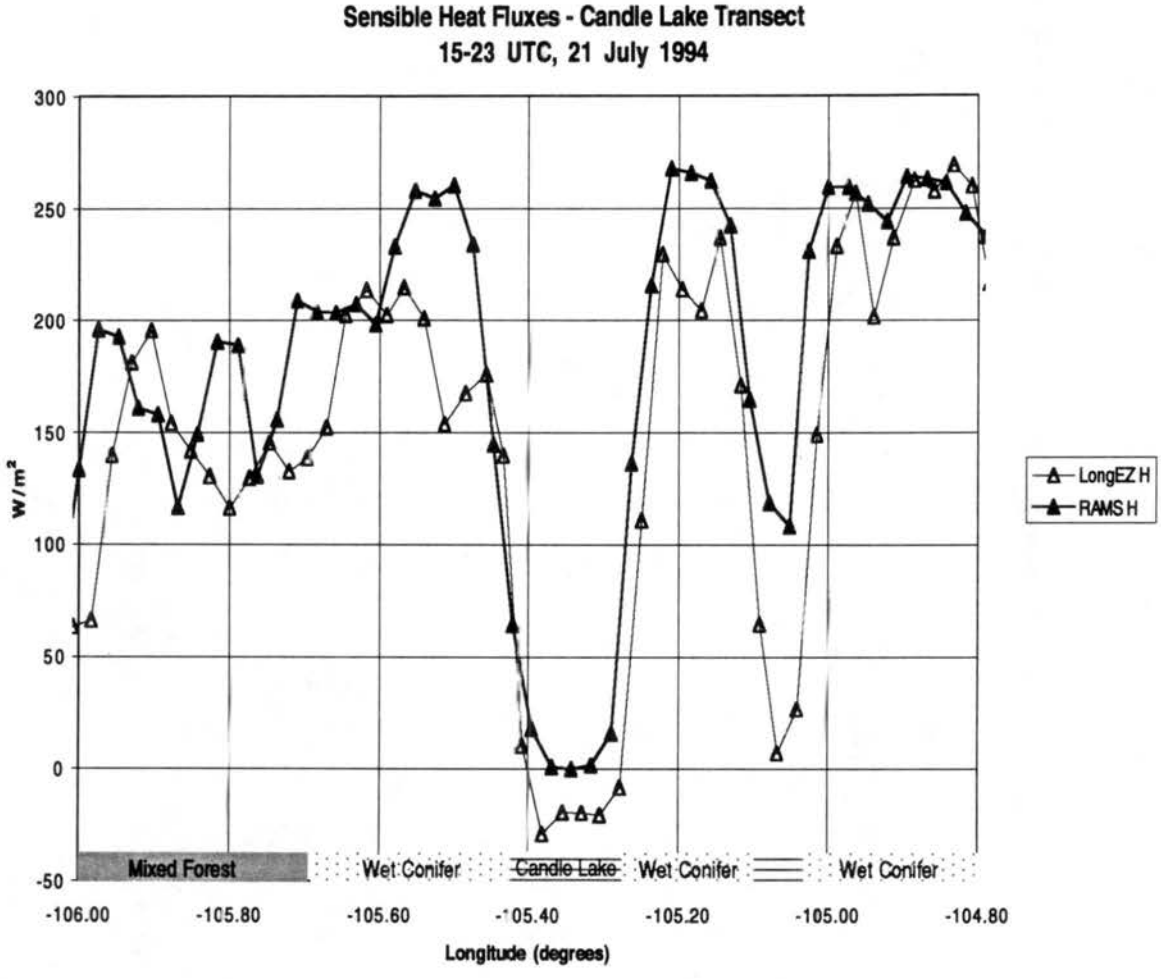

Figure 6.3: The average turbulent sensible heat fluxes over the Candle Lake transect for 21 July 1994. The LongEZ label refers to the NOAA/ATDD aircraft data; RAMS refers to the modeled fluxes.

was not as finely resolved as the measured one, but it is clear from the plot that the horizontally integrated heat input from the surface east of the lake was higher than that from west of the lake. The modeled sensible heat flux maximum, of 270 W m^{-2}, was (at point locations) about 75 to 100 W m^{-2} higher than observations, especially on the west side of the lake. The latent heat fluxes were about 30 W m^{-2} lower on average than the observed ones, while at point locations differing by as much as 100 W m^{-2}, in correspondence with points where sensible heat was too high. This incorrect partitioning is in part due to misclassification (as discusses later and visible in Fig. 4.5) and to incorrectly high albedo, so that the heat balance is maintained, although the bowen ratio is incorrect. Another possible factor in this discrepancy is the standing water at the soil surface, which was present for the Black Spruce class during IFC2 and is very hard to represent, since it depends on microtopography and on moss distribution, which we are unable to represent due to resolution and tc lack of information for model initialization.

Previous sensitivity tests suggested that the main controlling parameter for the surface fluxes calculated in the present version of LEAF-2 is the LAI. LAI was here indirectly specified (with a LUT approach) by the land cover classification, and not linked to remote sensing, so that the modeled spatial gradients in vegetation parameters are only representative at scales larger than actually occur along this transect (i.e., the aircraft, of course, measured fluxes from all patch sizes in the flight cross-sections, while the model used patch data that were limited to 2-3 km of effective resolution). The 100 W m^{-2} disagreement on the west bank of the lake is due to resolution and misclassification, as it appears in most simulations, under different environmental conditions. The pixels underlying that part of the transect register as 'burns' and 'unknown' (the latter reclassified as the high density wet conifer), but are probably too extensive in area (due to the predominant pixel technique) and are also difficult to parameterize, since there are no biophysical parameters for the burns class. The horizontally homogeneous sensible heat flux plateau over the mixed forest class on the west portion of the graph is also indicative of how the LUT approach is not capable of representing intra-class heterogeneity of biophysical parameters.

The important point for the modeling results described in the following sections is that the gradient between Candle Lake and its surrounding measured (at its peak time) over

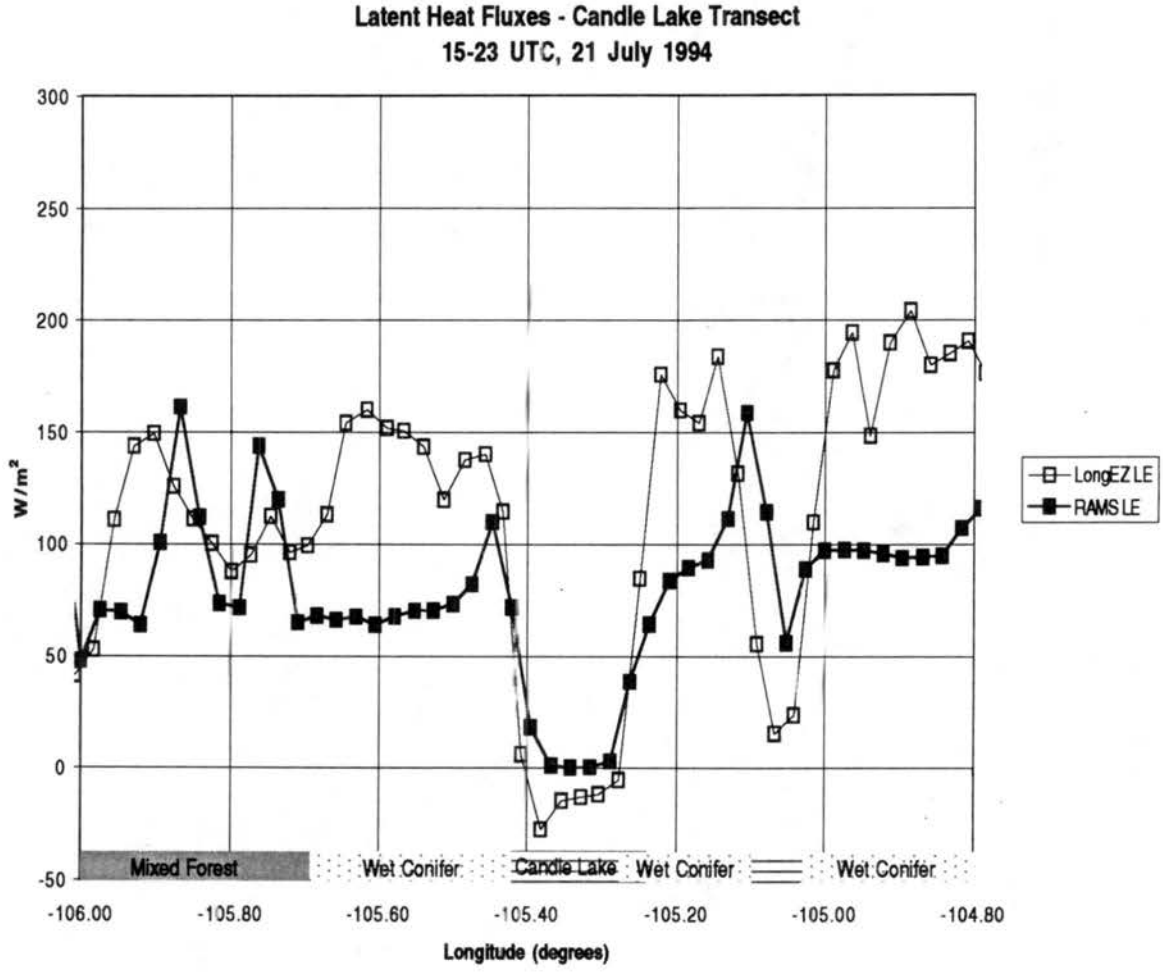

Figure 6.4: The average turbulent latent heat fluxes over the Candle Lake transect for 21 July 1994. The LongEZ label refers to the NOAA/ATDD aircraft data; RAMS refers to the modeled fluxes, data reproduced with permission of Crawford and Baldocchi.

400 W m^{-2} across about 20 km, and, according to linear theory, was sufficient to force a mesoscale circulation under the proper synoptic conditions.

Occurrences of a lake breeze over Candle Lake were successfully simulated with our atmospheric model for some calm wind days in June (IFC1) and July (IFC2) 1994 and their divergence/convergence patterns agreed well with the analysis of Sun et al. (1997a), which was conducted for Candle Lake during similar days. The contrast could also be seen in the temperature gradient over the same transect for the summer season (Figs. 2a and b in Sun et al. 1997a).

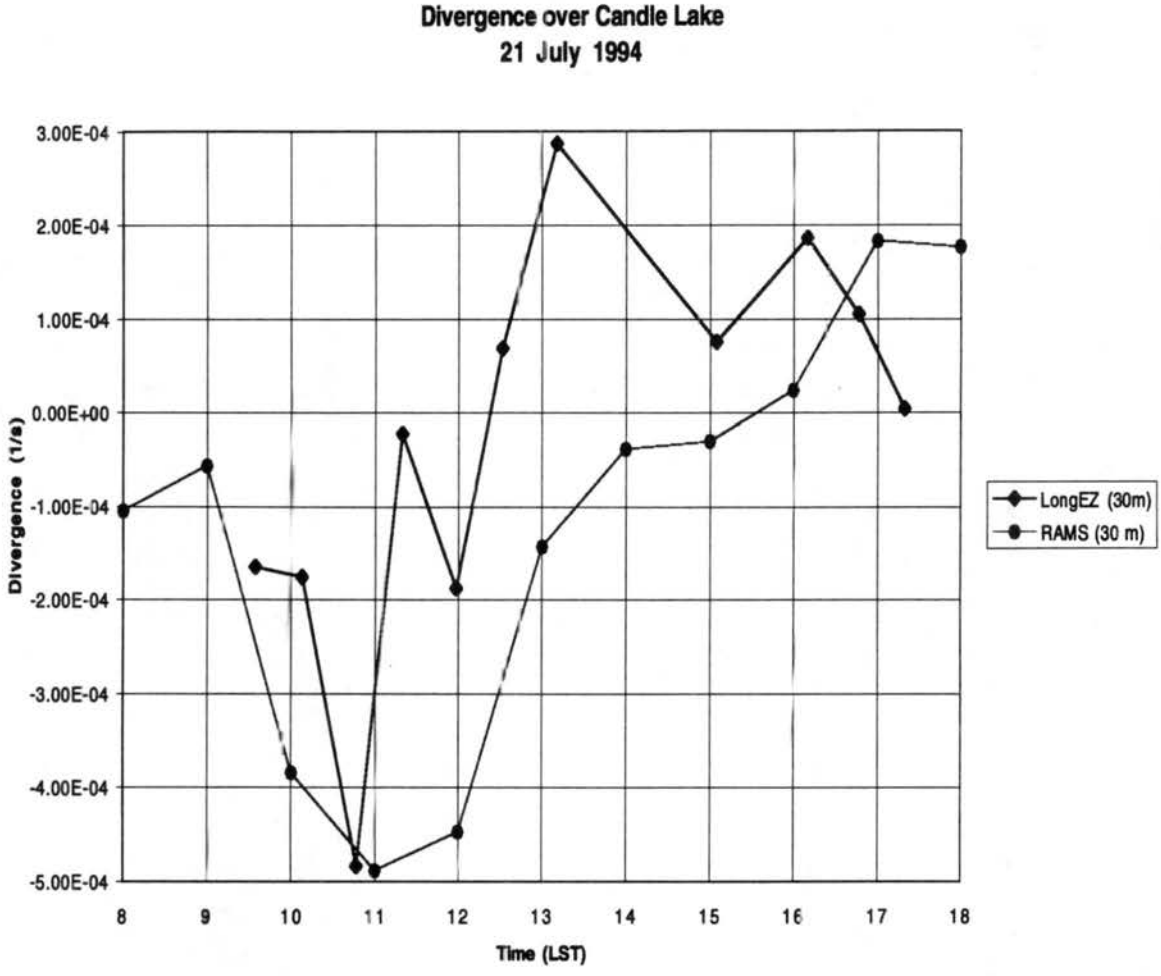

Figure 6.5: The average LongEZ leg divergence over the Candle Lake transect for 21 July 1994. The LongEZ label refers to the NOAA/ATDD aircraft data; RAMS refers to the modeled divergence. Data reproduced with permission by J. Sun.

On 21 July 1994, the date of our model simulation, a diurnal evolution of the horizontal wind divergence over the center of Candle Lake, derived from data of the LongEZ aircraft

(Fig. 6.5, data reproduced with permission of J. Sun), appeared as a clear lake breeze signature. The timing of the divergence pattern reflects both the two hour lag mentioned in Chapter 5 and the fact that the breeze cell was displaced to the NW, as will be shown later in this section. The mass divergence measured about 0.0002 s^{-1} during the heating period, between 13.00 and 17.00 local time (19 and 23 UTC), while a convergence (negative divergence, with peak of -0.0006 s^{-1}) was still present between 9 and 12 local time, at the end of the nocturnal cooling period. The divergence produced by RAMS over the same transect is also shown on Fig. 6.5.

6.3.2 Fluxes in Grid 1 (Δx = 10 km)

The grid 1 integration was carried out in two fashions by specifying the land cover over each grid cell at two different resolutions (for a graphical representation of the two modes, see Fig. 3.2):

- Coarse-grid run (or mosaic run), with grid separations as low as 10 km, in which the contributions from classes in the AVHRR product were included by statistics and the mesoscale was not fully resolved;

- Fine-grid run, with grid separations as low as 625 m, in which the resolution of the AVHRR product was matched at each grid point within grid 3 (and the mesoscale was fully resolved within this finest mesh). This is the same validation run mentioned in the previous section.

For the coarse-grid case we used a 10-patch representation of surface characteristics, while for the fine-grid case we used a 2-patch (predominant pixel) representation. The choice of ten patches was based on the number of existing vegetation classes (18) in the AVHRR product and on the high correlation between soil type and land cover class, so that we could ensure a good statistical representation of the local heterogeneity with 10 km horizontal grid spacing. The 2-patch approach in the fine-grid run is the minimal LEAF-2 configuration, and consists of using one vegetation type and one water patch per grid cell.

In both cases, RAMS was initialized at 00 UTC on 20 July 1994, using the ETA analysis, and then nudged over the grid 1 boundary exclusively, except for the top nudging,

which is domain-wide. For the fine-grid run, after one complete diurnal cycle, grids 2 and 3 were spawned and surface-atmosphere fluxes at scales as small as 2.5 km (corresponding to the 625 m grid spacing, since the resolution is defined as $4 \cdot \Delta x$, see discussion in Pielke 1984, page 327) were explicitly calculated over these finer meshes for a second, complete diurnal cycle. In the coarse-grid case, we were relying on a mosaic approach to the flux calculation (Avissar and Pielke 1989) and the nested grids were never spawned, thus truncating our effective resolution to 40 km, which limited our ability to represent surface heat flux gradients and associated mesoscale atmospheric circulations.

In terms of a local enhancement of turbulent effects, for example, a lake with dimensions of less than 10 by 10 km only contributed to the surface parameterized (turbulent) sensible heat fluxes as a grid cell fractional component, thus lowering the total grid cell flux intensity. On the other hand, a lake of similar size, within the fine mesh (grid 3), was capable of cooling the atmosphere above it directly, and, through resolved advection of cooler air, of ultimately enhancing the turbulent sensible heat fluxes from the land surrounding it.

The grid 1 sensible heat fluxes at 19 UTC (13 LT) on 21 July (Figs. 6.6 and 6.7) showed some general differences, in that the coarse-grid run produced slightly higher domain average surface sensible heat fluxes (differences of about 30 W m^{-2}) than the fine-grid run. The predominant pixel technique in the fine-grid run favored forests (which are more abundant and have larger patch scale) over disturbance regions, which are not very spatially organized and have larger albedo, smaller LAI, higher bare soil fraction and lower roughness length. Locally, however, e.g. in the Candle Lake (105.3W, 53.8N) and Montreal Lake regions, the coarse grid run produced patches of flux minima whereas the fine grid run produced sharper flux gradients between lake and forest. Again this is indicative of the different impact of a 'fully resolved' versus a 'mosaic' treatment of local surface flux gradients and the associated near-surface wind circulations. This is also to be contrasted with the aircraft data presented in Chapter 4 (Fig. 4.10) for a May case and with the results presented by Dobosy et al. (1997).

It is also possible to confirm that the orography has a local control on the wind patterns by contrasting the day-night surface wind maps over Figs. 6.7-6.8 with the topography map

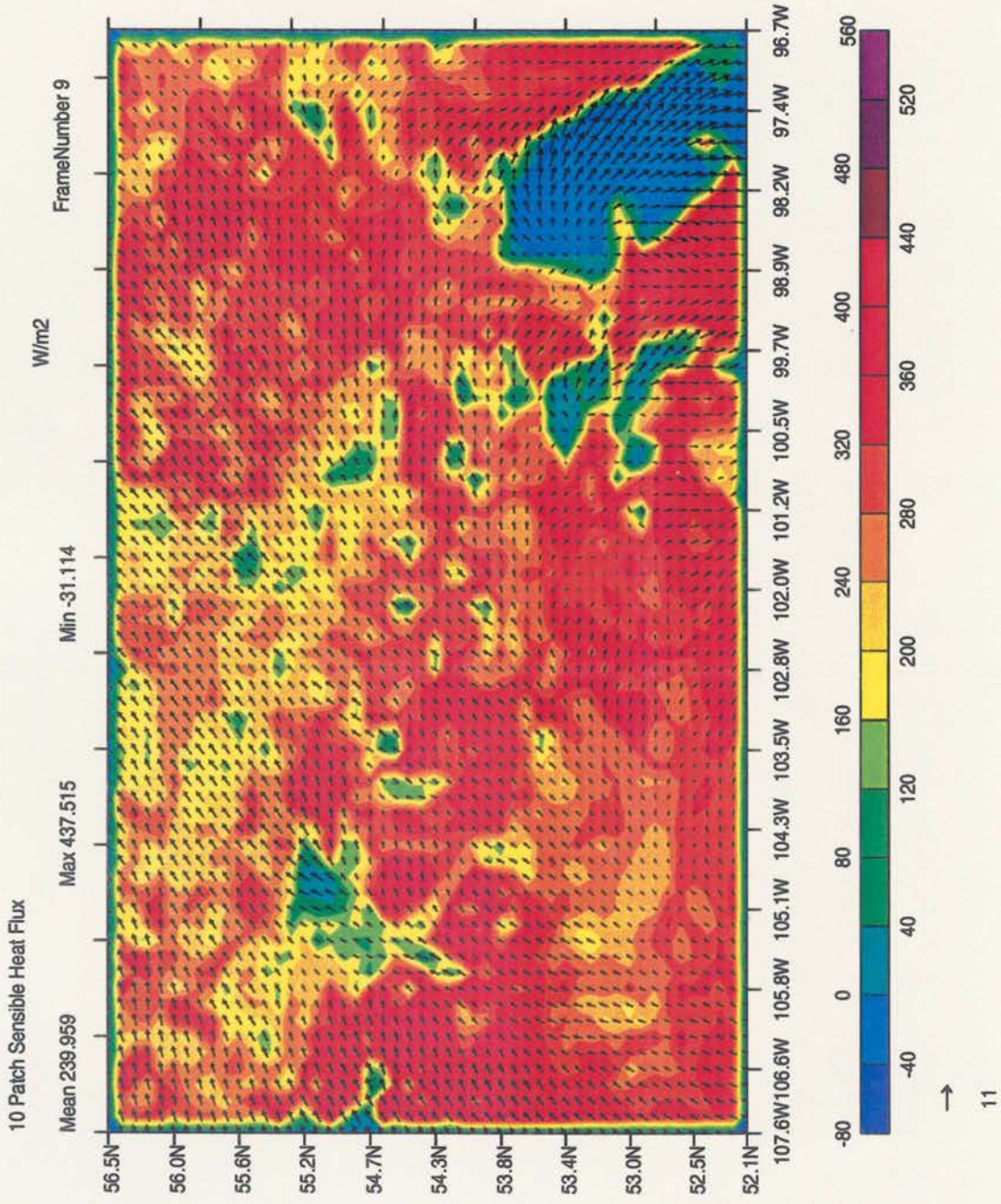

Figure 6.6: Coarse-grid run: the grid 1 surface sensible heat fluxes (W m^{-2}) at 19 UTC, 21 July 1994 and the near-surface (60 m) wind vectors. The color field and color bar represent the turbulent sensible heat flux. Tick marks are in decimal degrees.

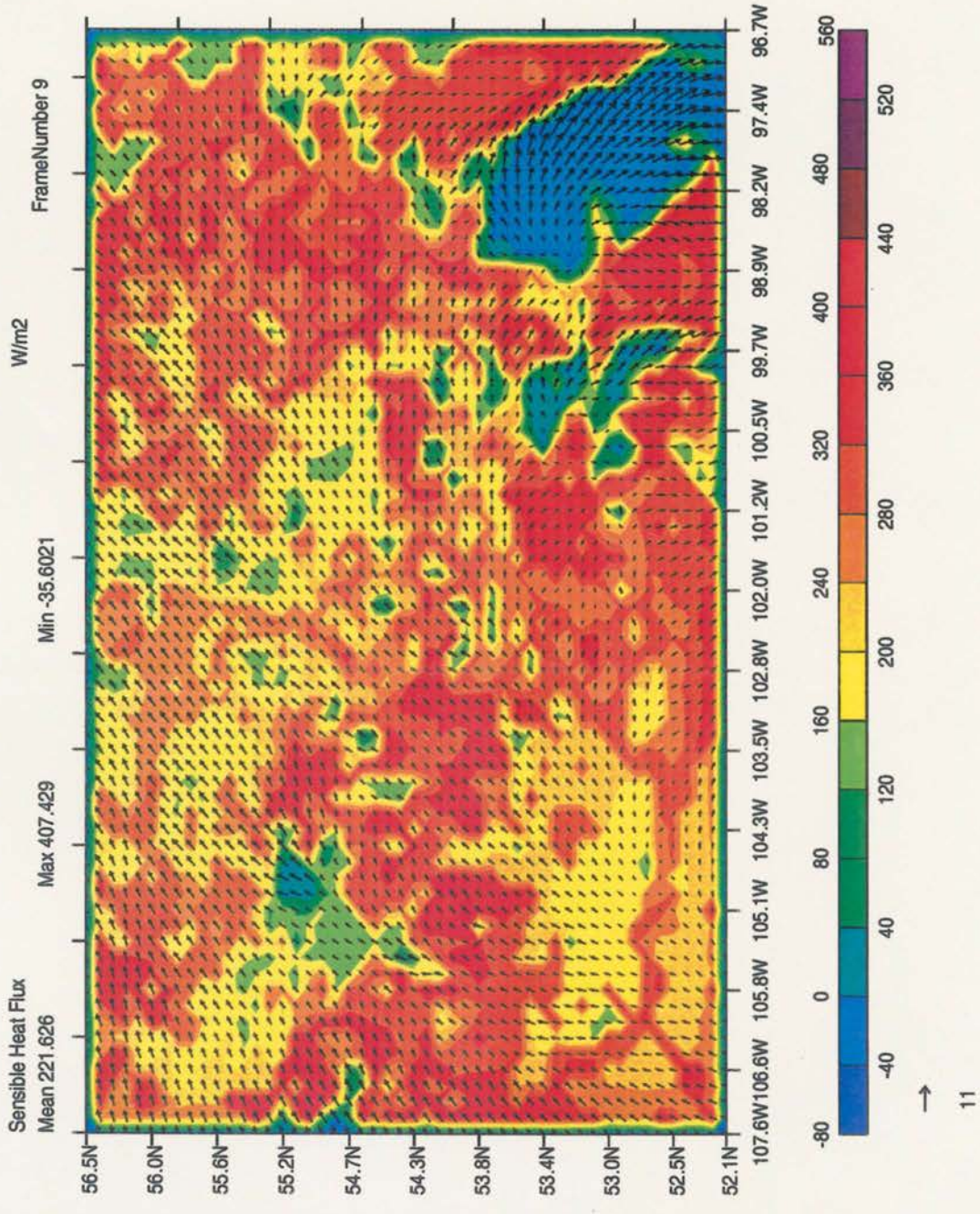

Figure 6.7: Fine-grid run: the grid 1 surface sensible heat fluxes (W m^{-2}) at 19 UTC, 21 July 1994 and the near-surface (60 m) wind vectors. The color field and color bar represent the turbulent sensible heat flux. Tick marks are in decimal degrees.

in Fig. 4.7. In these wind maps we have used a color representation of the surface parameterized sensible heat flux, which helps point to the presence of lakes (minima, corresponding to flux into the water), and wind arrows to represent the horizontal wind at 60 m.

During the day, for the fine-grid run in the grid 2 region (Fig. 6.9), a prevailing southwesterly flow turned northward in the direction of the local slope gradient, with a clear convergence signal on the northern boundary of Candle Lake (center of grid 2) and a divergence signal on the E and NE parts of the lake. The turning and acceleration of the wind to the N of Candle Lake was due to a combined effect of the lake breeze and of the uphill flow. On the NE part of the grid 2 domain the flow turned eastward, again in the direction of the slope.

During the night, over both grids 1 and 2 (Figs. 6.8, 6.11), the flow turned locally to SE, showing a tendency to join the drainage flow to the SE (53.5 S, 103.5 W). The local divergence and turning were stronger in the SE portion of the grid 2 domain (Fig. 6.11), aligned with the local slope. At the center of grid 2, over Candle Lake, there was local acceleration of the wind, due to decoupling caused by the formation of an intense nocturnal layer at the lake center (not shown).

Some larger features on the SW region of grid 1 (Fig. 6.8) were also capable of generating local circulations, even at 40 km resolution. The two terrain features on the southern boundary of grid 1 influenced the local flow, with uphill motion during the day and drainage during the night. The southwesterly flow to their West turned westerly to northwesterly locally, in the direction of the slopes. The divergence/convergence pattern over Lake Winnipeg (bottom right of Fig. 6.8) was also a very clear example of a local differential heating effect influencing atmospheric motions.

The coarse-grid run did not display the same local circulation characteristics around the grids 2 and 3 region, although retaining some of the flow sensitivity to larger-scale features.

6.3.3 Fluxes in Grid 2 ($\Delta x = 2500$ m)

Following the discussion in the previous section, turbulent surface sensible heat fluxes were quite pronounced over the grid 2 region. This could be explained by the large LAI of

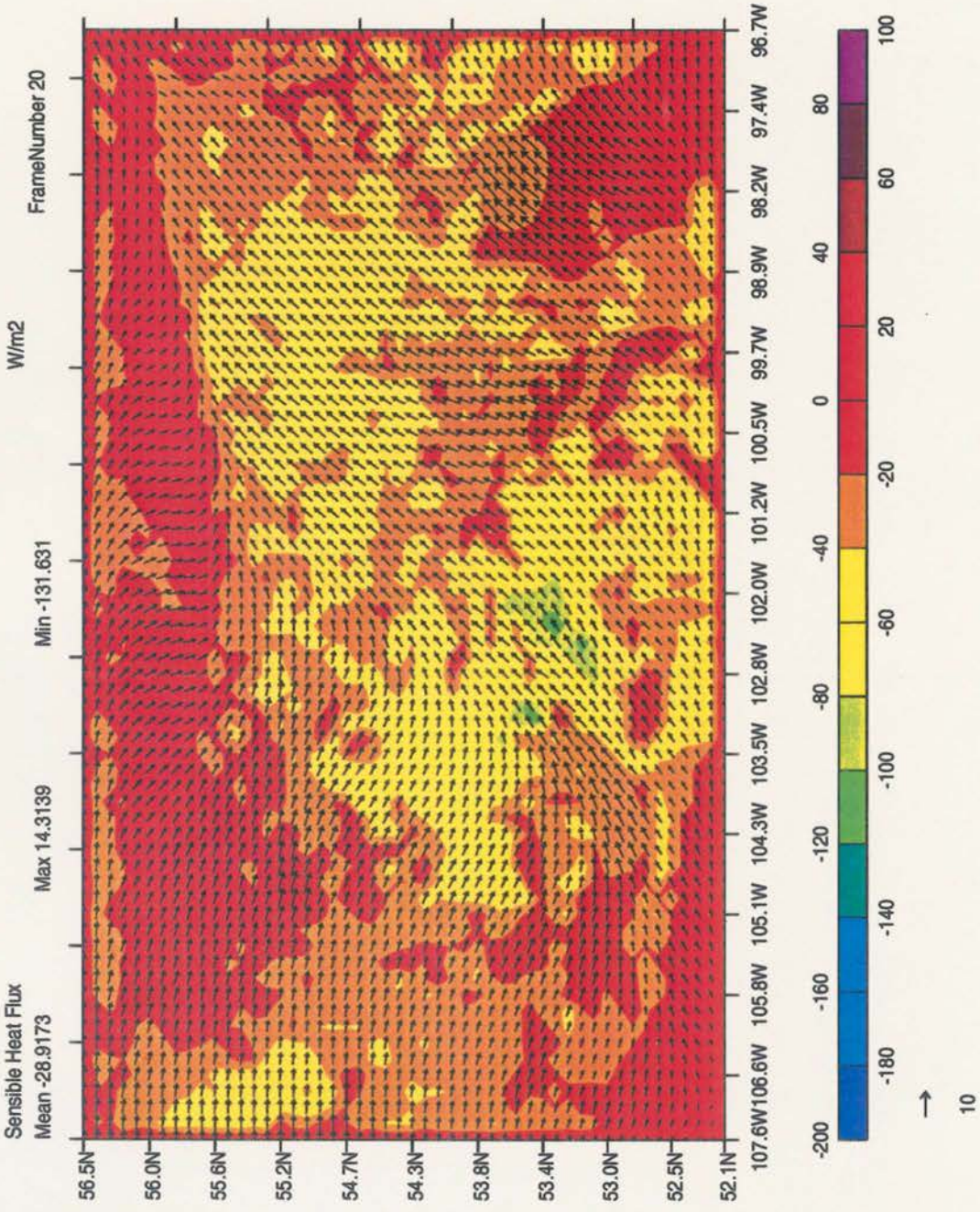

Figure 6.8: Fine-grid run: the grid 1 surface sensible heat fluxes (W m^{-2}) at 06 UTC, 22 July 1994 and the near-surface (60 m) wind vectors. The color field and color bar represent the turbulent sensible heat flux. Tick marks are in decimal degrees.

dense conifer, but also by horizontal advection of cooler air due to mesoscale circulations caused by differential heating between slope and valley (e.g. the local depression where Candle Lake is located), as discussed previously. The lowest sensible heat fluxes were found to correspond to the positions of Candle Lake (center) and Montreal Lake (NW). As a confirmation of the characteristics of the air advected from Candle Lake, Fig. 6.10 shows a potential temperature transect through Candle Lake roughly corresponding to the NOAA LongEZ transect. In this figure it is possible to see how the influence of Candle Lake on the potential temperature profile, in conjunction with predominant south-westerly flow, induced the formation of an internal boundary layer on the east bank of the lake, with a surface layer temperature change of 1 K over about 20 km between the two shores of the lake.

Turbulent fluxes over the grid 2 domain appeared to be highest around 19 UTC, with localized maxima of almost 400 W m^{-2} and presented large horizontal gradients associated with the vegetation cover type (Fig. 6.9). The wet conifer class (mainly Black Spruce, *Picea mariana*) generated the more intense sensible heat fluxes, as was also shown by the aircraft data. The lowest turbulent sensible heat fluxes were found to be concentrated in the southern portion of the grid 2 domain, where the forest transitions to agriculture. The latent heat fluxes (Fig. 6.12) were, on the other hand, much more homogeneous and had localized maxima of almost 270 W m^{-2}, mainly associated with the mixed forest cover class.

6.3.4 Results for Grid 3 (Δx = 625 m): The Candle Lake Breeze

Grid 3 was spawned around Candle Lake with the purpose of resolving possible lake-induced circulations. After one full diurnal cycle, the model developed a well defined lake breeze, identifiable in Fig. 6.13 (depicting vertical velocity at 1250 m), with a subsiding cell (-0.286 m s^{-1}) to the NW of the lake center and maximum ascending motion (0.157 m s^{-1}) at the west bank of the lake. The downward motion region revealed a shape and position that confirmed the influence of Candle Lake. The positive vertical velocity regions were distributed over the land around the lake, although shifted by the southwesterly winds.

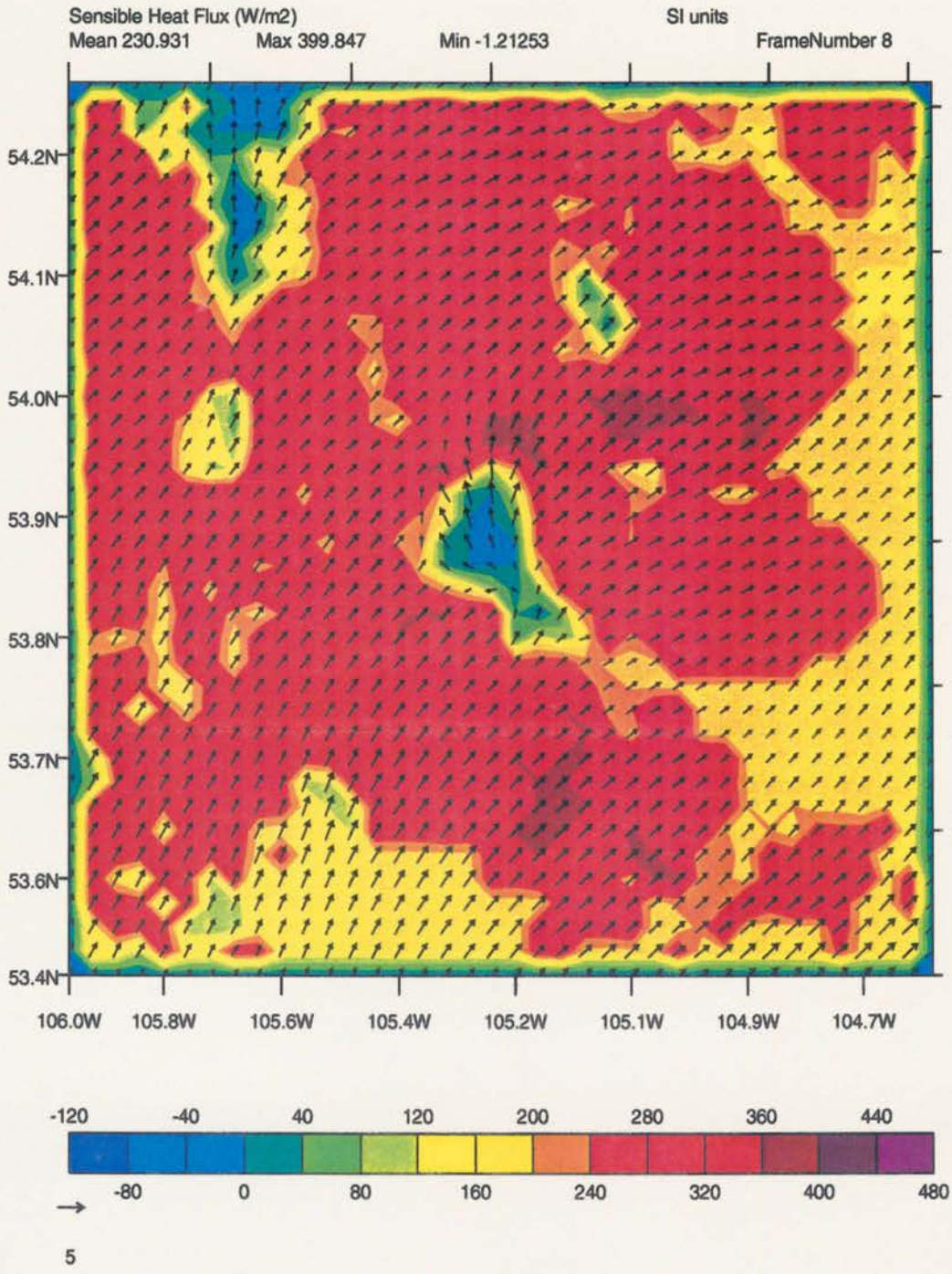

Figure 6.9: Fine-grid run: the grid 2 surface sensible heat fluxes (W m^{-2}) at 19 UTC, 21 July 1994 and the near-surface (60 m) wind vectors. The color field and color bar represent the turbulent sensible heat flux. Tick marks are in decimal degrees.

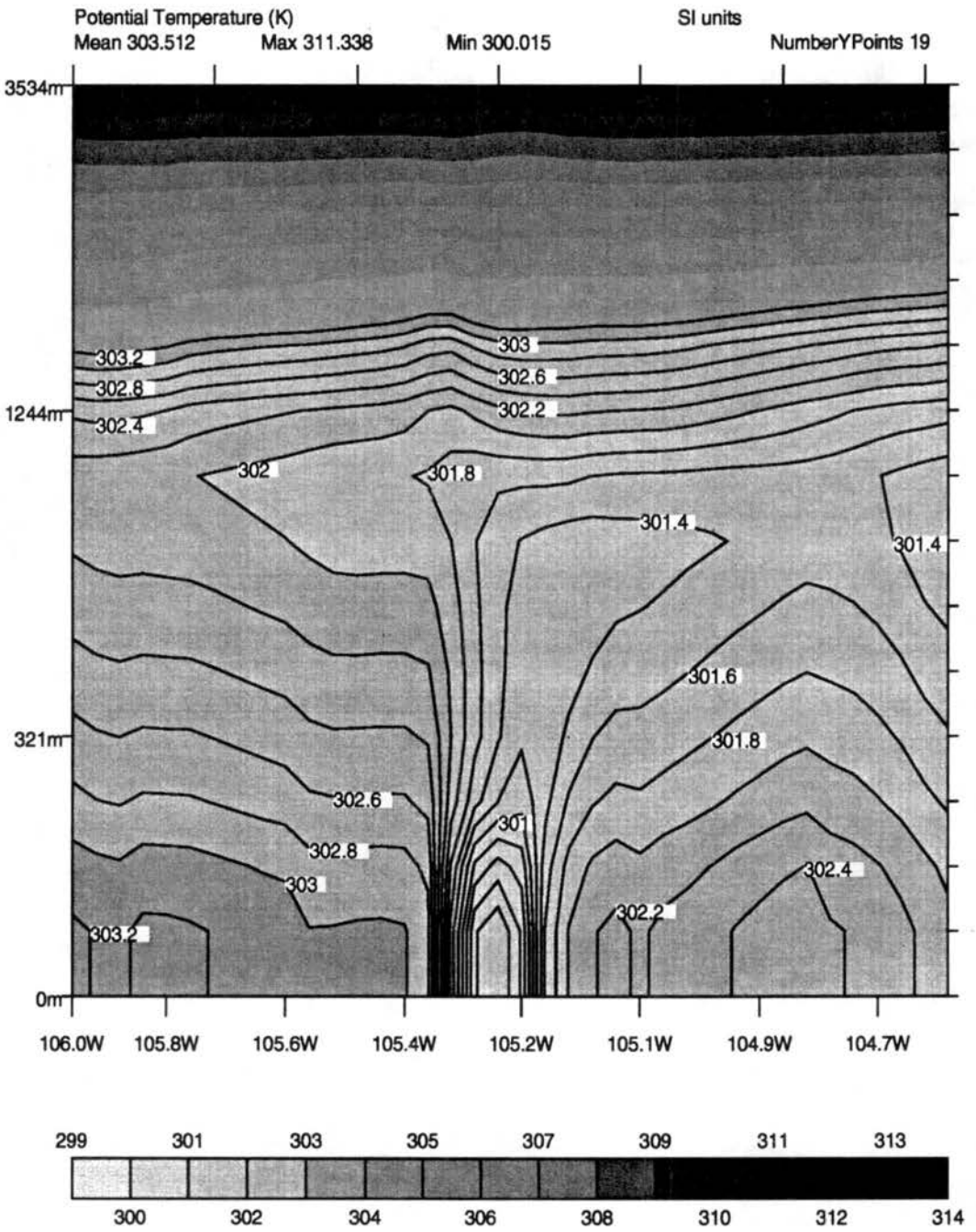

Figure 6.10: Fine-grid run: Modeled potential temperature profile over the grid 2 aircraft transect for 19 UTC, 21 July 1994. The lake is at the center of the domain, approximately between longitudes -105.35 and -105.25. Contour interval of 0.2 K. Tick marks are in decimal degrees.

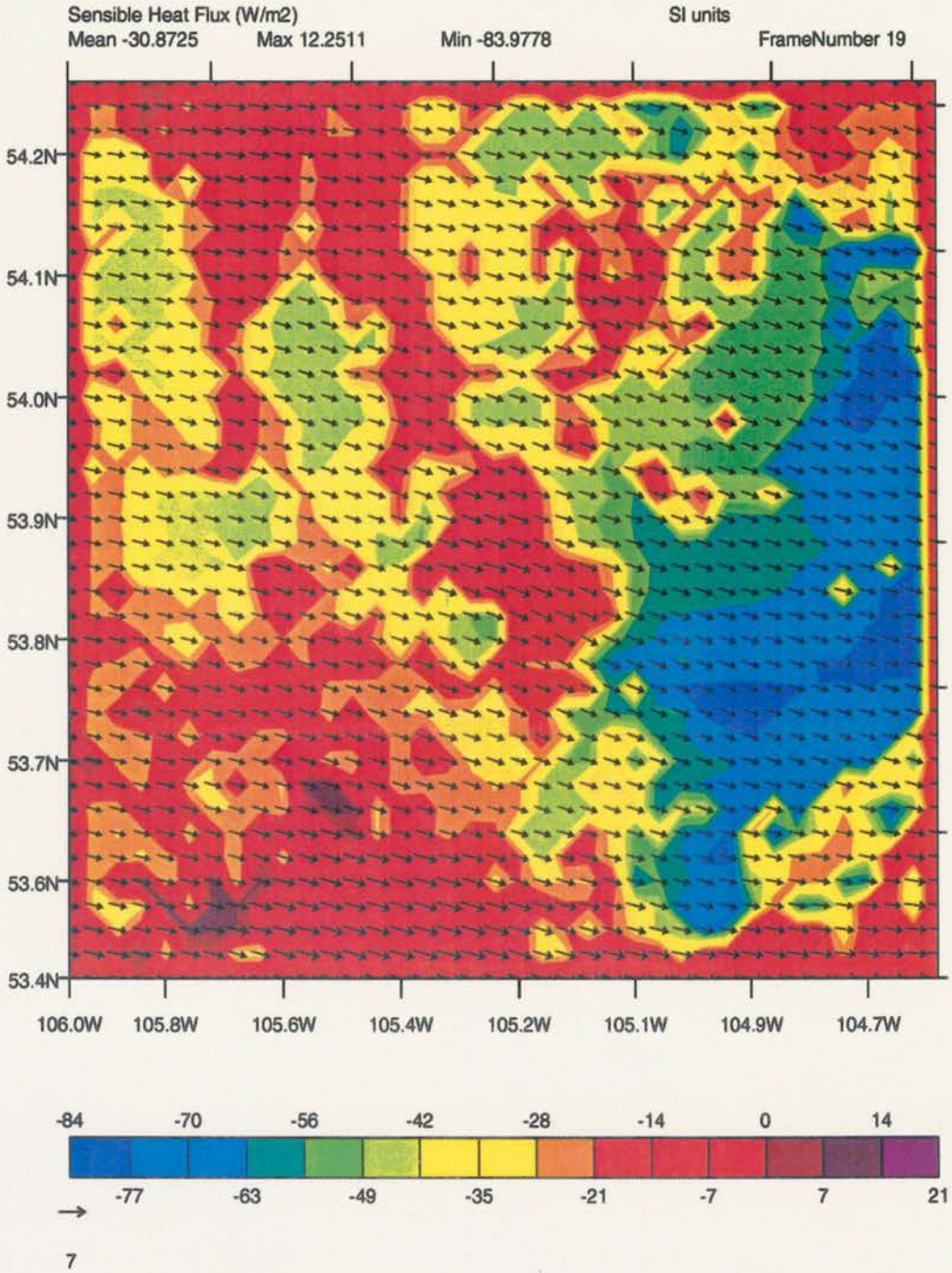

Figure 6.11: Fine-grid run: the grid 2 surface sensible heat fluxes (W m^{-2}) at 06 UTC, 22 July 1994 and the near-surface (60 m) wind vectors. The color field and color bar represent the turbulent sensible heat flux. Tick marks are in decimal degrees.

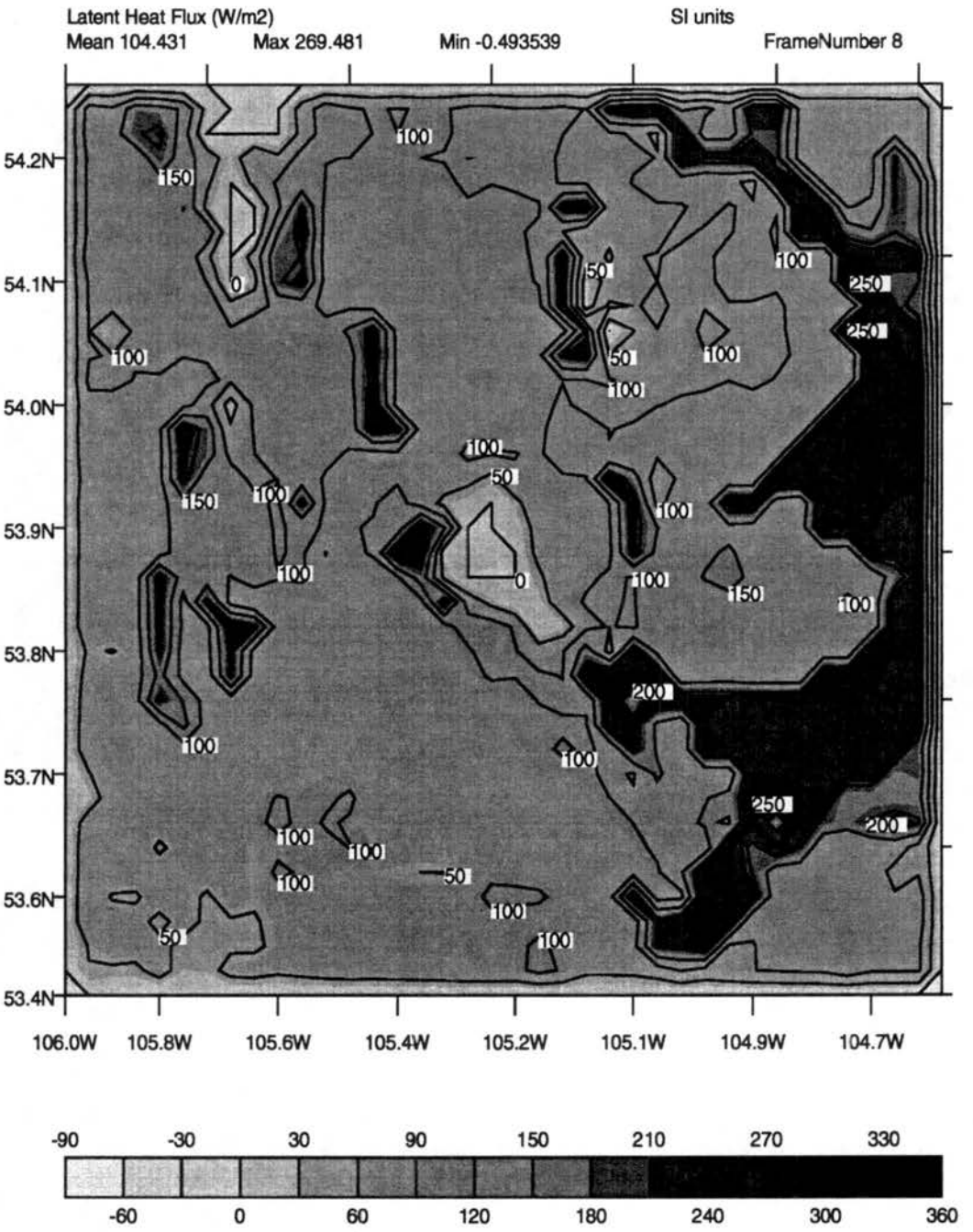

Figure 6.12: Fine-grid run: the grid 2 surface latent heat fluxes (W m^{-2}) at 19 UTC, 21 July 1994 and the near-surface (60 m) wind vectors. The gray scale field and gray scale bar represent the turbulent latent heat flux. Tick marks are in decimal degrees.

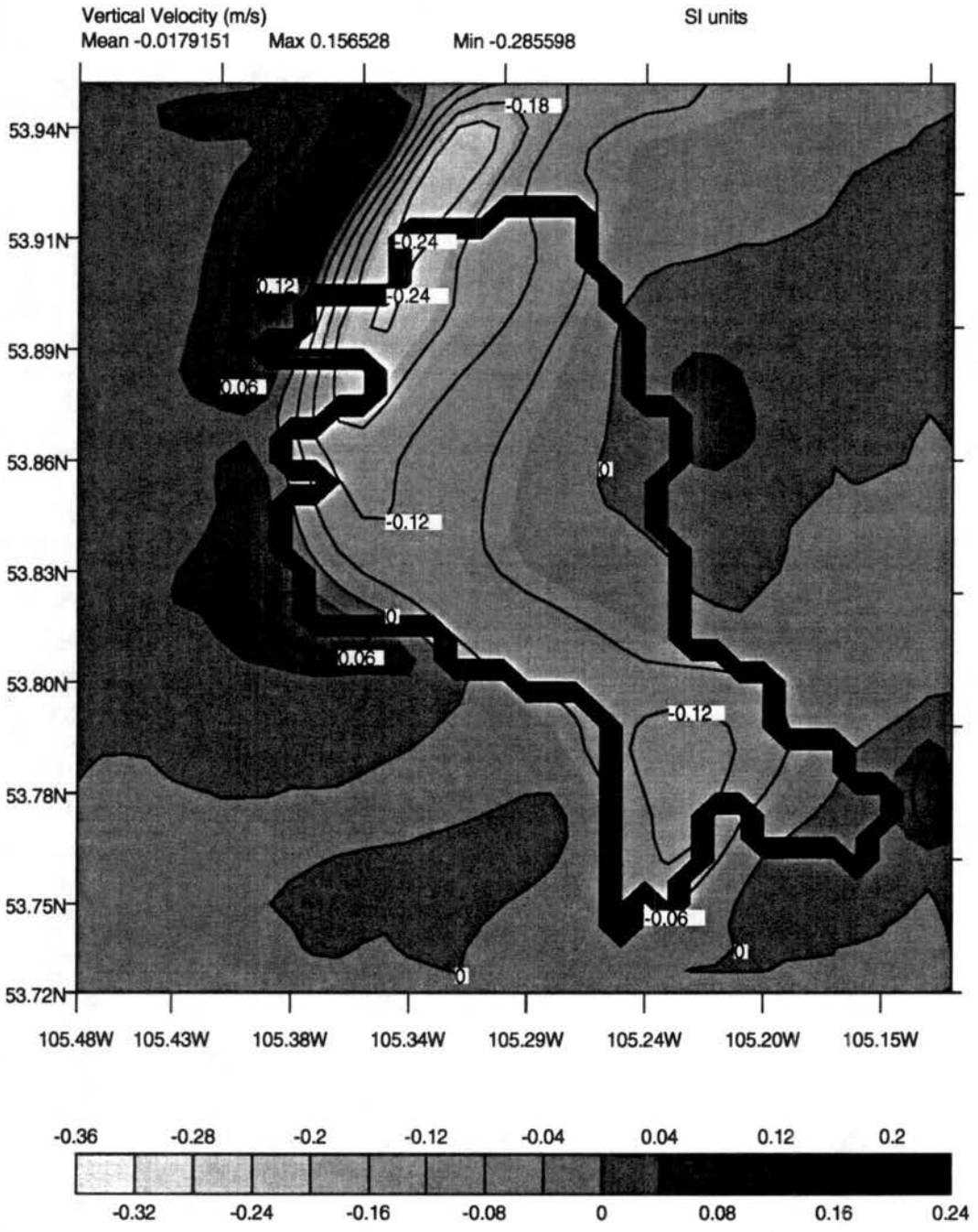

Figure 6.13: Fine-grid run: horizontal cross section of vertical velocity over Candle Lake for RAMS grid 3, 19 UTC, 21 July 1994 at 1250 m. Contour interval of 0.06 m^{-1}. Tick marks are in decimal degrees

A lake-induced circulation was also simulated at night (22 July 06 UTC, Fig. 6.14), with ascending motion (0.115 m s^{-1}) over the eastern part of the lake and descending motion (min. of -0.104 m s^{-1}) over the western lake boundaries. Most of the ascending motion over the central part of the lake was shifted eastward by the prevailing winds.

This pattern of ascending/descending motion corresponds to a diurnal cycle in mass divergence over the lake. A similar pattern was observed on 21 July by three aircraft, as discussed previously, and is portrayed in Fig. 6.5. During the diurnal heating period, with ascending motion over the lake boundaries and descending motion over the center of the lake, there was divergence at low levels near the lake center. During the nocturnal cooling period, there was descending motion over the lake boundaries and ascending motion at low levels near the lake center, where the land breeze converged with the prevailing flow. A typical conceptual model for the Candle Lake circulation was also given by Sun et al. (1997a), (see Fig. 2.1), consistent with our modeling results.

Superimposed on the lake breeze, the previous discussion of the wind fields pointed to contributions by the local orography (Candle Lake is positioned in a depression which slopes to the NE and NW with local terrain reliefs of 150 m within 50 km, which can control a coupled nocturnal surface flow converging at the lake center). Evidence of this influence on 21 July was present in Figs. 6.8 and 6.11 which shows how the surface winds turned towards the SE (downslope) as the nocturnal cooling was initiated. The nocturnal land breeze displayed an ascending cell over the east bank of the lake, illustrating how the prevailing flow shifted the convergence zone towards the N-NE. Another indication of the occurrence of this enhanced nocturnal convergence at low levels is that the vertical velocity in the nocturnal ascending cell had a considerably larger areal extent than the one during the daylight. The issue of the local coupling of the lake breeze with a mountain-valley type circulation needs to be explored through simulations of days with lower synoptic-scale winds.

6.3.5 Model Average Sounding and Diurnal Cycle Heating

The working hypothesis behind setting up a fine-grid run and a coarse-grid run over the grid 1 domain was that the coarse-grid run had truncated resolution and was not capable of

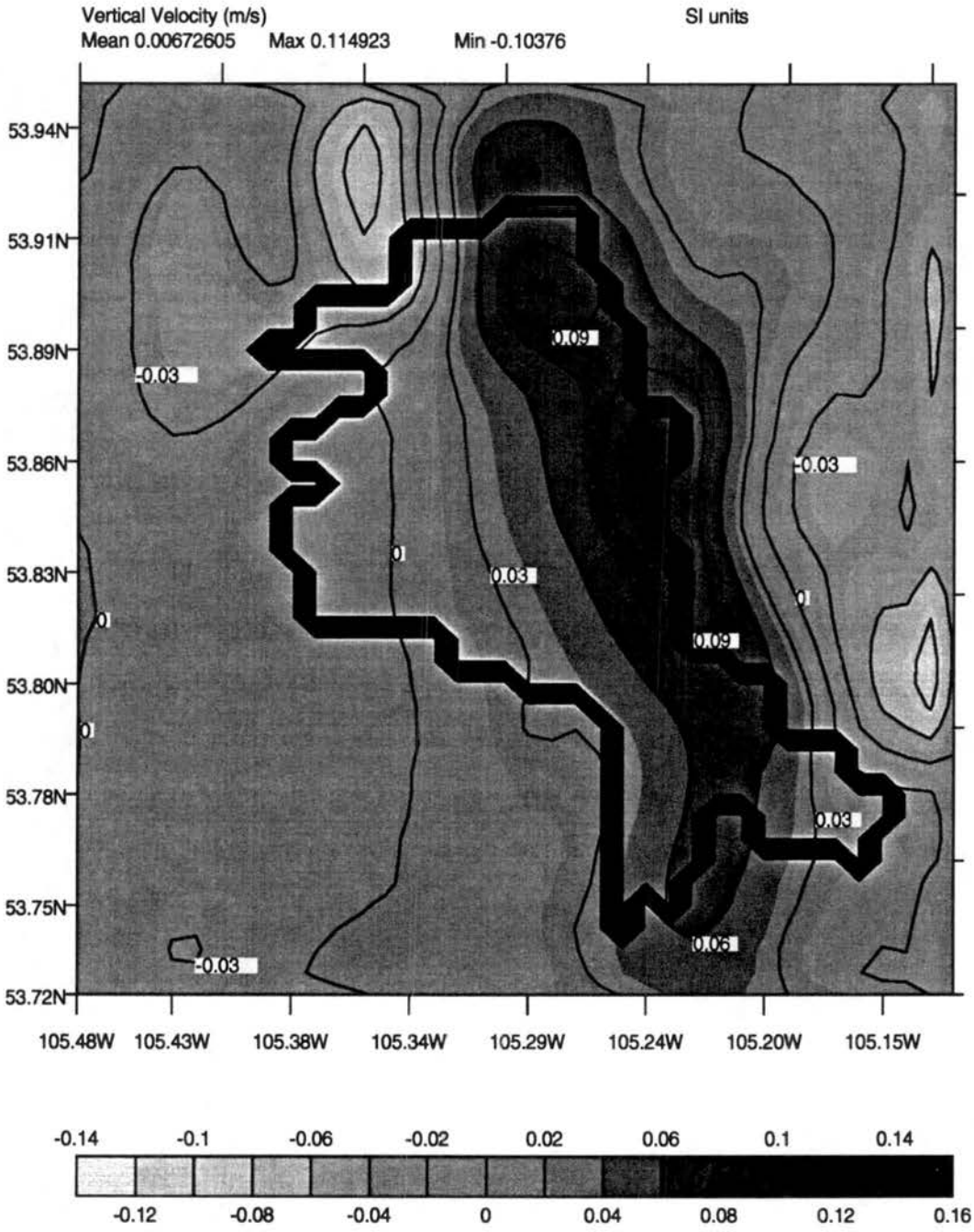

Figure 6.14: Fine-grid run: horizontal cross section of vertical velocity over Candle Lake for RAMS grid 3, 06 UTC, 22 July 1994 at 1250 m. Contour interval of 0.06 m^{-1}. Tick marks are in decimal degrees

effectively representing the full spectrum of mesoscale contributions (lacking both explicit and parameterized representation of mesoscale atmospheric processes with scales up to 40 km). We thus calculated horizontal averages of the vertical potential temperature (θ) profile for the region corresponding to a region of 40 by 40 km around grid 3 every 3600 s, by accumulating the tendencies at each time step. The rationale behind this averaging decision lies in the fact that we needed to compromise between being able to monitor the diurnal oscillation in the surface layer (which is strongly controlled by local heating, and therefore has a small footprint) and being able to represent the impact of the surface heterogeneity on the atmosphere. We chose a 40 km region because:

- we recognized the Candle Lake breeze as the strongest induced mesoscale circulation in this domain;
- by visual inspection of all cases we simulated, the lake breeze cells never left a boundary region of about 20 km around the lake;
- we wanted to include the small depression where Candle Lake lies on its 'lake valley' side only, in order to catch potential cold drainage effects;
- most point measurements were taken within about 20 km of the lake;
- it is equivalent to the coarse-scale run resolution;
- a variance analysis (i.e. an estimate of the departure of each atmospheric column from a domain average) of the model columns indicated this as a reasonable footprint for the CBL properties, although being rather large for the surface layer.

The conceptual model of what we expected to find in terms of a lake breeze impact is perhaps best summarized by looking Fig. 2.5 (adapted from Fig. 5, Dalu et al. 1996). In this figure, which shows the atmospheric response to an isolated heat patch, the top portion shows a situation with low predominant winds and a closed, mature circulation. With a positive vertical velocity at the center, the mesoscale heat flux is positive in the lower part of the CBL and negative in its upper part. The bottom portion of Fig. 2.5 shows the same

land surface forcing under higher winds, with an open circulation. In this case a vertical distribution of positive and negative vertical velocity nuclei, decaying in magnitude with height, is set up, and the mesoscale heat flux has a more complex vertical structure.

With this, we set out to compare to a set of soundings taken during the day of 21 July, in order to verify that our calculations were reasonable for the region. Our intent was not to reproduce the sounding, but rather to compare the two simulations. For this reason, once more, we decided against calibration and against calculating temperature profiles at the point nearest the sounding site.

The averages were taken over the exact same region in both the fine-grid and the coarse-grid runs. We then calculated a diurnal vertical temperature change curve by subtracting the horizontally averaged θ vertical profile at 23 UTC on 21 July from the horizontally averaged vertical θ profile at 11 UTC on the same day. Because of the mesoscale time lag of two hours (as compared to turbulence) indicated by the analysis in Chapter 5, later times would have been more revealing, but would not have been suitable for comparison to the data from the soundings at the Candle Lake station (the last sounding was taken at 23 UTC each day).

The results from our analysis are shown in Fig. 6.15 and overall seem to confirm the influence of a mesoscale perturbation in the heating pattern.

From comparison of the coarse-grid and the fine-grid diurnal temperature change patterns, the coarse-grid run showed less vertically integrated ΔT than the fine-grid run, although displaying a comparable surface layer diurnal amplitude and cooling in the layer from 610 hPa to approximately 450 hPa. The diurnal profile in the fine-grid run showed more intense T change within the boundary layer and a cooling in the 550 to 390 hPa layer.

Both the modeled and the observed (Old Jack Pine wind profiler) inversion height were near the 765 hPa layer. The detailed structure of ΔT at that level (common to other soundings) is thought to be due to entrainment.

From the discussion on the fluxes over the two grids, the near-surface turbulent sensible heat fluxes for the coarse-grid run were found, over the 21 July daytime, to be slightly less intense than those for the fine-grid run in the grid 3 model region. Our interpretation

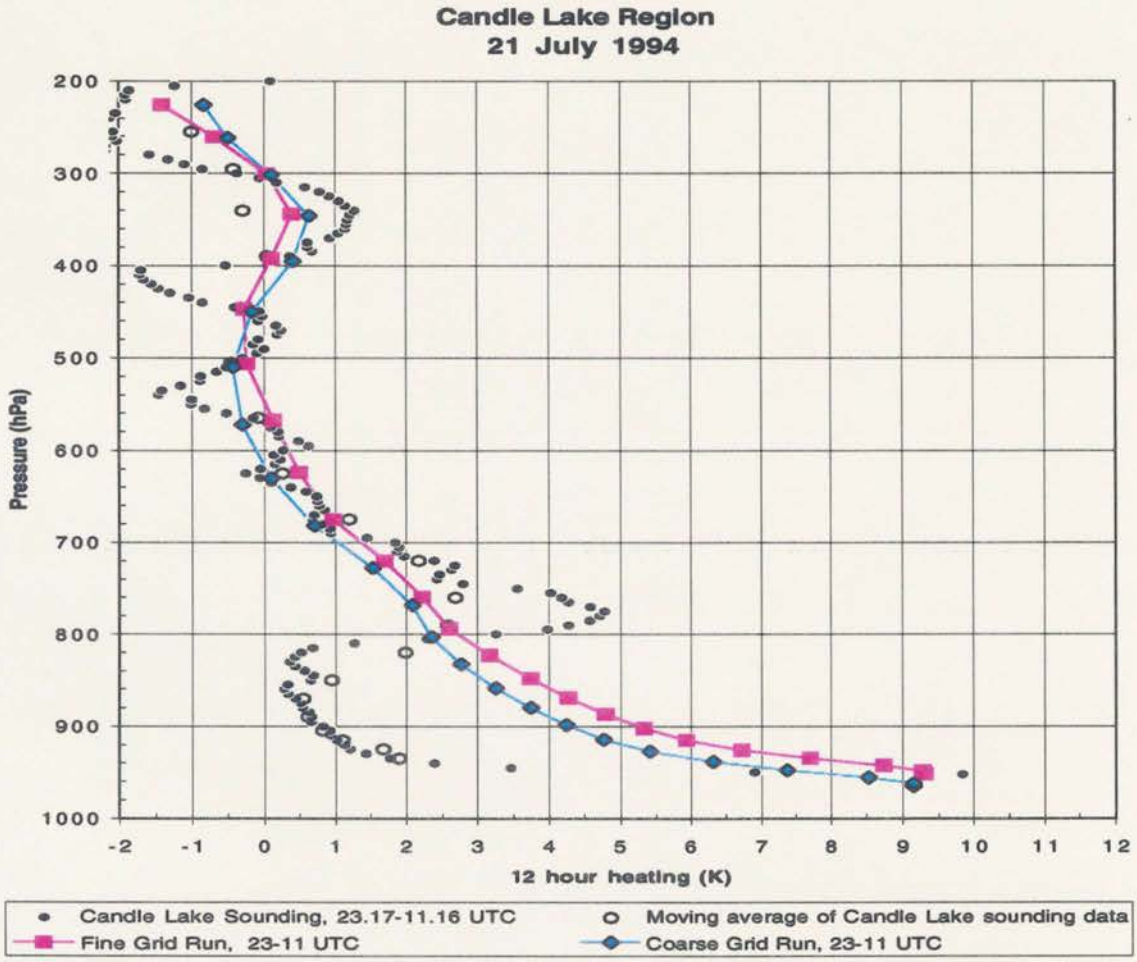

Figure 6.15: The Candle Lake diurnal temperature change from the Candle Lake sounding and the model runs, 21 July 1994 11-23 UTC.

is that the coarse-grid run, although developing less intense surface sensible heat fluxes, lacked a secondary mechanism for the vertical redistribution of heat, thus developing a large surface temperature oscillation over the 12 hours period. The fine-grid run produced larger sensible heat fluxes at the surface, but, through resolved mesoscale circulations, was capable of distributing this heat above the surface layer with more efficiency than if only parameterized turbulence had been active. Among the resolved circulations responsible for this vertical heat redistribution were the solenoidal circulations that we have shown to be active over the whole averaging period; that is, the diurnal lake breeze and the nocturnal drainage flow and land breeze.

In order to help interpret the comparison, we have also provided a data set (Fig. 6.15) that was derived from the original sounding data by using a vertical moving average with a variable window width, which simulated the effect of vertical resolution in our atmospheric model. The variable window width is necessary since the model vertical grid is telescopic, with higher resolution at low levels; data at each point was therefore averaged over four vertical grid separations.

The comparison of the observed and simulated ΔT curves shows how the model was capable of reproducing the surface layer diurnal range with accuracy. The lower part of the boundary layer, however, heated too much in comparison to the observations at Candle Lake. The reasons for the ΔT disagreement within the CBL are multiple:

- entrainment cannot be simulated by our local, downgradient vertical mixing scheme;
- the sounding is representative of a point measurement, the model profile is a 40 by 40 km average (roughly half land and half lake);
- the sounding was taken at the lake shore (see Fig. 4.4) and the low level wind was often coming from across the lake (winds from almost three quadrants would advect lake air to the sounding site);
- the model was colder than the sounding near the surface in the morning and warmer at the end of the day, thus the 12 hour tendency is a sum of two smaller errors;

- the morning sounding was receiving air from the NW, thus warmer air than the air over the land, which explains the model colder near-surface profile;
- the vertical resolution of the sounding is 5 hPa, the model has much lower resolution as soon as exiting the surface layer, as is seen in Fig. 6.15.

In order to better understand what is producing the differences between the two simulated diurnal ΔT profiles, we have also modified our atmospheric model to output tendencies for advection and diffusion (both horizontal and vertical) and for radiation. Since the simulated golden days had no precipitation and had absolutely clear skies, these are the main forcing quantities that are involved.

The radiation temperature tendency for both simulations in Fig. 6.16 shows no relevant differences; the only noticeable discrepancy is in the lowest model level where the coarse-scale run produces a much larger tendency, seemingly due to artificial horizontal mixing (in the fine-scale run, in the early hours of the day, a land breeze is formed and air flows from the land to the center of the lake, as confirmed by the divergence analysis).

The horizontal diffusion for the large-scale run always displays larger magnitude because it is proportional to the square of the grid spacing. Other than that, its contributions are modest. The vertical diffusion tendencies reflects the fact that the surface layer produced slightly higher fluxes for the fine-scale run, and also more heating within the CBL. The same figure shows the inversion height at approximately 780 mhPa, in agreement with the wind profiler estimate.

More general differences, especially above the CBL, are visible in the advection tendencies, in that the fine-scale run produced less warming from horizontal advection within the CBL (due to horizontal advection of lake air in the later part of the day). Within the CBL, the coarse-scale run produced some cooling, while the fine-scale run did not. In terms of the vertical advection tendency, it is clear that the fine-scale run produced more warming within the CBL, while producing far less than the coarse-scale run above it.

The mesoscale vertical flux divergence temperature tendency for the same period (calculated for the fine-scale run exclusively) showed how the lowest part of the CBL was heated

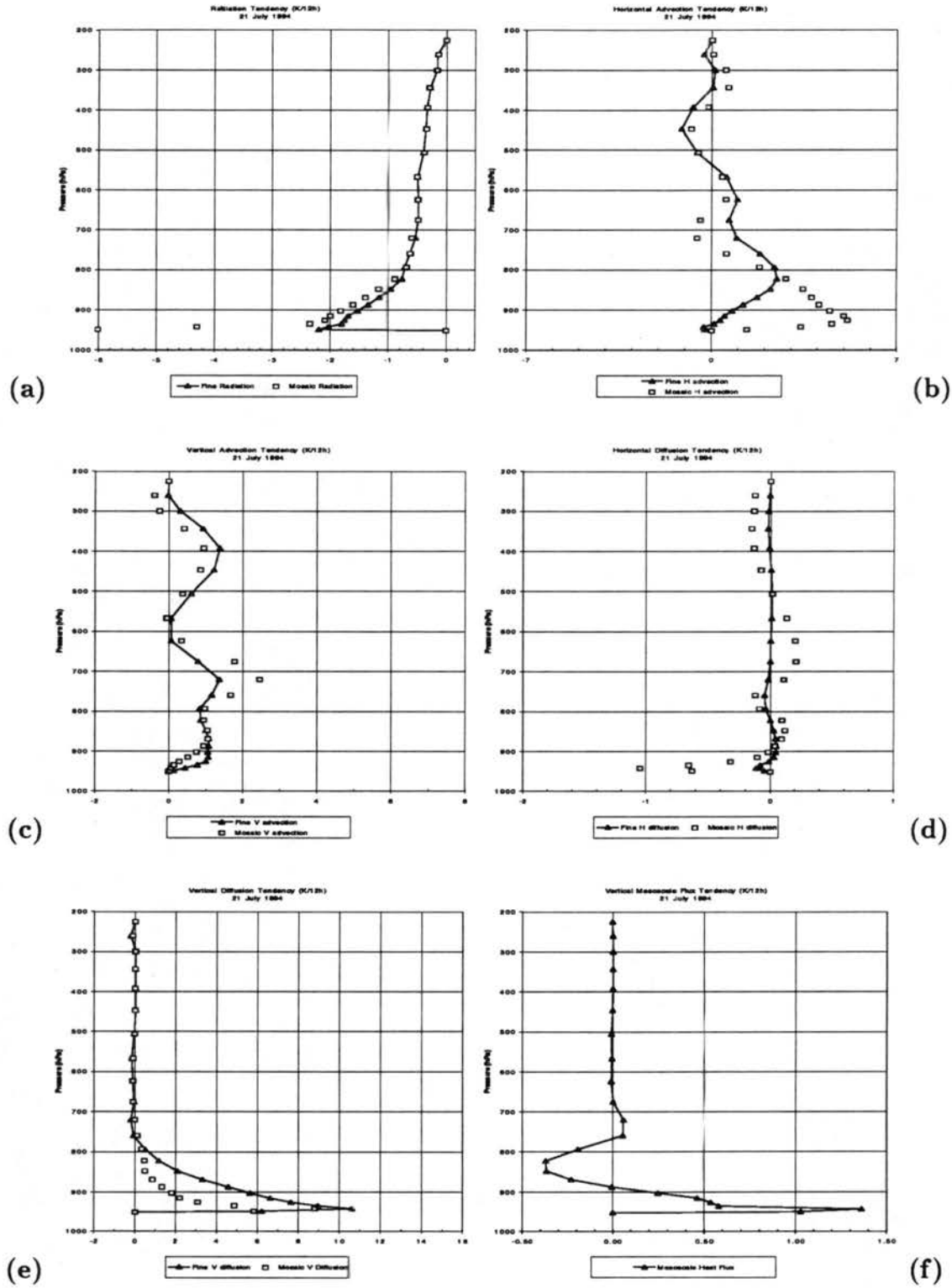

Figure 6.16: The RAMS accumulated temperature tendencies for 11-23 UTC, 21 July 1994: a) radiative tendency, b) horizontal advection tendency, c) vertical advection tendency, d) horizontal diffusion tendency, e) vertical diffusion tendency, f) vertical mesoscale flux tendency. Values are in K/12 hours. The values for the fine-scale run are connected by a black line.

and its upper part cooled, in agreement with linear theory. Just above the inversion, at about 750 hPa, there is another small heating profile, but no other structure above that. The temperature change magnitudes, as expected for a case with such sustained winds, is modest, reaching only a maximum value of 0.5 K in 12 hours.

The mesoscale heat flux divergence is in fact a portion of the vertical advection tendency, so that part of the difference in the two runs for Fig. 6.16c is explained by referring to Fig. 6.16f. Part of it must be dependent on the existence of a wavy vertical velocity perturbation, as confirmed by the correlation between the horizontal and vertical advection (less warming in the vertical corresponds to more warming in the horizontal and vice-versa), similar to the one generated by Candle Lake, that has a much larger horizontal scale than our averaging scale. Such a circulation is very probably in place over grid 2 because of the small topographical plateau within this domain, and is contaminating our base state vertical velocity. This same circulation is not well resolved in the mosaic run, because of the 40 km horizontal resolution.

6.4 A High Winds Case: The 7 June 1994 "Golden Day"

This day was also selected because of its clear skies and because of data availability.

The synoptic situation is depicted in Fig. 6.17. A weak low pressure system was present over the western part of the domain, and a weak high pressure system was present over the eastern part of the domain. Winds in the SSA were from the SE. The synoptic-scale winds in this case study were over 20 m s^{-1} at 850 hPa in the SSA region, so this was certainly the least ideal case for mesoscale circulations. The upper air showed a situation very similar to the one in the previous case, with a deep trough over the center of the domain and some acceleration to the west of the SSA. The vertical motion over this region, as diagnosed from the ETA model initialization, was -0.010 m s^{-1} on average for the diurnal period.

The Candle Lake sounding, Fig. 6.18 at 17.17 UTC (11.17 LT) showed an extremely dry atmosphere (perfect for RS work), a very shallow CBL (inversion at 850 hPa), with easterlies up to 370 hPa and westerlies the rest of the way to the tropopause.

The 7 June 1994 case was initialized on 6 June at 00 UTC (5 June, 18.00 Local Time) and run for 60 hours. The temperature of the lakes was set at 281 K. Soil temperature and

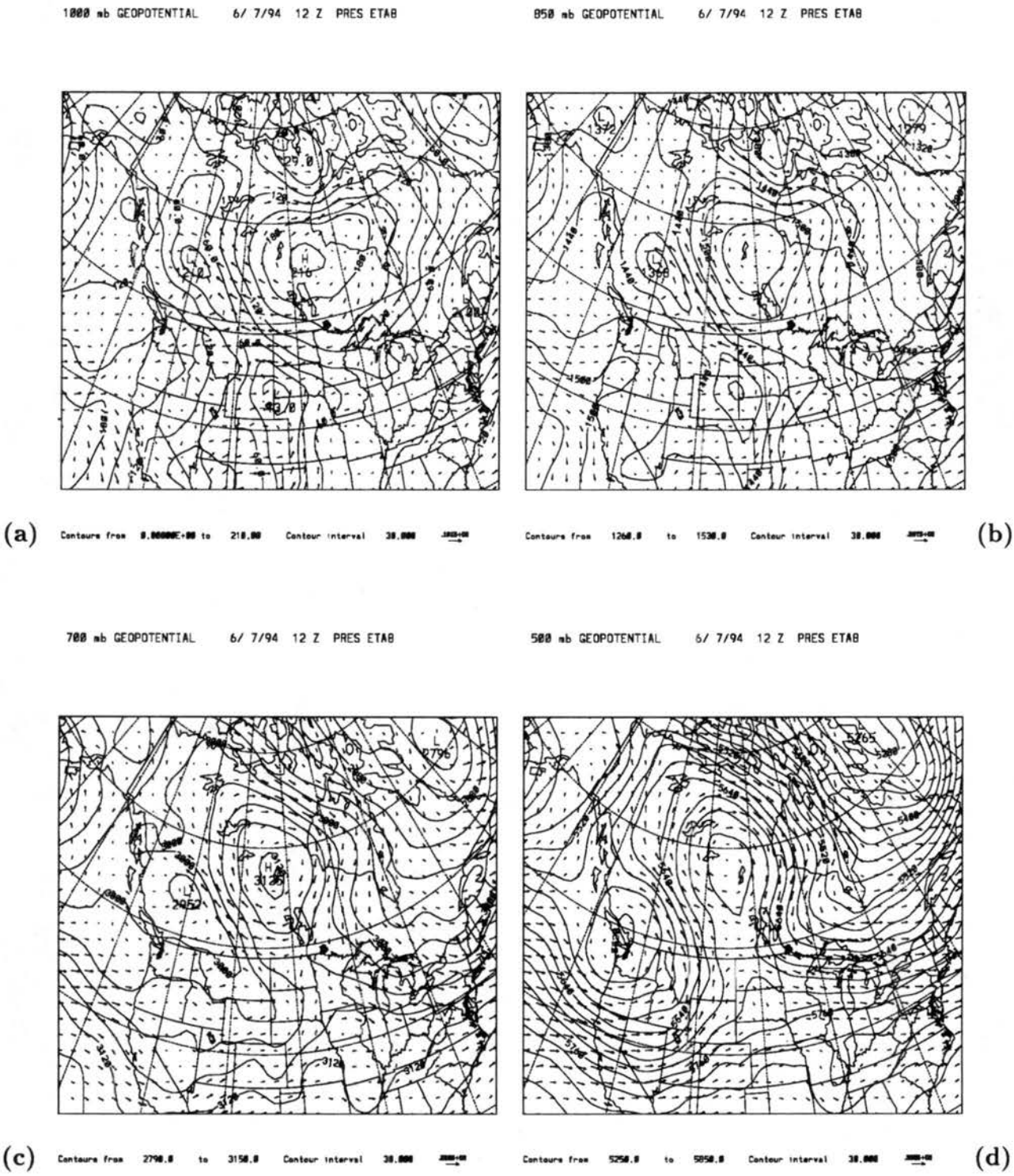

Figure 6.17: The 12 UTC ETA analysis for 7 June 1994: a) 1000 hPa geopotential height (m) and winds (m s^{-1}); b) 850 hPa geopotential height (m) and winds (m s^{-1}); c) 700 hPa geopotential height (m) and winds (m s^{-1}); d) 500 hPa geopotential height (m) and winds (m s^{-1})

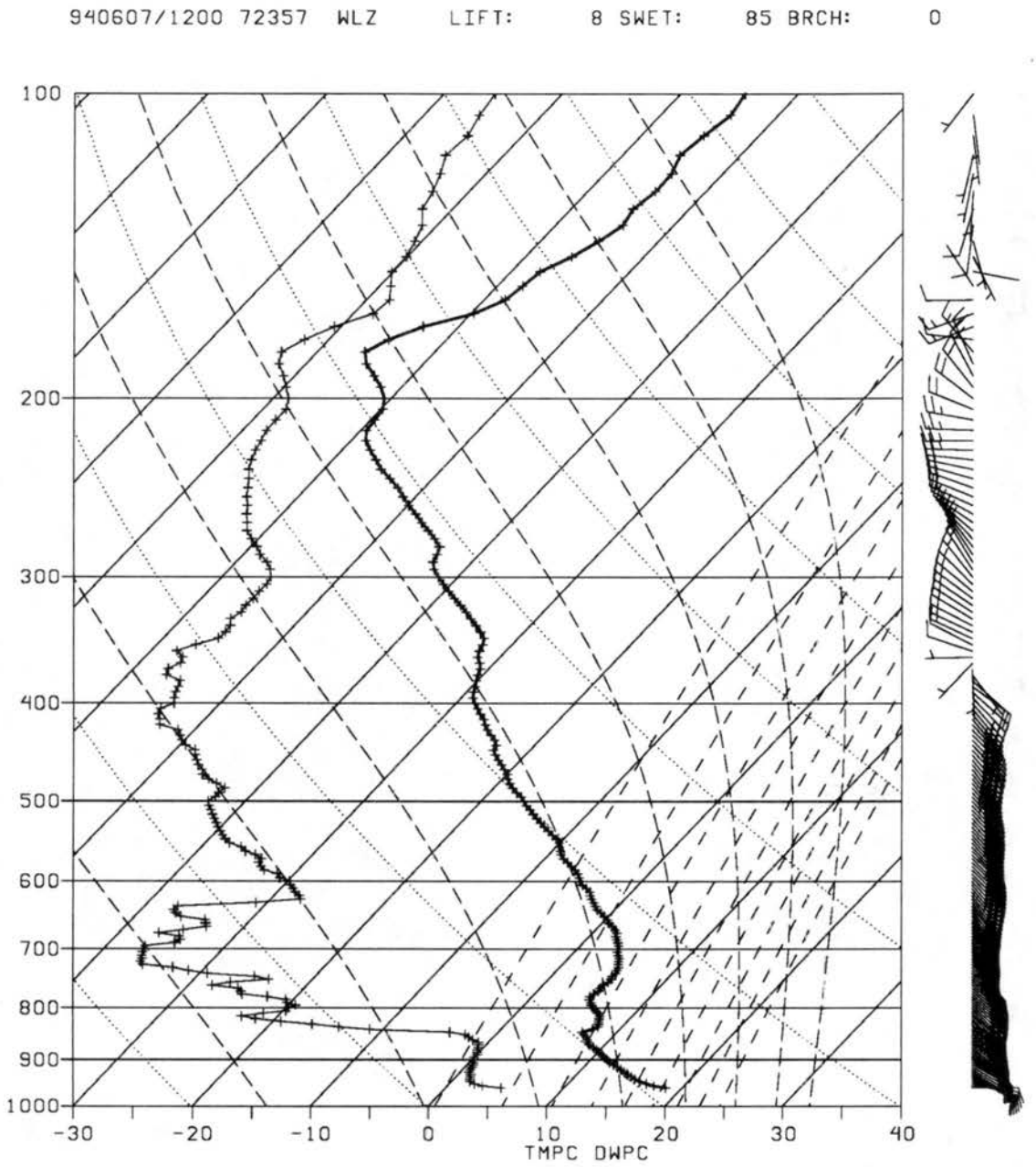

Figure 6.18: The 17 UTC Candle Lake skew-T diagram for 7 June 1994.

moisture profiles were initialized using information from the AMS and the AES networks on 6 June.

6.4.1 Second Comparison with Aircraft Measurements

Figure 6.19 (data here reproduced with permission of Crawford and Baldocchi) shows the surface turbulent sensible and latent fluxes, measured by the NOAA LongEZ aircraft and averaged over 10 legs, between 15.05 and 22.34 UTC on 7 June 1994 (transect indicated on Fig. 4.5b). The LongEZ measurements of sensible heat over Candle Lake for 7 June 1994 showed a sharp gradient in sensible heat fluxes, with values from 300 W m^{-2} over the forest to almost -20 W m^{-2} over the lake.

The same 100 W m^{-2} error appears on the west bank of the lake that was seen in the previous case, so that the pixel misclassification interpretation holds.

Figure 6.19 also shows the turbulent fluxes modeled by LEAF-2-RAMS, temporally averaged through the same period. As in the previous case, the model was capable of capturing the spatial pattern of the fluxes quite accurately, creating spatial gradients in the surface heating that could potentially drive a mesoscale circulation between lake and forest. The model skill in reproducing the latent heat fluxes seems to be better than in the previous case, probably due to more contributions from soil evaporation and less stressed vegetation (Fig. 6.20).

6.4.2 Fluxes in Grid 1 ($\Delta x = 10$ km)

As in the previous case, the grid 1 integration was carried out in two fashions by specifying the land cover over each grid cell at two different resolutions, with a grid spacing of 10 km for the coarse (mosaic) run and a minimum grid spacing (625 m) for the fine-scale run.

In both cases, RAMS was initialized at 00 UTC on 6 June 1994 (5 June, 18 LT), using the ETA analysis, and then nudged, with updates every six hours, over the outermost boundary and the top exclusively. Grids 2 and 3 were spawned after one full diurnal cycle.

The grid 1 sensible heat fluxes at 19 UTC (13 LT) on 7 June (Fig. 6.21) showed some general differences, in that the coarse-grid run produced slightly higher domain average

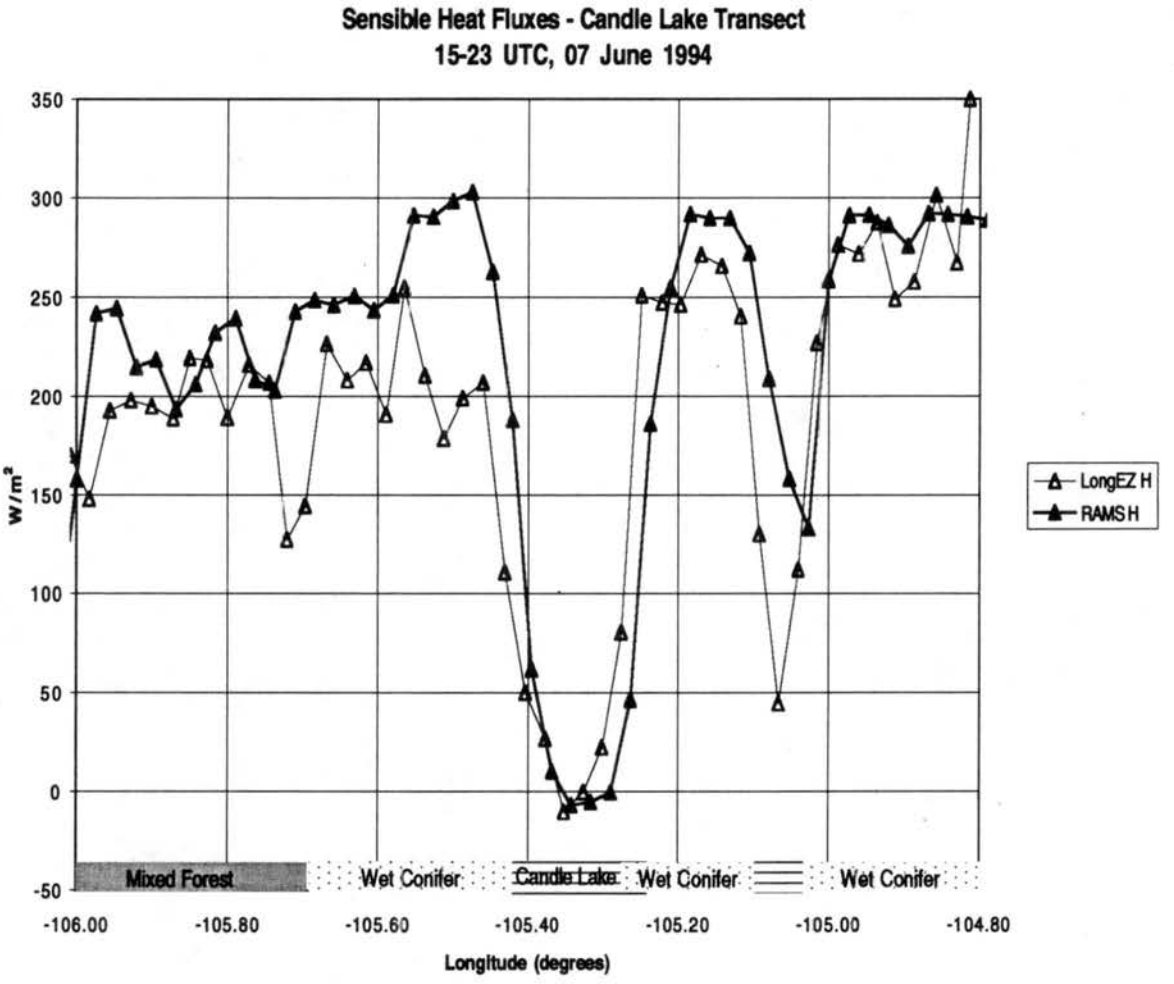

Figure 6.19: The average turbulent sensible heat fluxes over the Candle Lake transect for 7 June 1994. The LongEZ label refers to the NOAA/ATDD aircraft data; RAMS refers to the modeled fluxes.

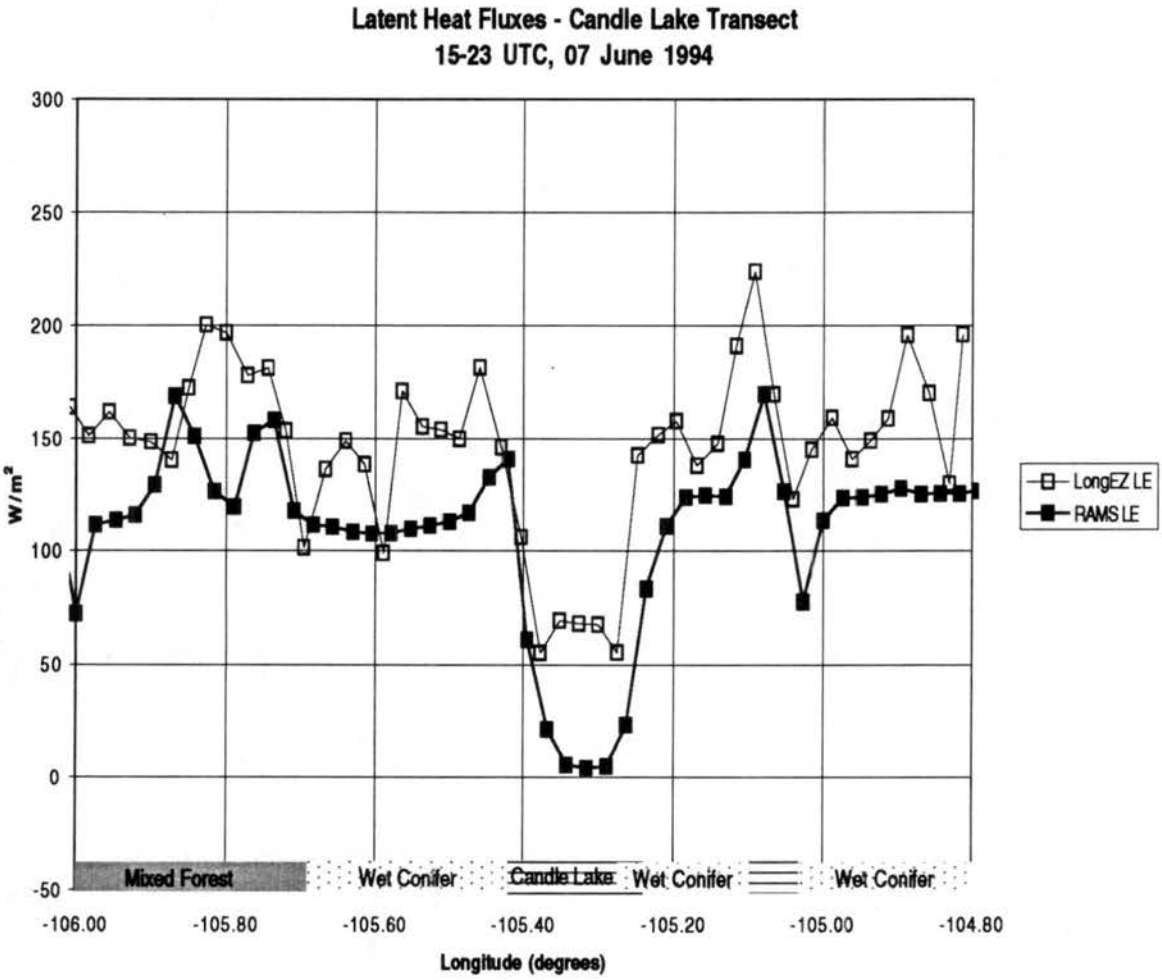

Figure 6.20: The average turbulent latent heat fluxes over the Candle Lake transect for 7 June 1994. The LongEZ label refers to the NOAA/ATDD aircraft data; RAMS refers to the modeled fluxes.

surface sensible heat fluxes (differences of about 40 W m^{-2}) than the fine-grid run (Fig. 6.22). Again, as in the previous case, this is due to the inclusion of less abundant classes with physiographical characteristics that favor a higher Bowen ratio. Also, the fine-scale run produced a tighter sensible heat flux gradient around Candle Lake, which is also confirmed by the vertical diffusion tendency discussed later.

While lake breezes were clearly active over Lac La Ronge and Lake Winnipeg, which are rather sizable lakes, only a minimal divergence trace is visible over Candle Lake (western bank). The only other noticeable difference between the runs, in the region around 103W, 53N, is a convergence zone in the fine-scale run that seems to be associated with channeling by the local orography, once the winds are strongly easterly. The higher sensible heat fluxes to the NW of this region, in the case of the mosaic run, seem to be driving the flow to a more westerly direction, somewhat diluting the convergence zone.

In terms of other local circulations, no distinct orographically-induced flow is visible, but a remarkable acceleration of the wind over lakes is in place, a roughness effect.

6.4.3 Results for Grid 3 (Δx = 625 m): The Candle Lake Breeze

Even under such southeasterlies, the model developed a well defined lake breeze, identifiable in Fig. 6.23 (depicting vertical velocity at 1250 m), with a subsiding cell (-0.152 m s^{-1}) to the SW of the lake center and maximum ascending motion (0.125 m s^{-1}) at the northwest bank of the lake. The downward motion region revealed a shape and position that confirmed the influence of Candle Lake (being also, as in the other two cases, the most persistent and intense feature present in the vertical velocity field over the grid 2 domain). The positive vertical velocity regions were distributed over the land around the lake, although shifted by the southeasterly winds.

A lake-induced circulation was also observed at night (7 June, 06 UTC, Fig. 6.24), with ascending motion (0.147 m s^{-1}) over the northwestern part of the lake and weak descending motion around the lake. Most of the ascending motion over the central part of the lake was shifted to the northwest by the prevailing winds.

Once more, although this day was not very favorable for a breeze over a lake of this area, a clear signature is present in the model and in the data.

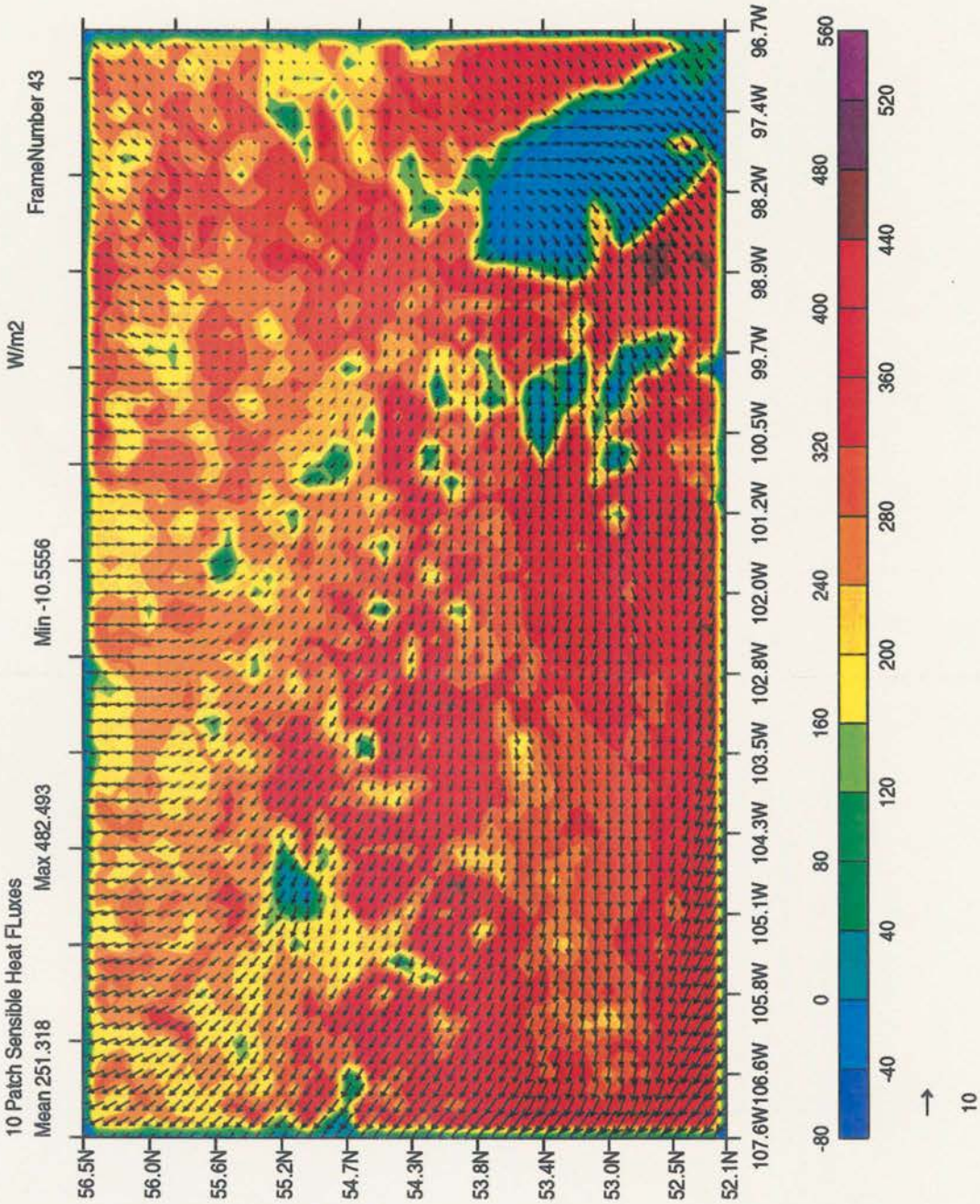

Figure 6.21: Coarse-grid run: the grid 1 surface sensible heat fluxes (W m^{-2}) at 19 UTC, 7 June 1994 and the near-surface (60 m) wind vectors. The color field and color bar represent the turbulent sensible heat flux. Tick marks are in decimal degrees.

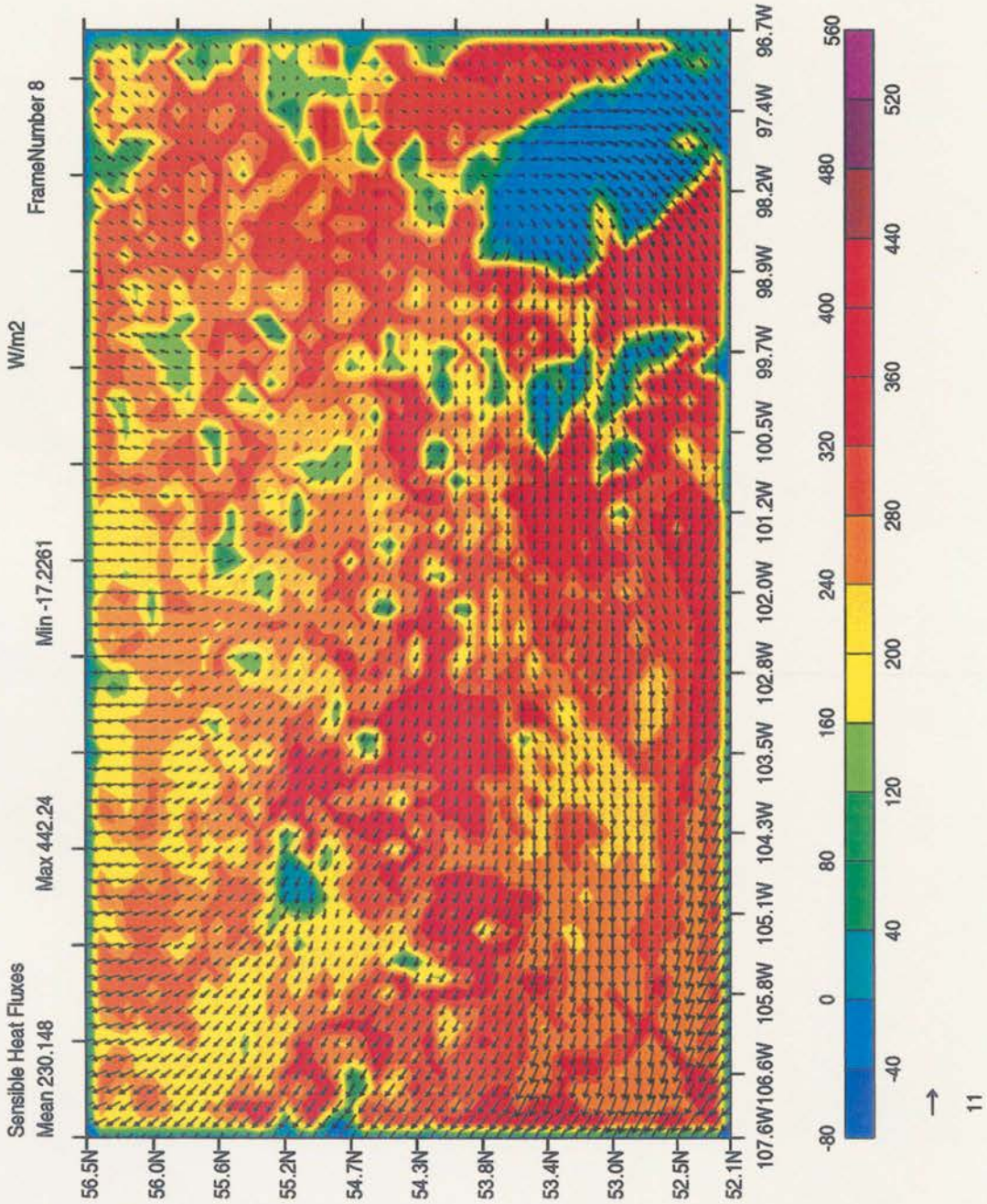

Figure 6.22: Fine-grid run: the grid 1 surface sensible heat fluxes (W m^{-2}) at 19 UTC, 7 June 1994 and the near-surface (60 m) wind vectors. The color field and color bar represent the turbulent sensible heat flux. Tick marks are in decimal degrees.

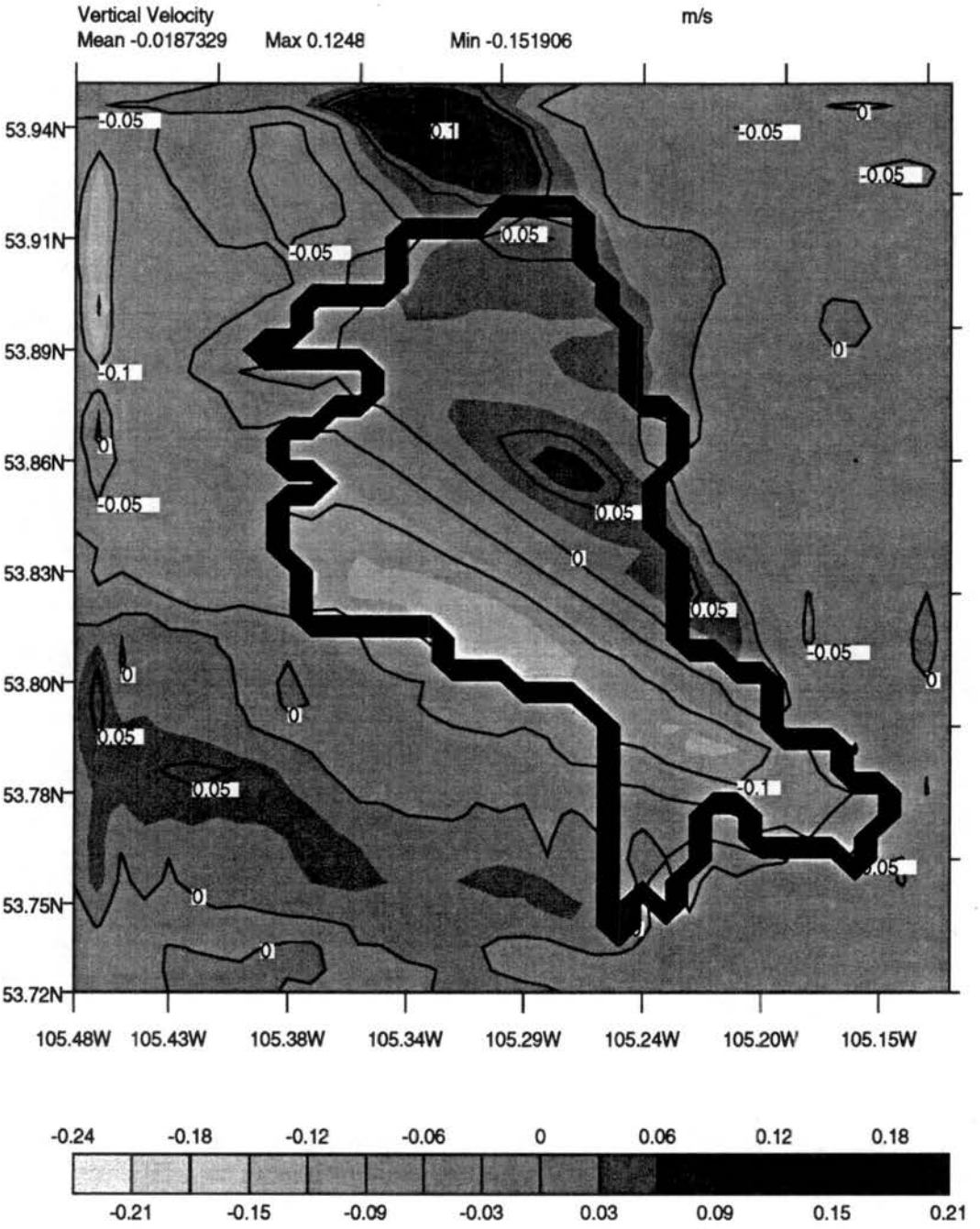

Figure 6.23: Fine-grid run: horizontal cross section of vertical velocity over Candle Lake for RAMS grid 3, 19 UTC, 7 June 1994 at 1250 m. Contour interval of 0.06 m^{-1}. Tick marks are in decimal degrees

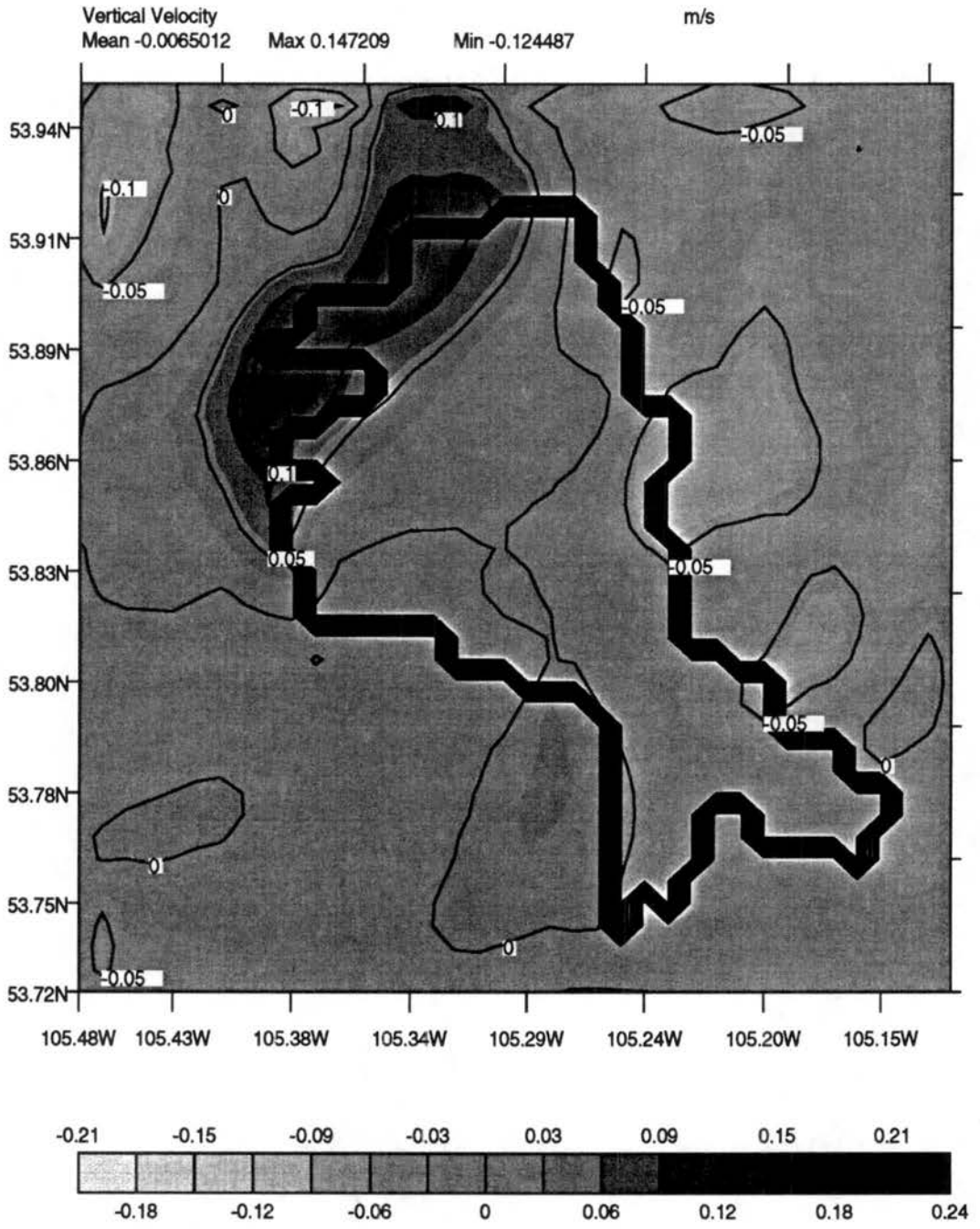

Figure 6.24: Fine-grid run: horizontal cross section of vertical velocity over Candle Lake for RAMS grid 3, 19 UTC, 7 June 1994 at 1250 m. Contour interval of 0.06 m^{-1}. Tick marks are in decimal degrees

6.4.4 Model Average Sounding and Diurnal Cycle Heating

As in the previous case, we calculated horizontal averages of the vertical potential temperature (θ) profile for a region of 40 km around grid 3. The diurnal vertical ΔT curves are shown in Fig. 6.25.

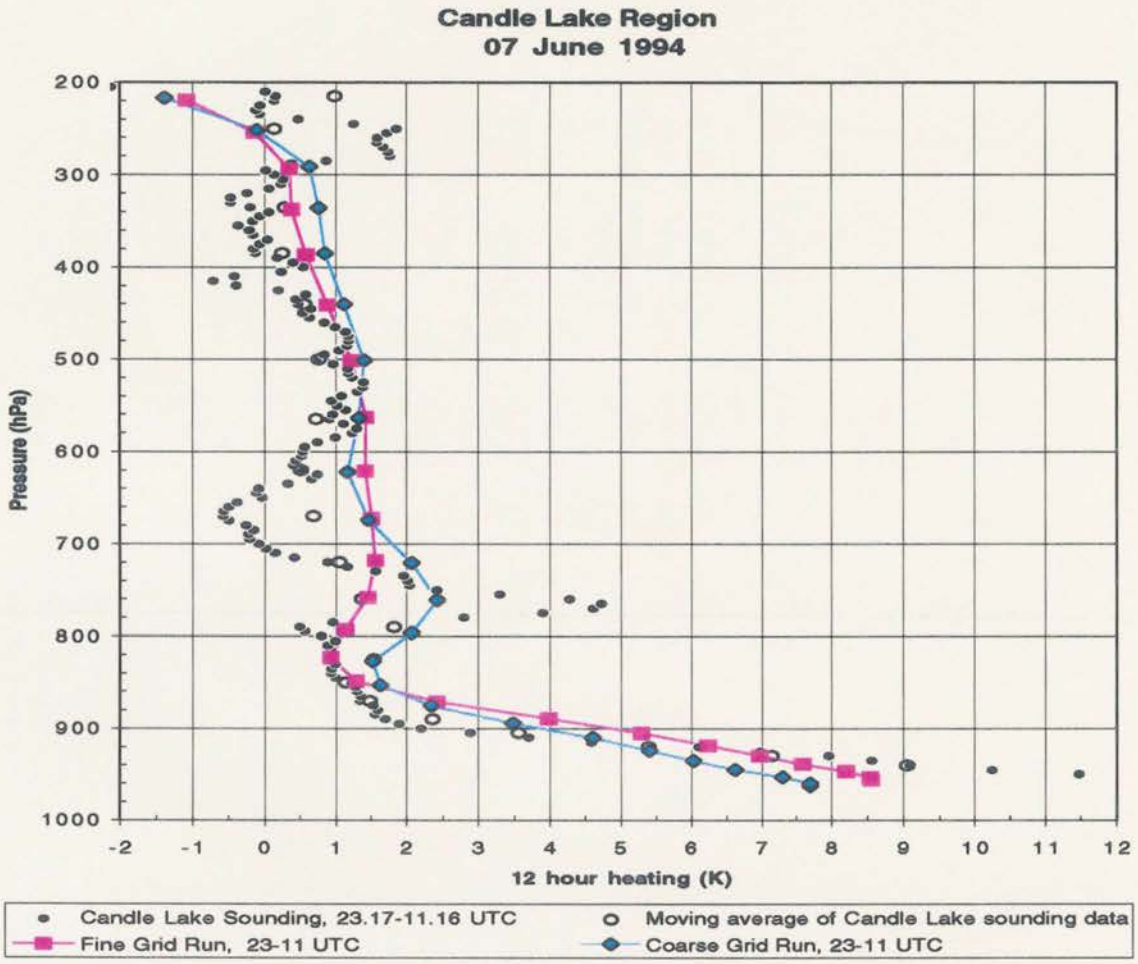

Figure 6.25: The Candle Lake diurnal temperature change from the Candle Lake sounding and the model runs, 7 June 1994 11-23 UTC.

From comparison of the coarse-grid and the fine-grid diurnal ΔT patterns, the coarse-grid run showed less warming within the surface layer and lower part of the CBL, while retaining more warming in the upper part of the CBL. Above these lower levels the fine-scale run seems to display slightly less warming than the mosaic run up to about 300 hPa. The largest difference between the two runs occurs just under the inversion (about 780 hPa).

Data from the high resolution sounding (interpolated to 5 hPa) at Candle Lake were used to calculate the 23.17 UTC - 11.16 UTC (17.17 to 5.16 Local Time) temperature change on 22 June 1994 and the resulting diurnal ΔT curve is shown on figure 6.25. Again the ΔT peak near 780 hPa is thought to be due to entrainment. The inversion height from the OJP profiler agrees with the modeled height. In this situation the prevailing winds, stronger (larger fetch) and from a different direction, allowed for a better model-sounding agreement.

The comparison of the observed and simulated ΔT curves shows how the model was capable of reproducing the surface layer diurnal range with some accuracy, although not catching the extreme diurnal oscillation at the very surface. It is important to notice that the general agreement between model and data is reproduced at higher levels where the sonde footprint is larger.

In order to better understand what is producing the differences between the two simulated diurnal temperature change profiles, as in the first case study, we have also modified our atmospheric model to output tendencies for advection and diffusion (both horizontal and vertical) and for radiation. Since the simulated golden days had no precipitation and absolutely clear skies, these are the main forcing quantities that are involved.

The 12 hour radiation tendency for both simulations (in Fig. 6.26 shows no significant differences; the only noticeable discrepancy being again in the lowest model level where extra horizontal mixing of lake characteristics in the coarse-scale run produces a shallow moist layer that is losing slightly more radiation to the clear sky.

The vertical diffusion tendency showed differences within the surface layer, in that the fine-scale run again developed a larger ΔT near the bottom of the CBL. Above the shallow CBL some cooling is present in both runs, more pronounced in the fine-scale run.

The strongest discrepancies between the two runs are visible in the advection tendencies, in that once more the fine-scale run is advecting cold lake air during the second part of the day, creating less warming. Vertically, the fine-scale case displays more warming up to 700 mb, well above the inversion. The two tendencies are largely compensating each other, in a pattern that would confirm our hypothesis about the setting up of a vertical

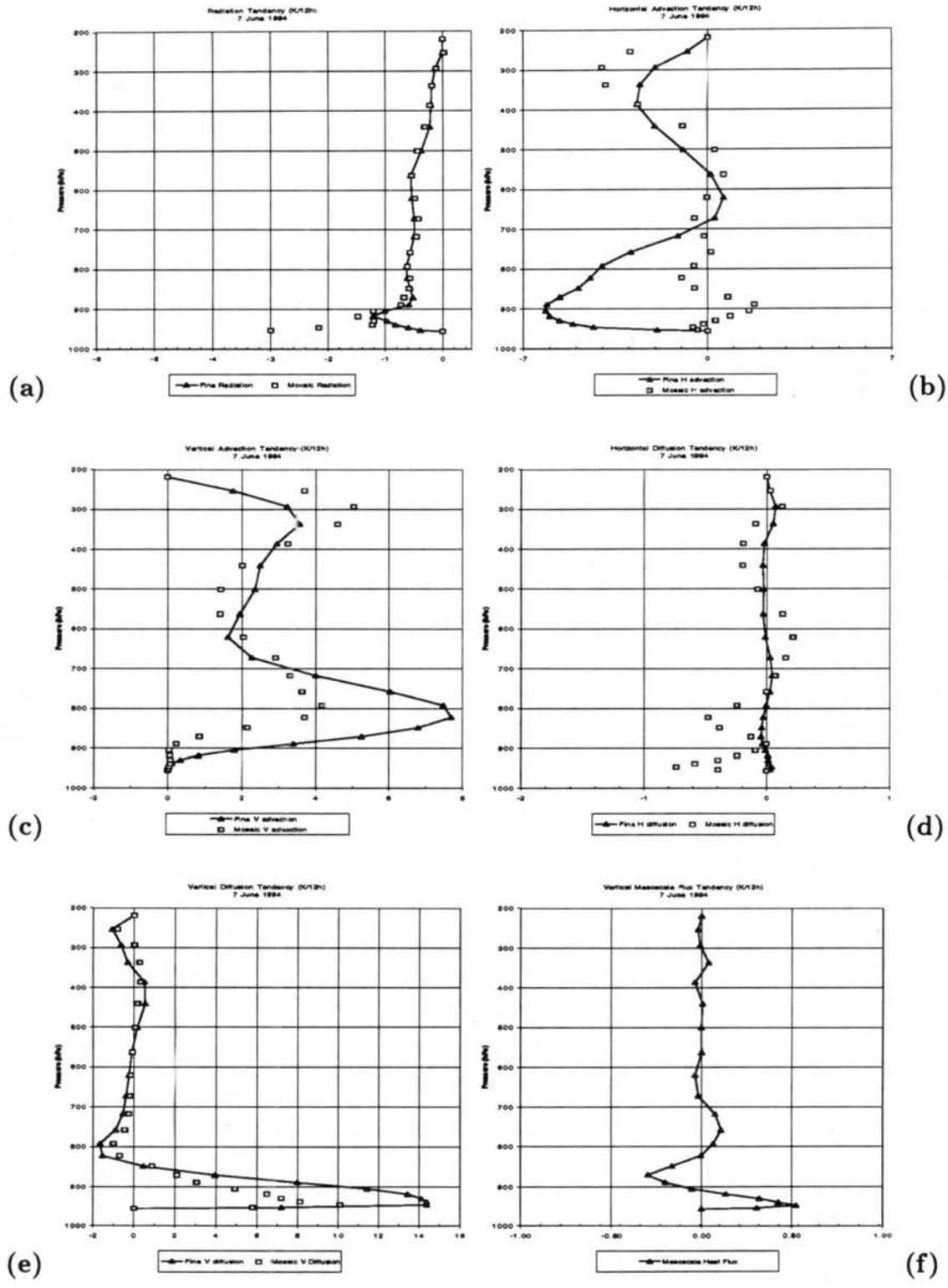

Figure 6.26: The RAMS accumulated temperature tendencies for 11-23 UTC, 7 June 1994: a) radiative tendency, b) horizontal advection tendency, c) vertical advection tendency, d) horizontal diffusion tendency, e) vertical diffusion tendency, f) vertical mesoscale flux tendency. Values are in K/12 hours. The values for the fine-scale run are connected by a black line.

wave in the horizontal convergence due to topography. In order to verify this hypothesis, we have plotted a vertical cross section of the vertical velocity at the latitude of Candle Lake, over the domain of grid 2. This is shown in Fig. 6.27. Clearly the vertical velocity is alternating in sign all the way to the tropopause with maximum strength at the center of Candle Lake.

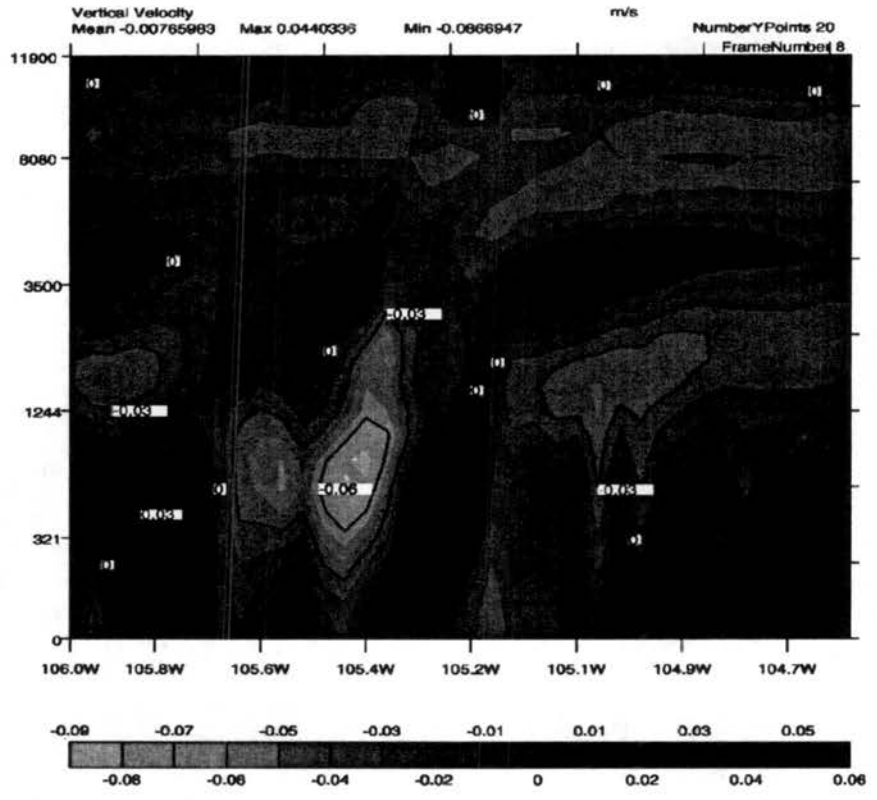

Figure 6.27: Fine-grid run: vertical cross section of vertical velocity over Candle Lake for RAMS grid 2, 18 UTC, 7 June 1994 at the latitude of Candle Lake. Contour interval of 0.03 m^{-1}. Tick marks are in decimal degrees. Candle Lake is at the center of the domain.

The 12 hour temperature tendency due to the vertical mesoscale flux, in this case, is the least of all three cases in magnitude, as expected from the higher predominant winds and from the less intense lake breeze, although retaining more structure in its vertical profile as expected from the analytical guidance.

6.5 A Lower Winds Case: 20-22 June 1994

This day was selected, although not a golden day, because of the need to investigate a day with lower wind speeds and also because of the noticeable CBL development reported by the wind profiler array (see Fig 6.28: the development appears to be the result of a sequence of days in which the CBL grew undisturbed by day, was then left over the nocturnal inversion as a residual layer, to then be reconnected on the following day as soon as the nocturnal layer was eroded).

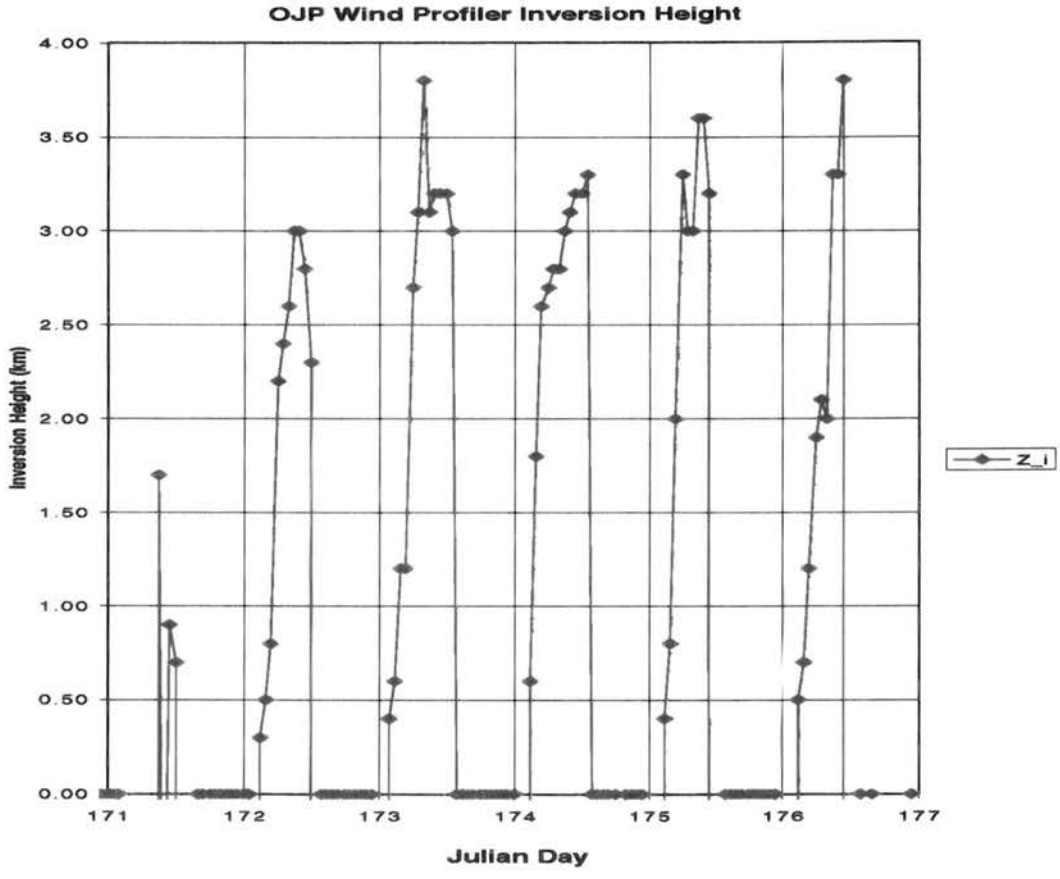

Figure 6.28: The OJP wind profiler inversion heights for 20-26 June 1994.

The synoptic situation on this day depicted in the four panel Fig. 6.29 was remarkably uneventful, with weak south-southwesterly flow near the SSA, about 10 m s^{-1} at 850 hPa.

The upper air showed a similar situation, with flow very much zonal and weak over the domain. The average vertical velocity over the day, for this region, was of -0.020 m s^{-1}.

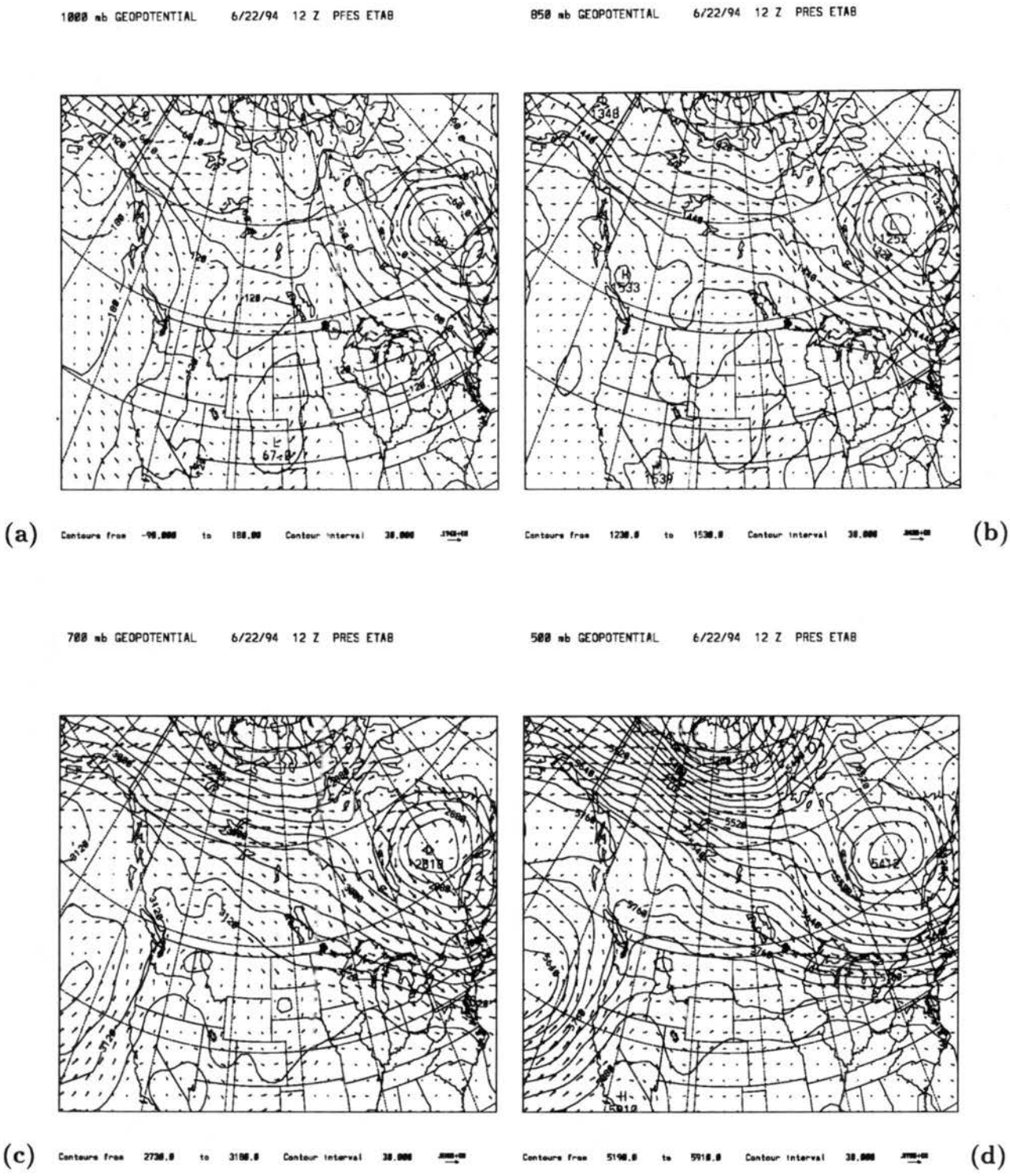

Figure 6.29: The 12 UTC ETA analysis for 22 June 1994: a) 1000 hPa geopotential height (m) and winds (m s^{-1}); b) 850 hPa geopotential height (m) and winds (m s^{-1}); c) 700 hPa geopotential height (m) and winds (m s^{-1}); d) 500 hPa geopotential height (m) and winds (m s^{-1})

No sounding was available for this day within the BOREAS domain or even within a 1000 km radius. The only information on the vertical atmospheric structure we have is from the wind profiler and from the ETA initialization. Both of them agreed that a very deep and dry CBL developed over a period of three days, to reach 3000 m on the day we analyzed.

The 22 June 1994 case was simulated by initializing the model on 21 June at 00 UTC (20 June, 18.00 Local Time) and running RAMS for 60 hours. The temperature of the Candle Lake water for 21-23 June 1994 was set at 281 K. Soil temperature and moisture profiles were initialized using information from the and the AES networks on 21 June.

No data for validation was present on this day, as it was not part of any IFC; nonetheless, after two successful simulations, we felt confident enough in the model capabilities to exercise it for this case.

6.5.1 Fluxes in Grid 1 ($\Delta x = 10$ km)

As in the previous two cases, the grid 1 integration was carried out in two fashions by specifying the land cover over each grid cell at two different horizontal grid interval spacings, with maximum resolutions of 40 km for the coarse grid (mosaic run) and 2.5 km for the fine grid (grid 3).

In both cases, RAMS was initialized and nudged using the ETA analysis. For the fine-grid run, after one complete diurnal cycle, grids 2 and 3 were spawned and surface-atmosphere fluxes at these finer scales were explicitly calculated for a second, complete diurnal cycle. The coarse grid run used the mosaic specification of the surface physiography.

Again the coarse-grid run produced slightly higher domain average surface sensible heat fluxes (differences of about 25 W m^{-2}) than the fine-grid run as in the previous two cases. It was possible to confirm that locally, e.g. in the Candle Lake (105.3W, 53.8N) and Montreal Lake regions, the coarse grid run produced patches of flux minima whereas the fine grid run produced sharper flux gradients between lake and forest. This is indicative of the different impact of a 'fully resolved' versus a 'mosaic' treatment of local surface flux gradients and the associated near-surface wind circulations.

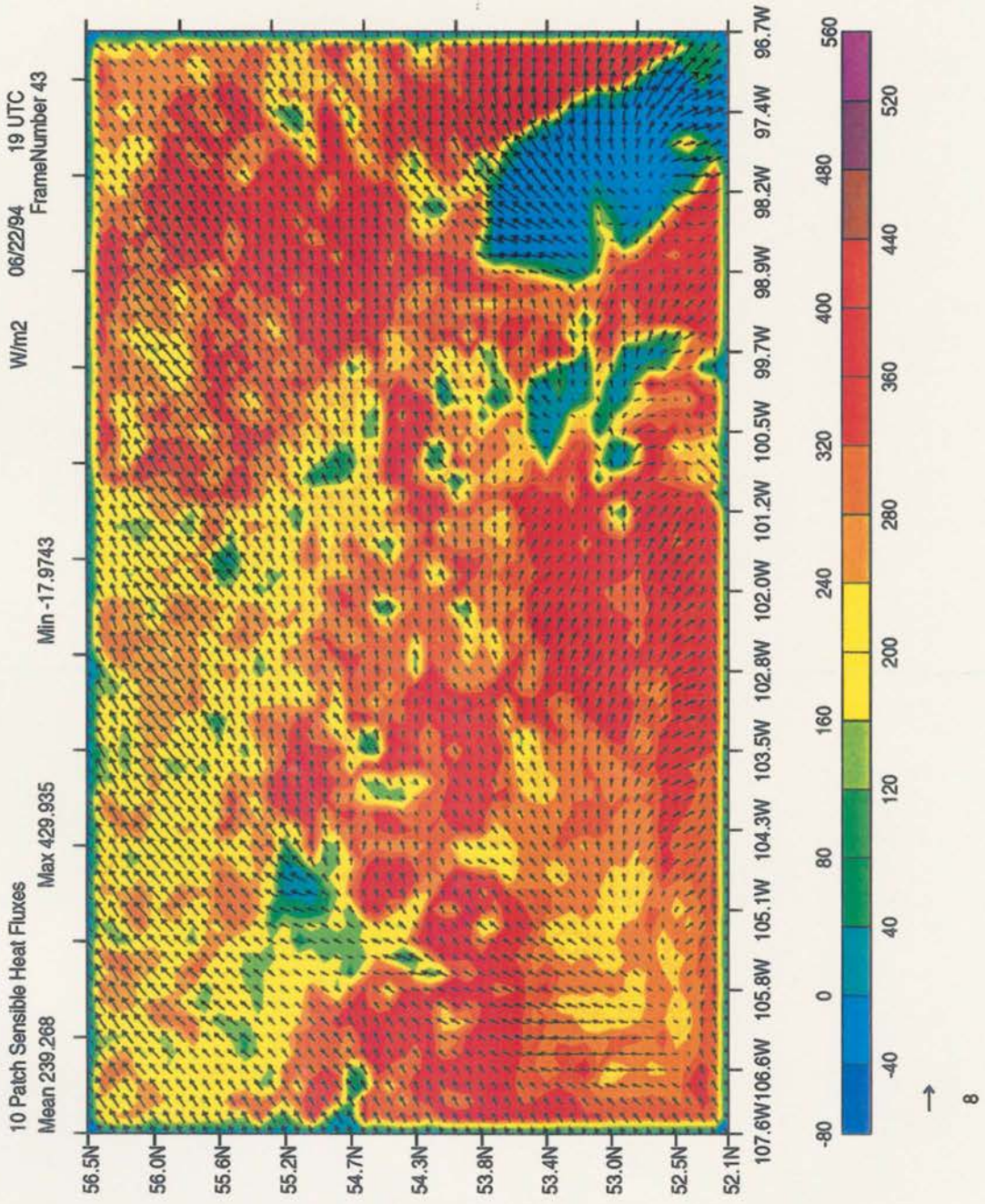

Figure 6.30: Coarse-grid run: the grid 1 surface sensible heat fluxes (W m^{-2}) at 19 UTC, 22 June 1994 and the near-surface (60 m) wind vectors. The color field and color bar represent the turbulent sensible heat flux. Tick marks are in decimal degrees.

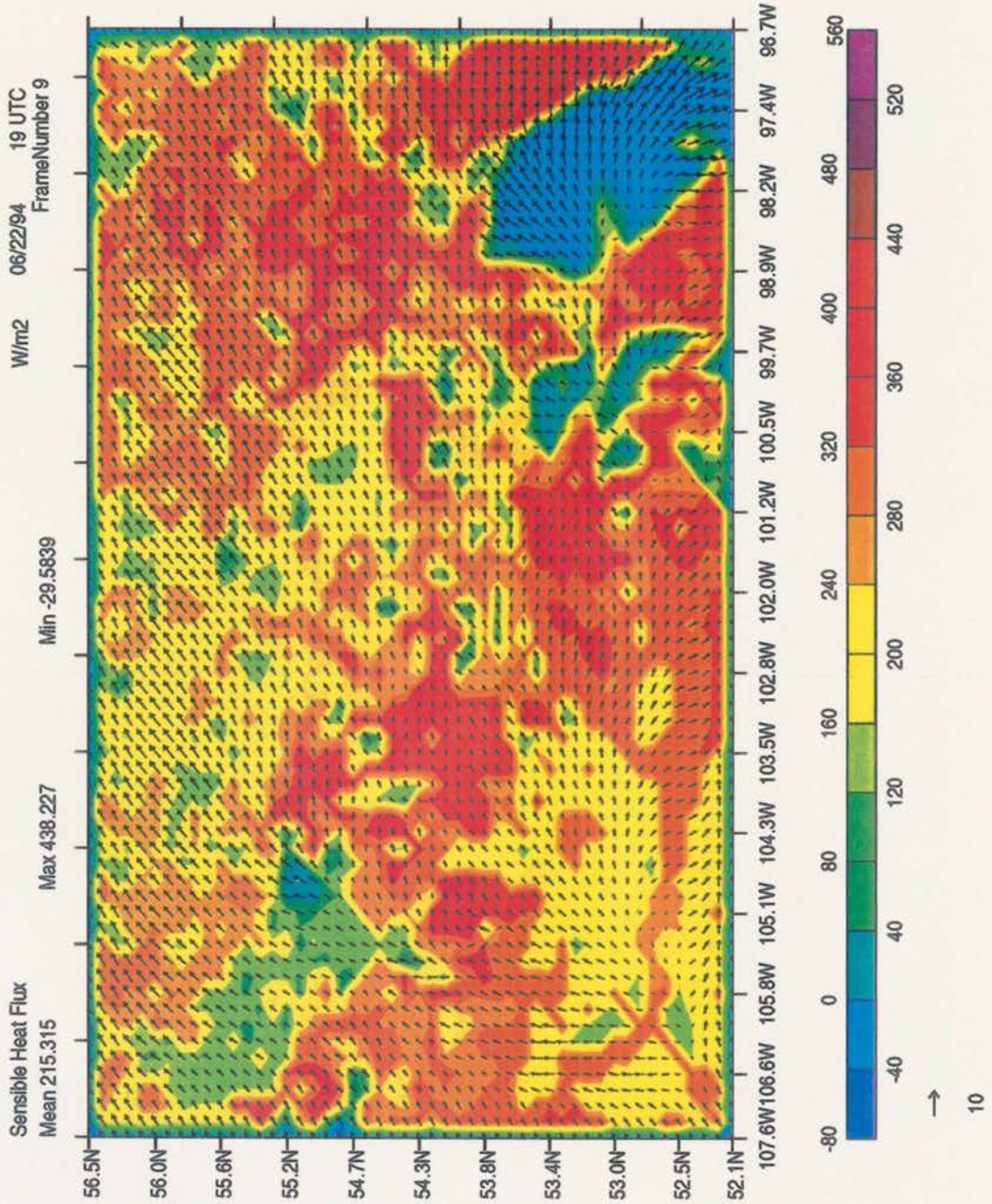

Figure 6.31: Fine-grid run: the grid 1 surface sensible heat fluxes (W m^{-2}) at 19 UTC, 22 June 1994 and the near-surface (60 m) wind vectors. The color field and color bar represent the turbulent sensible heat flux. Tick marks are in decimal degrees.

6.5.2 Results for Grid 3 (Δx = 625 m): The Candle Lake Breeze

Grid 3 was spawned around Candle Lake with the purpose of resolving possible lake-induced circulations. After one full diurnal cycle, the model developed a well defined lake breeze, identifiable in Fig. 6.32 (depicting vertical velocity at 1250 m), with a subsiding cell (-0.30 m s^{-1}) near the lake center and maximum ascending motion (0.30 m s^{-1}) at the north-west and SW banks of the lake. The downward motion region revealed a shape and position that confirmed the influence of Candle Lake. The positive vertical velocity regions were distributed over the land around the lake, although shifted by the southwesterly winds.

A lake-induced circulation was also observed at night (22 June, 06 UTC, Fig. 6.33), with ascending motion (0.06 m s^{-1}) over the eastern part of the lake and descending motion (a minimum of -0.06 m s^{-1}) around the lake boundaries. Most of the ascending motion over the central part of the lake was shifted eastward by the prevailing winds.

Superimposed on the lake breeze, the previous discussion of the wind fields pointed to contributions by the local orography. The evidence of this influence on 21 June was that the surface winds turned towards the SE (downslope) as the nocturnal cooling was initiated (not shown). The nocturnal land breeze displayed an ascending cell over the east bank of the lake, illustrating how the prevailing flow shifted the convergence zone towards the N-NE. Another indication of the occurrence of this enhanced nocturnal convergence at low levels is that the vertical velocity in the nocturnal ascending cell had a considerably larger areal extent than the one during the daylight.

6.5.3 Model Average Sounding and Diurnal Cycle Heating

As in the previous cases, we calculated horizontal averages of the vertical potential temperature (θ) profile for a region of 40 km around grid 3. The diurnal vertical temperature change curves are shown in Fig. 6.34.

This day presented very strong warming throughout the troposphere for both simulations. The value is consistent with the vertical velocity and the potential temperature profile in the ETA analysis, which implies about 5 K maximum warming in the column for the period.

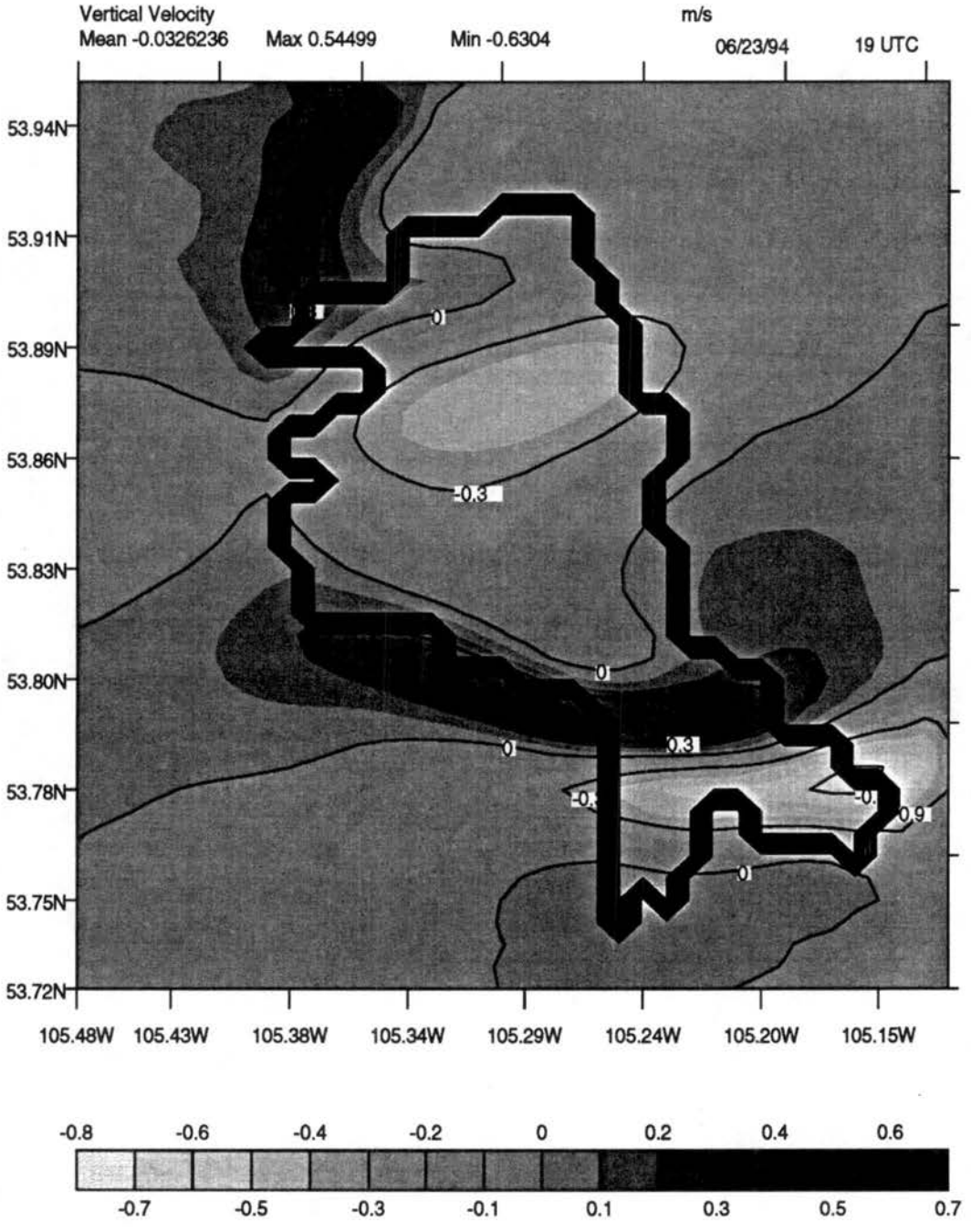

Figure 6.32: Fine-grid run: horizontal cross section of vertical velocity over Candle Lake for RAMS grid 3, 19 UTC, 22 June 1994 at 1250 m. Contour interval of 0.06 m^{-1}. Tick marks are in decimal degrees

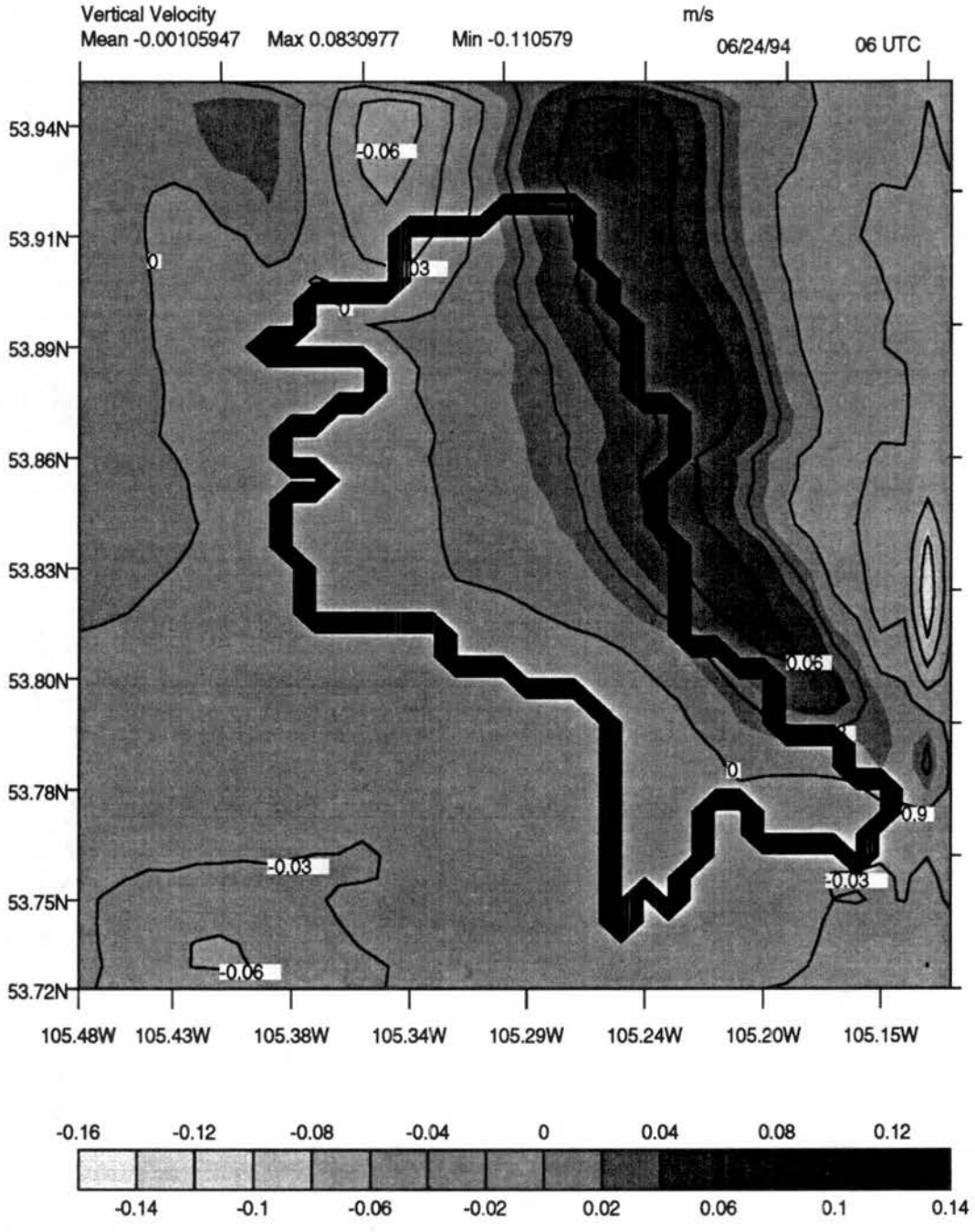

Figure 6.33: Fine-grid run: horizontal cross section of vertical velocity over Candle Lake for RAMS grid 3, 06 UTC, 22 June 1994 at 1250 m. Contour interval of 0.06 m^{-1}. Tick marks are in decimal degrees

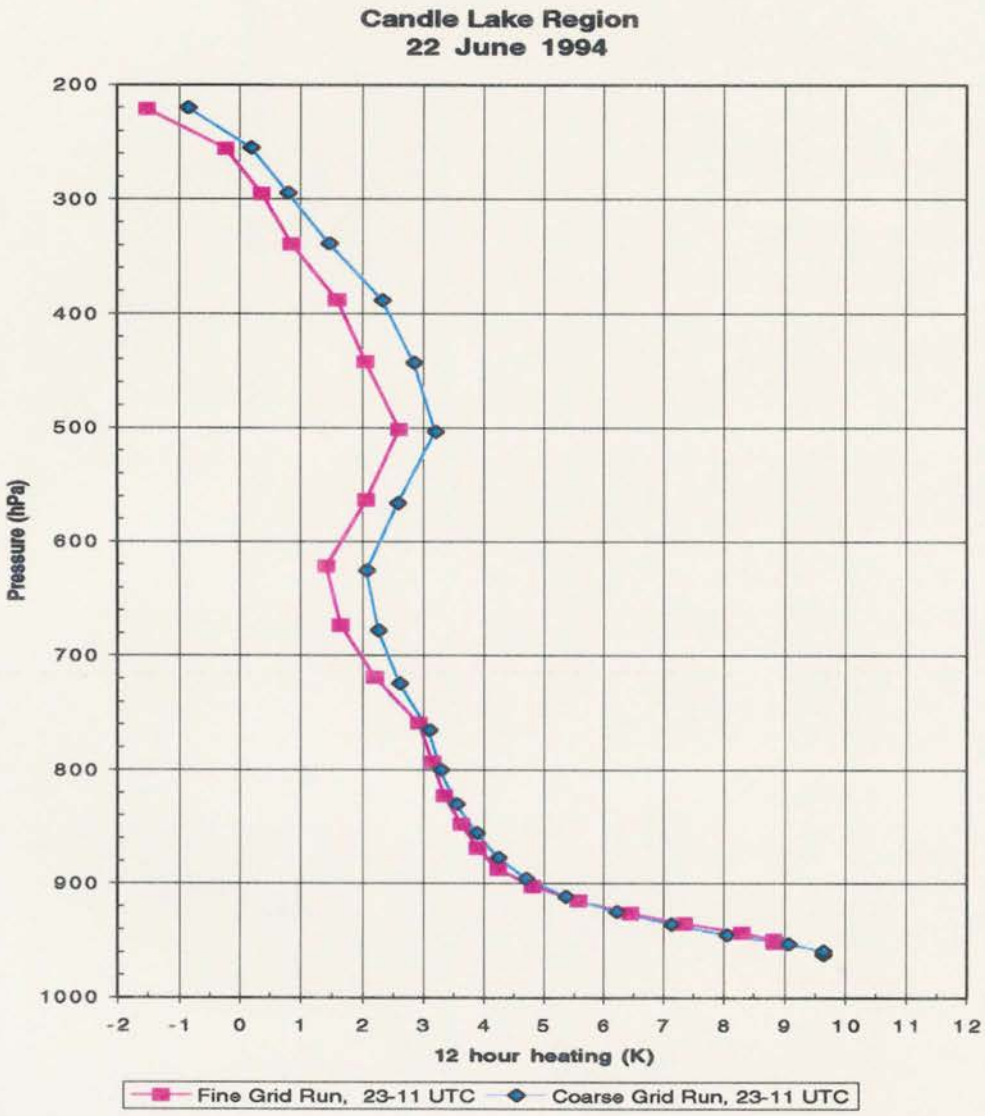

Figure 6.34: The Candle Lake diurnal temperature change from the Candle Lake sounding and the model runs, 22 June 1994 11-23 UTC.

The comparison between the coarse-grid and the fine-grid diurnal ΔT patterns shows a different pattern than the one observed in the previous two cases. The deep CBL developed very similar warming between the two runs, while differences arise above the CBL, where the fine grid run shows consistently less warming than the coarse grid run.

Once more, we looked at tendencies from the model in order to understand what caused the differences. The 12 hour radiation tendency for both simulations resembled the previous cases: the lowest model level displayed extra cooling for the coarse grid run.

The horizontal advection again showed how the fine-scale run has a tendency to warm less than the coarse-scale run, both at lower and upper levels. The vertical advection tendency shows almost 1 K more warming for the fine-scale run within the CBL, then less warming at higher levels. The two advection tendencies very much compensate each other, as in the previous cases, so that we do believe the differences in the two runs to be also caused by a perturbation in vertical velocity due to features with scales larger than 40 km.

The horizontal diffusion is once more enhanced by the different horizontal mesh sizes, with a stronger cooling tendency near the surface in the coarser resolution case. The vertical diffusion tendency confirms how the surface fluxes are enhanced in the fine-scale run, with lake air advection as the cause, and how the CBL is warmed through a slightly deeper layer in its lower portion.

The 12 hour vertical mesoscale flux tendency, in this case, is the most pronounced, with the same vertical profile seen before: a positive near surface value of nearly 3 K in 12 hours and a deep cooling layer between 880 and 680 hPa, then a warming layer up to 500 hPa and another cooling layer between 500 and 400 hPa. This vertical pattern points to a wavy regime. While less of an open circulation was expected in this case, because of the lower predominant winds, the lake breeze is a stronger feature, so that it is capable of forcing a stronger vertical response.

6.6 Summary

We have analyzed numerical fields of surface fluxes of sensible and latent heat, and the circulations induced by them. These horizontal sensible heat patterns were forced

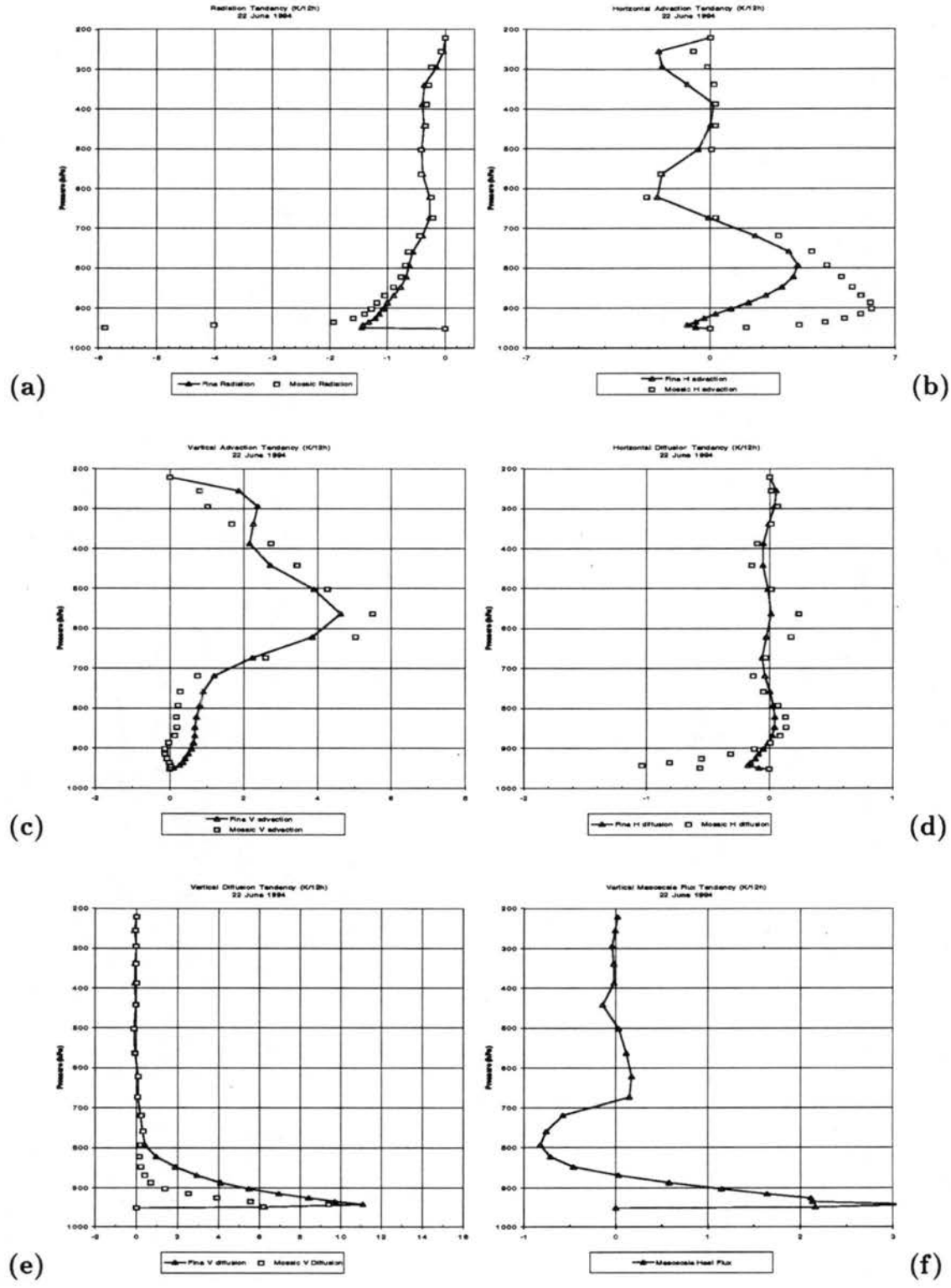

Figure 6.35: The RAMS accumulated temperature tendencies for 11-23 UTC, 22 June 1994: a) radiative tendency, b) horizontal advection tendency, c) vertical advection tendency, d) horizontal diffusion tendency, e) vertical diffusion tendency, f) vertical mesoscale flux tendency. Values are in K/12 hours. The values for the fine-scale run are connected by a black line.

by imposing surface boundary conditions derived from remotely sensed data sets that were constructed for the BOREAS campaign, using the guidance of scaling criteria that were established through atmospheric dynamics principles. We have found that both the physiography and the surface heat fluxes do in fact exhibit organized patchiness that would be within the size interval necessary to generate mesoscale circulations, mainly due to lake-forest contrasts. The RAMS-LEAF-2 coupled model, using biophysical characteristics of the land surface from BOREAS data sets, was able to capture the surface turbulent flux variability across a portion of the BOREAS region with reasonable accuracy, without the need for special calibration. Once this capability was established, there is more confidence that the circulations generated by the model can be trusted to be representative of the local effects of the surface heterogeneity on the atmosphere. We have found that integrating the model in two different fashion, a) with a mosaic representation of fluxes under the 40 km scale, and b) with full resolution of the mesoscale (within a smaller domain), results in different vertical 12-hour temperature change patterns over the course of the diurnal cycle within a 40 by 40 km region. This region contains most of the BOREAS point measurement sites, so that the regional representativeness of data collected at those sites might need to be re-interpreted.

Chapter 7

CONCLUSIONS AND FUTURE WORK/FUTURE APPLICATIONS

We have investigated the problem of how to correctly produce maps of surface sensible and latent heat fluxes that are representative of the BOREAS region. We approached this problem from several directions, including evidence from measurements taken during the field campaign and also exercising analytical and numerical tools by forcing them with data from two of the IFCs.

We find that, in general, the ideas developed within our research group in the past are applicable in this context and were useful for guidance and interpretation.

In Chapter 4 we addressed some of the research problems in BOREAS, mainly the strategy for the upscaling of surface measurements, which can be linear or physically-based, using an atmospheric model as a complex interpolator. We have seen aircraft data evidence that mesoscale processes are probably in place around lakes, enhancing the surface fluxes through horizontal advection over an influence region surrounding those negative flux regions (for sensible heat, positive for moisture and carbon), and breaking the linear upscaling assumptions.

We have found, in Chapter 5, that this region is potentially the theater of mesoscale circulations that are forced by landscape heterogeneity, resulting principally in lake-forest heating gradients, that have lifetimes of several hours and spatial scales of the order of 100 km. We have also found that these effects are indeed more pronounced at lower predominant wind speeds, in which regime they affect the BL almost exclusively, but that, under higher synoptic winds, they cannot be dismissed, since they are capable of forcing vertical gravity-inertia waves that influence the higher atmosphere. We have also used the analytical tools to specify scales for the numerical simulations, so that numerical grids could be deployed over the region with some theoretical justification.

We have also learned that the key relationship for scaling is the one between patch scale, surface forcing gradient magnitude and predominant wind speed. At lower wind speeds, small patches with large heating gradients are sufficient to generate a significant mesoscale circulation. At large wind speeds, heating gradients can be diluted even for large patches, but hilly terrain can be effective in generating local vertical circulations.

In Chapter 6 we have used a regional vegetation classification, developed for BOREAS, in order to define the surface boundary conditions in our coupled numerical model, RAMS-LEAF-2. The performance of this tool, as modified for this task, was good, given the generality of the approach. For instance, we decided against calibration, and we retained the AVHRR product as the sole remotely sensed forcing product, so that we could assess the usefulness of a type of data set that is available to modelers at present. With this limitation, we found the AVHRR product, used in conjunction with detailed ancillary data sets, to be immensely useful for the correct definition of the surface forcings, even at the rather coarse resolution of 2-3 km. It must be remembered, however, that the availability of such ancillary data sets is somehow exceptional, and the same kind of modeling exercise might not be so successful over, for instance, the Siberian boreal forest, for which we are limited by BATS classes (2 conifer types, 2 deciduous types to cover thousands of km^2) and 'global' parameters. For this reason the general applicability of future RS products from the Earth Observing System (EOS) seem very attractive.

We have found that the surface heating gradient between Candle Lake and the surrounding forest exceeds 400 W m^{-2} in all simulated cases at its peak, and about 300 W m^{-2} on a daily average, a magnitude sufficient to generate a lake breeze over most days. We have also been able to confirm, through data analysis and numerical simulations, that this lake breeze is capable of influencing the surface fluxes at the lake boundaries, increasing the Bowen ratio on a rim of forest around the lake.

The relative contributions of mesoscale (due to the Candle Lake breeze, because of our averaging choices) and turbulent fluxes of sensible heat, expressed as temperature tendencies, confirm that the former are more important under lower predominant winds within the CBL, but that under strong winds they can exceed the magnitude of turbulent fluxes above the inversion height.

We have found that we cannot reject the hypothesis that mesoscale circulations need to be included in the total HWM flux calculations, even under significant synoptic-scale winds. Furthermore, we have to reject the hypothesis that sub-grid HWM budgets can be linearly upscaled to mesh sizes of hundreds of km over regions of high surface heterogeneity such as BOREAS. This rejection is supported by our calculation of the differences in diurnal warming magnitude and profile between the two methods (linear and physically based).

We find that we could not reject the second sub-hypothesis, given the field and simulations evidence that surface fluxes are enhanced near strong gradients in surface heterogeneity. It is also important to mention that agreement between the observed and modeled diurnal inversion heights was achieved only after the inclusion of the cold roots effect.

7.1 Implications for NWP, GCM Modeling, Regional Climate Modeling and Future Model Design

The work presented here implies that mesoscale processes should be parameterized over regions of high surface heterogeneity, such as BOREAS. While the off-line models are performing rather well in reproducing single point measurements (although always with local calibration), the same is not immediately true as soon as these models are 'bolted' into a three-dimensional, large-scale atmospheric model.

7.1.1 Scaling Lessons

We have seen how averaging fluxes linearly fails when mesoscale effects are significant. In order for realistic scaling rules to be produced, however, more case studies need to be completed, particularly in the very low wind speed range. These case studies should be simulated with a version of the model that includes a more sophisticated turbulence parameterization, and at least one of them should be run in a LES mode, so that the mechanism for the vertical transfer of heat can be better evaluated. At this time, the three-way relationship between patch size, heating gradient size and wind speed seems to be the most needed tool for the upscaling decisions to be made for BOREAS data sets.

7.2 Future Work

The work presented here needs to be continued in many directions. At least two main avenues are clear at this point, and both are important for the confirmation of the results so far achieved. To begin with, as mentioned above, a more detailed validation campaign needs to be undertaken, with close help from the aircraft investigators that were involved in the field campaigns and data from the 1996 campaigns. This will help to build more confidence in the model capabilities and will address some of the aircraft-tower intercomparison issues, together with the definition of footprints for each instrument.

Several recent improvements to our atmospheric model, for instance the new radiation parameterization (Harrington 1997) , the new soils (van Genuchten 1980), but most of all a stomatal closure scheme based on carbon assimilation (SiB2, Sellers et al. 1996), will allow us to produce maps of carbon fluxes at very fine scales, in order to better understand the spatial variability of carbon and feedbacks from ecological processes (e.g. test the CO_2 hypothesis of Sun et al. 1997b and the diurnal rectifier effect of Denning et al. 1996a, b).

We also need to implement a more sophisticated turbulence parameterization that will allow us to:

1. Simulate the Candle Lake breeze with much finer resolution, in LES mode, in order to address the issue of the sonde footprint;

2. Explore the finer details of the Candle Lake breeze and its influence on measurement sites;

3. Simulate entrainment effects (and countergradient effects in general);

4. Use the Thematic Mapper (TM) vegetation classification at 30 m resolution (Hall et al. 1997), without the need to develop aggregation rules disconnected from atmospheric dynamics.

In a second, synthesis phase, model and data analysis are needed in order to explore intra and inter-seasonal time scales over the full BOREAS domain, so that the role of

the BOREAS ecosystem in the climate context can be better defined. We have partially started on this avenue, using NCEP re-analysis data to try and identify a mesoscale thermal signature over grid points that cover most of the North American boreal forest. We have already run this analysis, correlating results with surface heterogeneity, but uncertainties in some of the budget terms are still preventing us from presenting it at this time. Because the problems we have encountered in this analysis are linked to the physics of the model used for the NCEP re-analysis (which is still not capable of representing surface processes over BOREAS in a realistic fashion), we are also planning on supplementing it with time series of satellite radiances, which might be a more direct method to test our synthesis hypotheses.

From the numerical modeling point of view, we plan to perturb the surface conditions (with the support of the BIOME-BGC group at the University of Montana) and run hypothetical study cases (with limited duration) in the following fashion:

- high and low fractal dimension landscape (resulting from different aggregation rules of the surface heterogeneity, through relative abundance thresholds in the mosaic composition);
- stressed and unstressed vegetation conditions (simulating possible extreme growing season conditions in different years);
- different specification of biophysical parameters, as defined from remote sensing, and as defined from linear extrapolation of surface surveys;
- synthetic definition of surface vegetation cover, through an artificial expansion and an artificial reduction of the biome occupied by the Boreal Forest;
- substitution of the areas influenced by human activities (agriculture, logging) with the natural vegetation state, to explore the issue of modification to the local climate due to the progression of human intervention.

7.2.1 New RS Products and Numerical Modeling

Another exciting future research theme is the exploration of special RS products that represent a preview of what will be available operationally in the next few years, as soon as some of the EOS platforms become available.

During the past work for BOREAS we have acquired robust GIS capabilities and we have created a RS repository for use in RAMS. Vegetation classifications (coming from AVHRR or TM data), soil maps and LAI maps are among the products we have used intensely, especially to supplement the point observations available inside the Study Areas. By processing these images, we confirmed the existence of a strong correlation between soil type and vegetation class, which helped complete our physiography data base, but we also noticed other features that seem worth exploring.

Figure 7.1 shows a map of water bodies and of disturbance regions (mainly burn scars) for the BOREAS domain. There seems to be an association between lakes and large burn scars in the NE part of the domain. The working hypothesis (also justified by our linear studies) is that lakes in that region are sufficiently large to produce solenoidal circulations which may phase-lock a portion of the convection and may alter the areal distribution of lightening discharges, hence influencing the positioning of the burned regions (Knowles 1993). A further positive feedback may be in place, in that the disturbed regions display higher sensible heat fluxes than the forested regions, thus, creating a stronger heating gradient between lake and land.

These hypotheses need to be initially explored by statistical analysis of the images (spatial coherence analysis) and also through time series of cloudiness and of precipitation at different points over the domain. This can be accomplished by analyzing the visible images acquired during the BOREAS campaign.

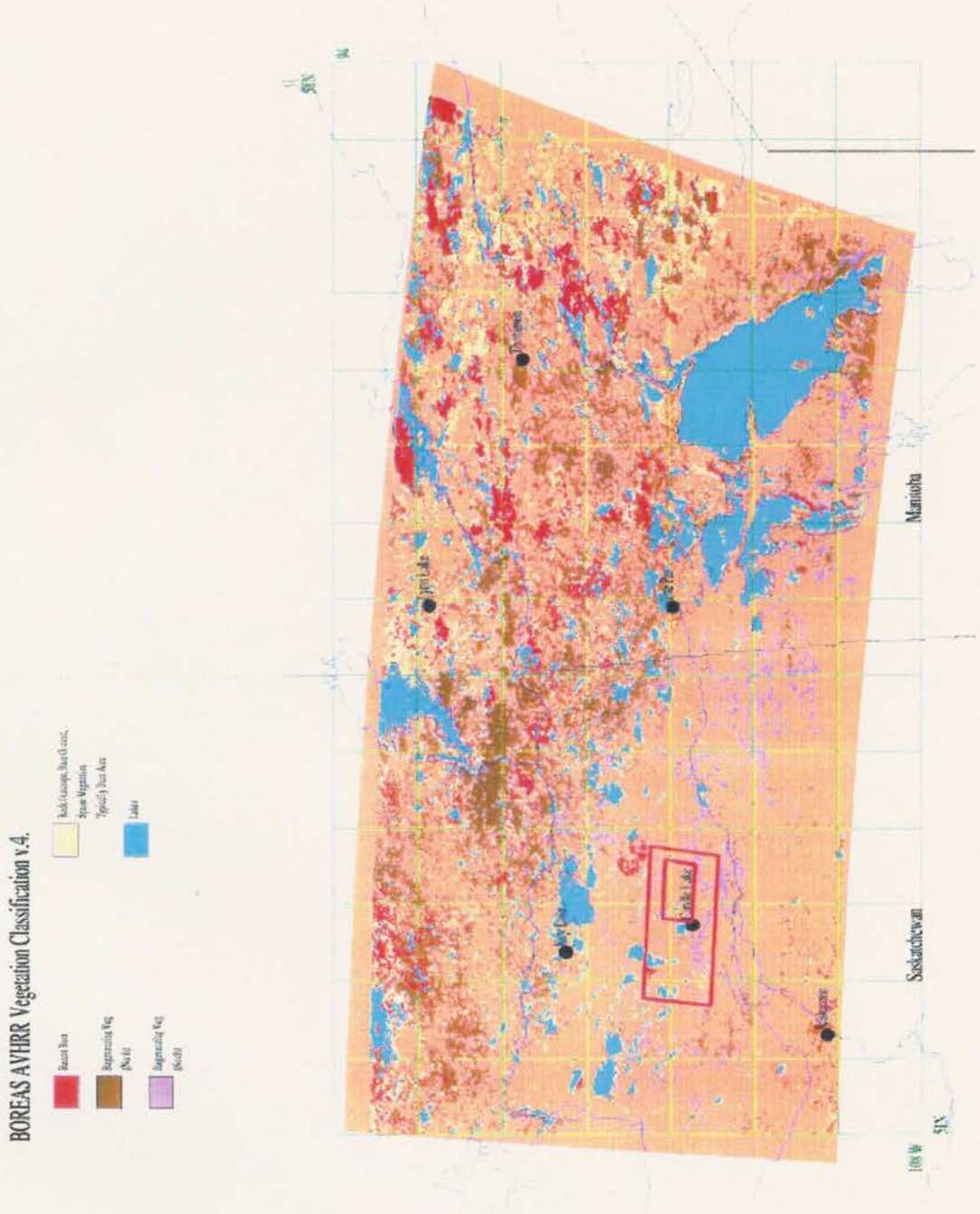

Figure 7.1: Data from the AVHRR classification of Steyaert et al. (1997), illustrating the spatial distribution of recent burns and lakes over BOREAS. The pixel size is 1 km.

REFERENCES

Anderson, J.R., E.E. Hardy, J.T. Roach, and R.E. Witmer, 1976: A land use and land cover classification system for use with remote sensor data. U.S. Geological Survey Professional Paper 964, Reston, Virginia, USGS.

André, J.-C., P. Bougeault, J.-F. Mahfouf, P. Mascart, J. Noilhan, and J.-P. Pinty, 1989a: Impact of forests on mesoscale meteorology. *Phil. Trans. Roy. Soc. London*, **324**, 407-422.

André, J.-C., J.P. Goutorbe, T. Schmugge, and A. Perrier, 1989b: HAPEX-MOBILHY: Results from a large-scale field experiment. In: *Remote sensing and large-scale global processes*, A. Rango, Ed., Wallingford, UK, International Association of Hydrological Sciences, 13-20.

Avissar, R. 1995: Recent advances in the representation of land-atmosphere interactions in general circulation models. *Rev. Geophys.*, Supplement to Volume 33, Part 2, US National Report 1991-1994, 1005-1010.

Avissar, R. and F. Chen, 1993: Development and analysis of prognostic equations for mesoscale kinetic energy and mesoscale (subgrid-scale) fluxes for large-scale atmospheric models. *J. Atmos. Sci.*, **50**, 3751-3774.

Avissar, R., and Y. Mahrer, 1988: Mapping forest-sensitive areas with a three-dimensional local-scale numerical model. Part I: Physical and numerical aspects. *J. Appl. Meteor.*, **27**, 400-413.

Avissar R. and R.A. Pielke, 1989: A parameterization of heterogeneous land surfaces for atmospheric numerical models and its impact on regional meteorology. *Mon. Wea. Rev.*, **117**, 2113-2136.

Ball, J.T., 1988: An analysis of stomatal conductance. Ph.D. thesis, Stanford University, 89 pp.

Balling, R.C., Jr., 1988: The climatic impact of a Sonoran vegetation discontinuity. *Climatic Change*, **13**, 99-109.

Banta, R.M. and R.T. McNider, 1997: Intra-regional variability of mixing height during the 1995 Southern Oxidants Study near Nashville, Tennessee. *12th Symposium on Boundary Layers and Turbulence*, Vancouver, British Columbia, July.

Beljaars, A.C.M., and A.A.M. Holtslag, 1991: Flux parameterization over land surfaces for atmospheric models. *J. Appl. Meteor.*, **30**, 327-341.

Belward A.S., and T.R. Loveland., 1995: The IGBP-DIS 1 km land cover project: Remote sensing in action. *Proc. 21st Annual Conference of the Remote Sensing Society*, Southampton, United Kingdom, 1099-1106.

Betts, A.K., and J.H. Ball, 1997: Albedo over the boreal forest. *J. Geophys. Res.*, **102**, 28901-28909.

Betts, A.K., and A.C.M. Beljaars, 1993: Estimation of effective roughness length for heat and momentum from FIFE data. *Atmos. Res*, **30**, 251-261.

Betts, A.K., J.H. Ball, and A.C.M. Beljaars, 1993: Comparison between the land surface response of the European Centre model and the FIFE 1987 data. *Quart. J. Roy. Meteor. Soc.*, **119**, 975-1001

Betts, A.K. S.-Y. Hong, and H.-L. Pan, 1996: Comparison of NCEP/NCAR reanalysis with 1987 FIFE data. *Mon. Wea. Rev.*, **124**, 1480-1498.

Betts, A.K., F. Chen, K. Mitchell, and Z. Janjic, 1997a: Assessment of land-surface and boundary layer models in 2 operational versions of the Eta Model using FIFE data. *Mon. Wea. Rev.*, **125**, 2896-2916.

Betts, A.K., J.H. Ball, B.J. Smith, and S.R. Shewchuk, 1997b: Comparison of BOREAS and Atmospheric Environment Service humidity sensors at Meadow Lake, Saskatchewan. *J. Geophys. Res.*, **102**, 28911-28913.

Betts, A.K., P. Viterbo, and A.C.M. Beljaars, 1998: Comparison of the land-surface interaction in the ECMWF reanalysis model with the 1987 FIFE data. em Mon. Wea. Rev., **126**, 186-198.

Beven, K.J., 1982: On subsurface stormflow: an analysis of response times. *Hydrol. Sci. Journal*, **27**, 505-521.

Beven, K.J., 1984: Infiltration into a class of vertically non-uniform soils. *Hydrol. Sci. Journal*, **29**, 424-434.

Beven, K.J., and M.J. Kirkby, 1979: A physically based, variable contributing area model of basin hydrology. *Hydrolog. Sci. Bull.*, **24**, 43-69.

Black, T.L., 1994: The new NMC mesoscale Eta model: Description and forecast examples. *Wea. Forecasting,* **9**, 265-278.

Blackadar, A.K., 1962: The vertical distribution of wind and turbulent exchange in a neutral atmosphere. *J. Geophys. Res.*, **67**, 3095-3102.

Bolle, H.-J., J.-C. André, J.L. Arrue, H.K. Barth, P. Bessemoulin, A. Brasa, H.A.R. de Bruin, J. Cruces, G. Dugdale, E.T. Engman, D.L. Evans, R. Fantechi, F. Fiedler, A. van de Griend, A.C. Imeson, A. Jochum, P. Kabat, T. Kratzsch, J.-P. Lagouarde, I. Langer, R. Llamas, E. Lopez-Baeza, J. Miralles, L.S. Muniosguren, F. Nerry, J. Noilhan, H.R. Oliver, H.R. Roth, S.S. Saatchi, J. Diaz, M. de Santa Olalla, W.J. Shuttleworth, H. Sogaard, H. Stricker, J. Thornes, M. Vauclin, and D. Wickland, 1993: EFEDA: European Field Experiment in a Desertification threatened Area. *Ann. Geophys.*, **11**, 173-189.

Bonan, G.B., D. Pollard, and S.L. Thompson, 1993: Influence of subgrid-scale heterogeneity in leaf area index, stomatal resistance, and soil moisture on grid-scale land-atmosphere interactions. *J. Climate*, **6**, 1882-1897.

Chen F. and R. Avissar, 1994: Impact of land-surface moisture variabilities on local shallow convective cumulus and precipitation in large-scale models. *J. Appl. Meteor.*, **33**, 1382-1394.

Chen, J.M., and J. Cihlar, 1996: Retrieving leaf area index in boreal conifer forests using Landsat TM images. *Remote Sens. Environ.*, **55**, 153-162.

Clark, C.A. and R.W. Arritt, 1995: Numerical simulations of the effect of soil moisture and vegetation cover on the development of deep convection. *J. Appl. Meteor.*, **34**, 2029-2045.

Coughlan, J.C., 1994: Preliminary results from the terrestrial modeling exercise for the BOREAS Experiment. American Geophysical Union, Fall 1995.

Collins, D.C. and R. Avissar, 1994: An evaluation with the Fourier Amplitude Sensitivity Test (FAST) of which land surface parameters are of greatest importance in atmospheric modeling. *J. Climate*, **7**, 681-703.

Cotton, W.R. and R.A. Pielke, 1995: *Human Impacts on Weather and Climate*, Cambridge University Press, New York, 288 pp.

Dalu, G.A. and R.A. Pielke, 1993: Vertical heat fluxes generated by mesoscale atmospheric flow induced by thermal inhomogeneities in the PBL. *J. Atmos. Sci.*, **50**, 919-926.

Dalu, G.A., R.A. Pielke, R. Avissar, G. Kallos, M. Baldi, and A. Guerrini, 1991: Linear impact of thermal inhomogeneities on mesoscale atmospheric flow with zero synoptic wind. *Ann. Geophys.*, **9**, 641-647.

Dalu, G.A., R.A. Pielke, M. Baldi, and X. Zeng 1996: Heat and momentum fluxes induced by thermal inhomogeneities. *J. Atmos. Sci.*, **53**, 3286-3302.

Dalu, G.A., R.A. Pielke, P.L. Vidale, and M. Baldi, 1998: Diabatic heat transport and weakening of the static stability induced by mesoscale flows. In preparation.

Davies, H.C., 1983: Limitations of some common lateral boundary schemes used in regional NWP models. *Mon. Wea. Rev.*, **111**, 1002-1012.

De Ridder, K. and G. Schayes, 1997: The IAGL land surface model. *J. Appl. Meteor.*, **36**, 167-182.

Denning, A.S., J.G., Collatz, C. Zhang, D.A. Randall, J.A. Berry, P.J. Sellers, G.D. Colello, and D.A. Dazlich, 1996a: Simulations of terrestrial carbon metabolism and atmospheric CO_2 in a general circulation model. Part 1: Surface carbon fluxes. *Tellus*, **48B**, 521-542.

Denning, A.S,, D.A. Randall, G.J. Collatz, and P.J. Sellers, 1996b: Simulations of terrestrial carbon metabolism and atmospheric CO_2 in a general circulation model. Part 2: Spatial and temporal variations of atmospheric CO_2. *Tellus*, **48B**, 543-567.

Dickinson, R.E., 1995: Land-atmosphere interaction. *Rev. Geophys.*, Supplement to Volume 33, Part 2, US National Report 1991-1994, 917-922.

Dickinson, R.E., A. Henderson-Sellers, P.J. Kennedy, and M.F. Wilson, 1986: Biosphere-Atmosphere Transfer Scheme (BATS) for the NCAR Community Climate Model. Technical Report NCAR/TN-275+STR, National Center for Atmospheric Research, Boulder, Colorado, USA.

Dobosy, R.J., T.L. Crawford, J.I. MacPherson, R.L. Desjardins, R.D. Kelly, S.P. Oncley, and D.H. Lenschow, 1997: Intercomparison among four flux aircraft at BOREAS in 1994. *J. Geophys. Res.*, **102**, 29101-29111.

Doran, J.C., and S. Zhong, 1995: Variations in mixed-layer depths arising from inhomogeneous surface conditions. *J. Climate*, **8**, 1965-1973.

Doran, J.C., F.J. Barnes, R.L. Coulter, T.L. Crawford, D.D. Baldocchi, L. Balick, D.R. Cook, D. Cooper, R.J. Dobosy, W.A. Dugas, L. Fritschen, R.L. Hart, L. Hipps, J.M. Hubbe, W. Gao, R. Hicks, R.R. Kirkham, K.E. Kunkel, T.J. Martin, T.P. Meyers, W. Porch, J.D. Shannon, W.J. Shaw, E. Swiatek, and C.D. Whiteman, 1992: The Boardman regional flux experiment. *Bull. Amer. Meteor. Soc.*, **73**, 1785-1795.

Doran, J.C., J.M. Hubee, J.C. Liljegren, W.J. Shaw, and S. Zhong, 1997: Observations and modeling of the response of the boundary layer to spatially varying surface fluxes of sensible and latent heat. *Proceedings, Special Symposium on Boundary Layer and Turbulence*, 32-38, Long Beach, CA, February 2-7, 1997, AMS, Boston.

Eastman, J.L., R.A. Pielke, and D.J. McDonald, 1998: Calibration of soil moisture for large eddy simulations over the FIFE area. *J. Atmos. Sci.*, in press.

Farquhar, G.D., S. von Cemmerer, and J.A. Berry, 1980: A biochemical model of photosynthetic CO_2 assimilation in C_3 plants. *Planta*, **149**, 78-90.

Gash, J.H.C. and W.J. Shuttleworth, 1991: Tropical deforestation: Albedo and the surface-energy balance. *Climatic Change*, **19**, 123-133.

Gash, J.H.C., J.S. Wallace, C.R. Lloyd, A.J. Dolman, M.V.K. Sivakumar, and C. Renard, 1991: Measurements of evaporation from fallow Sahelian Savannah at the start of the dry season. *Quart. J. Roy. Meteor. Soc.*, **117**, 749-760.

Giorgi, F., 1997a: An approach for the representation of surface heterogeneity in land surface models: Part I: Theoretical framework. *Mon. Wea. Rev.*, **125**, 1885-1899.

Giorgi, F., 1997b: An approach for the representation of surface heterogeneity in land surface models: Part II: Validation and sensitivity experiments. *Mon. Wea. Rev.* , **125**, 1885-1899.

Goutorbe J.-P., T. Lebel, A. Tinga, et al., 1994: HAPEX-Sahel: A large-scale study of land-atmosphere interactions in the semi-arid tropics. *Annales de Géophysique.* **12** 53-64.

Grasso, L., 1996: Numerical simulation of the May 15 and April 26, 1991 tornadic thunderstorms, Atmos. Sci. Paper #596, Colorado State University, Dept. of Atmospheric Science, Fort Collins, CO 80523, 151 pp.

Guo, Y., and P.H. Schuepp, 1994: An analysis of the effect of local heat advection on evaporation over wet and dry surface strips. *J. Climate*, **7**, 641-652.

Hall, F.G., Y.E. Shimabukuro and K.F. Huemmrich, 1995: Remote sensing of forest biophysical structure in boreal stands of Picea Mariana using mixture decomposition and geometric reflectance models. *Ecol. Appl.*, **5**, 993-1013.

Hall, R.G., D.E. Knapp, and K.F. Huemmrich, 1997: Physically based classification and satellite mapping of biophysical characteristics in the southern boreal forest. *J. Geophys. Res.*, **102**, 29567-29580.

Harrington, J.Y., 1997: The effects of radiative and microphysical processes on simulated warm and transition season Arctic stratus. Ph.D. dissertation, Atmospheric Science Paper No. 637, Colorado State University, Dept. of Atmospheric Science, Fort Collins, CO 80523, 289 pp.

Haurwitz, B., 1947: Comments on the sea-breeze circulation. *J. Meteor.*, **4**, 1-8.

Henderson-Sellers, A., Z.-L. Yang, and R.E. Dickinson, 1993: The project for intercomparison of land-surface parameterization schemes. *Bull. Amer. Meteor. Soc.*, **74**, 1335-1349.

Henderson-Sellers, A., A.J. Pitman, P.K. Love, P. Irannejad and T.H. Chen, 1995: The Project for Intercomparison of Land surface Parameterization Schemes (PILPS): Phases 2 & 3. *Bull. Amer. Met. Soc.*, **76**, 489-503.

Jarvis, P.G., 1976: The interpretation of the variation in leaf water potential and stomatal conductance found in canopies in the field. *Philos. Trans. Roy. Soc. London, Ser. B.*, **273**, 593-610.

Knowles, Captain John B., 1993, M.S. Thesis: The influence of forest fire induced albedo differences on the generation of mesoscale circulations. Department of Atmospheric Science, Colorado State University, 86 pp.

Kosta, R.D., and M.J. Suarez, 1992: A comparative analysis of two land surface heterogeneity representations. *J. Climate*, **5**, 1379-1390.

Lee, T.J., 1992: The impact of vegetation on the atmospheric boundary layer and convective storms. Ph.D. dissertation, Department of Atmospheric Science, Colorado State University, Fort Collins, Colorado, USA.

Lee, T.J., R.A. Pielke, and P.W. Mielke, Jr., 1995: Modeling the clear-sky surface energy budget during FIFE87. *J. Geophys. Res.*, **100**, 25585-25593.

Li, B., and R. Avissar, 1994: The impact of spatial variability of land-surface heat fluxes. *J. Climate*, **7**, 527-537.

Louis, J. F., M. Tiedke, and J.-F. Geleyn, 1982: A short history of the PBL parameterization at the ECMWF. *Workshop on Planetary Boundary Layer Parameterization*, Shinfield Park, Reading, United Kingdom, ECMWF, 59-80.

Lüpkes, C. and K.H. Schlünzen, 1996: Modelling the Arctic convective boundary-layer with different turbulence parameterizations. *Bound.-Layer Meteor.*, **79**, 107-130.

Mahrt, L. and M. Ek, 1993: Spatial variability of turbulent fluxes and roughness lengths in HAPEX-MOBILHY. *Bound.-Layer Meteor.*, **65**, 381-400.

Mahrt, L., J.L. McPherson, and R. Desjardins, 1994a: Observations of fluxes over heterogeneous surfaces. *Bound.-Layer Meteor.*, **67**, 345-367.

Mahrt, L., J. Sun, D. Vickers, J.I. MacPherson, and J.R. Pederson, 1994b: Observations of fluxes and inland breezes over a heterogeneous surface. *J. Atmos. Sci.*, 2484-2499.

Mahrt, L., J. Sun, J.I. MacPherson, N.O. Jensen, and R.L. Desjardins, 1997: Formulation of surface heat flux: Application to BOREAS. *J. Geophys. Res.*, **102**, 29641-29649.

Manabe, S., 1969: Climate and the ocean circulation. I: The atmospheric circulation and the hydrology of the earth's surface. *Mon. Wea. Rev.*, **97**, 739-774.

Manqian, M., and J. Jinjun, 1993: A coupled model on land-atmosphere interactions – simulating the characteristics of the PBL over a heterogeneous surface. *Bound.-Layer Meteor.*, **66**, 247-264.

Meeson, B.W., F.E. Corprew, J.M.P. McManus, D.M. Myers, J.W. Closs, K.-J. Sun, D.J. Sunday, and P.J. Sellers, 1995: ISLSCP initiative I-global data sets for land-atmosphere models, 1987-1988. Volumes 1-5, Published on CD by NASA (USA_NASA_GDAAC_IS USA_NASA_GDAAC_ISLSCP_005).

Miller, N., 1993: Applications of a hierarchical systems flux scheme for interactively coupling subgrid land surface models with atmospheric models. University of California-Lawrence Livermore National Laboratory Technical Report UCRL-JC-114100, 27 pp.

Monteith, J.L., 1965: Evaporation and the environment. *Symp. Soc. Expl. Biol.*, **19**, 205-234.

Moran, M.D. and R.A. Pielke, 1996a: Evaluation of a mesoscale atmospheric dispersion modeling system with observations from the 1980 Great Plains mesoscale tracer field experiment. Part I: Data sets and meteorological simulations. *J. Appl. Meteor.*, **35**, 281-307.

Moran, M.D. and R.A. Pielke, 1996b: Evaluation of a mesoscale atmospheric dispersion modeling system with observations from the 1980 Great Plains mesoscale tracer field experiment. Part II: Dispersion simulations. *J. Appl. Meteor.*, **35**, 308-329.

Mukabana, J.R., and R.A. Pielke, 1996: Investigating the influence of synoptic-scale monsoonal winds and mesoscale circulations on diurnal weather patterns over Kenya using a mesoscale numerical model. *Mon. Wea. Rev.*, **124**, 224-243.

Nicholls, M.E., R.A. Pielke, J.L. Eastman, C.A. Finley, W.A. Lyons, C.J. Tremback, R.L. Walko, and W.R. Cotton, 1995: Applications of the RAMS numerical model to dispersion over urban areas. In: Wind Climate in Cities, J.E. Cermak et al., Editors. Kluwer Academic Publishers, The Netherlands, 703-732.

Noilhan, J., J.C. André, P. Bougeault, J. Goutorbe, P. Lacarrere, 1991: Some aspects of the HAPEX-MOBILHY programme: The data base and the modeling strategy. *Surv. Geophys.*, **12**, 31-61.

Ogunjemiyo, S, P.H. Schuepp, J.I. MacPherson and R.L. Desjardins, 1998: Analysis of flux maps vs. surface characteristics from twin otter grid flights in BOREAS 1994. *J. Geophys. Res.*, submitted.

Olson, J.S. and Watts, J.A. 1982. Major world ecosystem complex map. Oak Ridge TN, Oak Ridge National Laboratory.

Ooyama, K.V., 1980: Conceptual evolution of the theory and modeling of tropical cyclone. *J. Meteorol. Soc. Japan*, **60**, 369-380.

Orlansky, I., 1975: A rational subdivision of scales for atmospheric processes. *Bull. Amer. Meteor. Soc.*, **56**, 527-530.

Pielke, R.A., 1984: *Mesoscale meteorological modeling.* Academic Press, New York, N.Y., 612 pp.

Pielke, R.A., W.R. Cotton, R.L. Walko, C.J. Tremback, W.A. Lyons, L.D. Grasso, M.E. Nicholls, M.D. Moran, D.A. Wesley, T.J. Lee, and J.H. Copeland, 1992: A comprehensive meteorological modeling system – RAMS. *Meteor. Atmos. Phys.*, **49**, 69-91.

Pielke, R.A., T.J. Lee, J.H. Copeland, J.L. Eastman, C.L. Ziegler, and C.A. Finley, 1997: Use of USGS-provided data to improve weather and climate simulations. *Ecological Applications*, **7**, 3-21.

Pielke, R.A. Sr., G.E. Liston, L. Lu, R.A. Pielke, Jr., and R. Avissar, 1998: Land-atmosphere hydrology – heterogeneity and preliminary assessment of feedbacks. *J. Hydrology*, submitted.

Pitman, A.J., 1994: Assessing the sensitivity of a land-surface scheme to the parameter values using a single column model. *J. Climate*, **7**, 1856-1869.

Pleim, J.E. and A. Xiu, 1995: Development and testing of a surface flux and planetary boundary layer model for application in mesoscale models. *J. Appl. Meteor.*, **34**, 16-32.

Qu, W., A. Henderson-Sellers, A. Pitman, T.C.F. Abramopoulos, A. Boone, S. Chang, F. Chen, Y. Dai, R. Dickinson, L. Duemenil, M. Ek, N. Gedney, Y.G.J. Kim, R. Koster, E. Kowalczyk, D. Lean, X. Liang, J.-F. Mahfouf, H.-T., Mengelkamp, K. Mitchell, O. Nasonova, J. Noilhan, A. Robock, C. Rosenzweig, J.S.C. Schlosser, J.-P. Schulz, A. Shmakin, D. Verseghy, P. Wetzel, E. Wood, Z.-L. Yang, Q. and Zeng, 1998: Sensitivity of latent heat flux from PILPS land-surface schemes to perturbations of surface air temperature. *J. Atmos. Sci.*, in press.

Raupach, M.R., 1991: Vegetation-atmosphere interaction in homogeneous and heterogeneous terrain: Some implications of mixed layer dynamics. In: *Vegetation and climate interactions in semi-arid regions*, Henderson-Sellers and Pitman, Eds., Dordrecht, The Netherlands, Kluwer Academic Publishers, 105-120.

Rotunno, R., 1983: On the linear theory of land and sea breeze. *J. Atmos. Sci.*, **40**, 1999-2009.

Schädler, G., N. Kalthoff, and F. Fiedler, 1990: Validation of a model for heat, mass, and momentum exchange over vegetated surfaces using LOTREX 10E/HIBE88 data. *Contrib. Atmos. Phys.*, **63**, 85-100.

Segal, M. and R.W. Arritt, 1992: Non-classical mesoscale circulations caused by surface sensible heat-flux gradients. *Bull. Amer. Meteor. Soc.*, **73**, 1593-1604.

Segal M., R. Avissar, M.C. McCumber and R.A. Pielke, 1988: Evaluation of vegetation effects on the generation and modification of mesoscale circulations. *J. Atmos. Sci.*, **45**, 2268-2292.

Segal, M., W. Schreiber, G. Kallos, R.A. Pielke, J.R. Garratt, J. Weaver, A. Rodi, and J. Wilson, 1989: The impact of crop areas in northeast Colorado on midsummer mesoscale thermal circulations. *Mon. Wea. Rev.*, **117**, 809-825.

Sellers, P.J., F.G. Hall, G. Asrar, D.E. Strebel, and R.E. Murphy, 1992: An overview of the First ISLSCP Field Experiment. *J. Geophys. Res.* **97**-D17, 18455-18466.

Sellers, P.J. et al. 1995a: Remote sensing of land surface for studies of global change: Models-Algorithms-Experiments. *Remote Sens. Environ.*, **5**, 3-26.

Sellers, P.J., F.G. Hall, H. Margolis, B. Kelly, D. Baldocchi, J. den Hartog, J. Cilhar, M. Ryan, B. Goodison, P. Crill, J. Ranson, D. Lettenheimer, D. Wickland, 1995b: The Boreal Ecosystem-Atmosphere Study (BOREAS): An overview and early results from the 1994 field year. *Bull. Amer. Meteor. Soc.* **76**, 1549-1577.

Sellers, P.J., B.W. Meeson, J. Closs, J. Collatz, F. Corprew, D. Dazlich, F.G. Hall, Y. Kerr, R. Koster, S. Los, K. Mitchell, M. McManus, D. Myers, K.-J. Sun, and P. Try, 1995c: An overview of the ISLSCP Initiative global data sets. On: ISLSCP Initiative

1-global data sets for land-atmosphere models, 1987-1988. Volumes 1-5. Published on CD by NASA. Volume 1: USA_NASA_GDAAC_ISLSCP_001.OVERVIEW.DOC.

Sellers, P.J., M.D. Heiser, F.G. Hall, S.J. Goetz, D.E. Strebel, S.B. Verma and R.L. Desjardins, 1995d: Effects of spatial variability in topography, vegetation cover and soil moisture on area-averaged surface fluxes: a case study using the FIFE 1989 data. *J. Geophys. Res.*, **100**, 25607-25629.

Sellers, P.J., D.A. Randall, G.J. Collatz, J.A. Berry, C.B. Field, D.A. Dazlich, C. Zhang, G.D. Collelo, and L. Bounoua, 1996: A revised land surface parameterization (SiB2) for atmospheric GCMs. Part I: Model formulation. *J. Climate*, **9**, 676-705.

Sellers, P.J., F.G. Hall, R.D. Kelly, A. Black. D. Baldocchi, J. Berry, M. Ryan, K.J. Ranson, P.M. Crill, D.P. Lettenmaier, H. Margolis, J. Cihlar, J. Newcomer, D. Fitzjarrald, P.G. Jarvis, S.T. Gower, D. Halliwell, D. Williams, B. Goodison, D.E. Wickland, and F.E. Guertin, 1997: BOREAS in 1997: Experiment overview, scientific results, and future directions. *J. Geophys. Res.*, **102**, 28731-28769.

Shaw, B.L., 1995: The effect of soil moisture and vegetation heterogeneity on a Great Plains dryline: A numerical study. Atmospheric Science Paper No. 576, Colorado State University, R.A. Pielke, P.I., 93 pp.

Shaw, B.L., R.A. Pielke, and C.L. Ziegler, 1997: The effect of soil moisture heterogeneity on a Great Plains dryline: A numerical study. *Mon. Wea. Rev.*, **125**, 1489-1506.

Shuttleworth, W.J., 1985: Daily variations of temperature and humidity within and above Amazonian forest. *Weather*, **40**, 102-108.

Simpson, J.E., 1994: *Sea breeze and local wind*, Cambridge University Press, New York, 234 pp.

Smith, E.A., A.Y. Hsu, W.L. Crosson, R.T. Field, L.J. Fritschen, R.J. Gurney, E.T. Kanemasu, W.P. Kustas, D. Nie, W.J. Shuttleworth, J.B. Stewart, S.B. Verma, H.L.

Weaver, and M.L. Wesley, 1992: Area-averaged surface fluxes and their time-space variability over the FIFE experimental domain. Paper No. 91JD03060, *J. Geophys. Res.*, **97**, 18599-18622.

Steyaert, L.T., F.G. Hall, and T.R. Loveland, 1997: Land cover mapping, fire regeneration, and scaling studies in the Canadian boreal forest with 1 km AVHRR and Landsat TM data. *J. Geophys. Res.*, **102**, 29581-29598.

Sun, J. and L. Mahrt, 1995: Relationship of surface heat flux to microscale temperature variations: Applications to BOREAS. *Bound.-Layer Meteor.*, **76**, 291-301.

Sun, J. D.H. Lenschow, L. Mahrt, T. L. Crawford, K.J. Davis, S.P. Oncley, J.I. MacPherson, Q. Wang, R.J. Dobosy, and R.L Desjardins, 1997a: Lake-induced atmospheric circulations during BOREAS. *J. Geophys. Res.*, **102**, 29155-29166.

Sun, J., R.L. Desjardins, L. Mahrt and J.I. MacPherson, 1997b: The influence of lakes in the atmospheric transport of CO_2, water vapor and O_3 in BOREAS. *J. Geophys. Res.*, accepted.

Taylor, C.M., R.J. Harding, R.A. Pielke, Sr., P.L. Vidale and R.L. Walko, 1998: Snow breezes in the boreal forest. *J. Geophys. Res.*, under review.

Timbal B., A. Hahmann, A. Pitman, and A.Henderson-Sellers, 1998: New developments for the Project for Intercomparison of Land-surface Parameterisation schemes: Phase 4, Proceedings of the Workshop: Continental-scale Hydrological Models: Charting the Future, To be published in WCRP series by WMO.

Tremback, C.J., and R. Kessler, 1985: A surface temperature and moisture parameterization for use in mesoscale numerical models. Seventh Conference on Numerical Weather Prediction, 17-20 June 1985, Montreal, Canada, American Meteorological Society, Boston, Massachusetts, USA.

van Genuchten, M.T., 1980: A closed-form equation for predicting the hydraulic conductivity of unsaturated soils. *Soil Sci. Soc. Am. J.*, **44**, 892-898.

Vidale, P.L., R.A. Pielke, A. Barr, L.T. Steyaert, 1997: Case study modeling of turbulent and mesoscale fluxes over the BOREAS region. *J. Geophys. Res.*, **102**, 29167-29188.

von Caemmerer, S. and G.D. Farquhar, 1985: Kinetics and activation of Rubisco an some preliminary modeling of RuP2 pool sizes. *Proc. of the 1983 Conf. at Tallinn*, J. Vill, G. Grishina, and A. Laisk, Eds. Estonian Academy of Sciences, 46-58.

Walko, R.L. and R.A. Pielke, 1994: Simulations of PROJECT WIND cases with RAMS. Chapter 11 in *AMS Meteorological Monograph on Mesoscale Modeling of the Atmosphere*, R.A. Pielke and R.P. Pearce, Eds., *25*, 97-122.

Walko, R.L., C.J. Tremback, R.A. Pielke, and W.R. Cotton, 1995: An interactive nesting algorithm for stretched grids and variable nesting ratios. *J. Appl. Meteor.*, **34**, 994-999.

Walko, R.L., R.A. Pielke, J. Baron, D. Schimel, W.J. Parton, D. Ojima, T.G.F. Kittel, T.J. Lee, and C.J. Tremback, 1998: Methods of coupling RAMS with ecosystem models. In preparation.

Wallace, J.S., I.R. Wright, and J.B. Stewart, 1991: The Sahelian Energy Balance Experiment (SEBEX): Ground based measurements and their potential for spatial extrapolation using satellite data. *Adv. Space Res.*, **11**, 131-142.

Wang, J.E., A.B. Eltahir, and R.L. Bras, 1998: 3D numerical simulation of mesoscale circulations forced by land surface thermal heterogeneities of random distribution. *J. Atmos. Sci.*, in press.

Wood, E.F., D.P. Lettenmaier, and V.G. Zartarian, 1992: A land-surface hydrology parameterization with subgrid variability for general circulation models. *J. Geophys. Res.*, **97**, 2717-2728.

Wright, I.R., J.H.C. Gash, H.R. Da Rocha, W.J. Shuttleworth, C.A. Nobre, G.T. Maitelli, C.A.G.P. Zamparoni, and P.R.A. Carvalho, 1992: Dry season micrometeorology of central Amazonian ranch-land. *Quart. J. Roy. Meteor. Soc.*, **118**, 1083-1099.

Ye, Z. and R.A. Pielke, 1995: A parameterization of Bowen ratio with respect to soil moisture availability. *Adv. Atmos. Sci.*, **12**, 449-474.

Zeng, X. and R.A. Pielke, 1995a: Further study on the predictability of landscape-induced atmospheric flow. *J. Atmos. Sci.*, **52**, 1680-1698.

Zeng, X. and R.A. Pielke, 1995b: Landscape-induced atmospheric flow and its parameterization in large-scale numerical models. *J. Climate*, **8**, 1156-1177.

Zhong, S., and J.C. Doran, 1995: A modeling study of the effects of inhomogeneous surface fluxes on boundary-layer properties. *J. Atmos. Sci.*, **52**, 3129-3142.

Ziegler, C.L., W.J. Martin, R.A. Pielke, and R.L. Walko, 1995: A modeling study of the dryline. *J. Atmos. Sci.*, **52**, 263-285.

Ziegler, C.L., T.J. Lee, and R.A. Pielke, 1997: Convective initiation at the dryline: A modeling study. *Mon. Wea. Rev.*, **125**, 1001-1026.

Appendix A

A.1 Land-Water

This is the case that describes a periodic, sinusoidal distribution of CBL height due to a periodic distribution of land and water. The height of the CBL at the time of maturity for the induced mesoscale circulations is:

$$h = h_0 \frac{1}{2}[1 + a\sin(kx)] \;\; ; \;\; h_0 = \frac{2Q_0}{\lambda N_0^2} \tag{A.1}$$

$$a = \frac{\lambda k U}{(\lambda + Kk^2)^2 + k^2U^2)} \tag{A.2}$$

where a is the amplitude of the sinusoidal modulation of the height of the CBL, which decays as $1/(kU)$ and k is the horizontal wavenumber of the land/water distribution. K is dissipation, U is the environmental wind speed, λ represents linear friction, Q_0 is the surface heating magnitude, N_0^2 is the Brunt-Väisälä frequency.

The MAPE is calculate as the difference in potential energy at the mature stage (i.e. a distribution of mesoscale circulations is in place over the terrain) and that at a state of rest, where every circulation has completely decayed and the CBL has uniform height in the horizontal. All cases have a perfectly mixed layer, so that there is no surface layer and the atmosphere is immediately stable above the inversion height.

We derive MAPE as in Dalu et al. 1996:

$$MAPE = \int_{-R_0}^{R_0} \int_0^h \left(\frac{gz\theta_i}{\Theta}\right) dzdx - \int_{-R_0}^{R_0} \int_0^{h_0/2} \left(\frac{gz\theta_f}{\Theta}\right) dzdx \tag{A.3}$$

where g is gravity, z is height above the ground, Θ is the environmental potential temperature, θ_i is the initial potential temperature perturbation, θ_f is the final potential temperature perturbation (which minimizes PE), R_0 is the local Rossby radius, h_0 is the asymptotic CBL height.

$$\theta_i = \Theta_z h \ ; \ \theta_f = \Theta_z h_0/2 \tag{A.4}$$

where Θ_z is the environmental potential temperature change with height.

$$MAPE = \frac{g}{\Theta} \cdot \Theta_z \int_{-R_0}^{R_0} dx \left[\int_0^h dz\,(zh) - \int_0^{h_0/2} dz\,(zh_0/2)\right] =$$

$$\frac{g\Theta_z}{\Theta} \int_{-R_0}^{R_0} dx \left(\frac{h^3}{2} - \frac{h_0^3}{16}\right) =$$

$$= g\frac{\Theta_z}{\Theta} \int_{-R_0}^{R_0} dx \cdot \left(\frac{h_0^3}{16}\left[(1 + a\sin kx)\right]^3 - \frac{h_0^3}{16}\right) =$$

$$= g\frac{\Theta_z}{\Theta} \int_{-R_0}^{R_0} \left[\frac{h_0^3}{16}\left(1 + 3a^2\sin^2 kx + 3a\sin kx + a^3\sin^3 kx\right) - \frac{h_0^3}{16}\right] =$$

After canceling terms that integrate to even functions:

$$= g\frac{\Theta_2}{\Theta}\left(\frac{h_0}{2}\right)^3 \int_{-R_0}^{R_0} dx \left[3a^2\sin^2 kz\right]$$

$$= g\frac{\Theta_2}{\Theta}\frac{h_0^3}{8}\left[3a^2\int_{-R_0}^{R_0}\sin^2 kx dx\right]$$

$$= g\frac{\Theta_2}{\Theta}\frac{h_0^3}{8}\left[3a^2\left[\frac{x}{2}-\frac{1}{4k}\sin 2kx\right]\Big|_{-R_0}^{R_0}\right]$$

$$= g\frac{\Theta_z}{\Theta}\frac{h_0^3}{8}\left\{3a^2\left[\frac{1}{4k}\sin 2kR_0+\frac{1}{4k}\sin -2kR_o\right]\right\}$$

$$= g\frac{\Theta_z}{\Theta}\frac{1}{6}\frac{h_0^3}{8}\left\{3a^2\cdot\left(2R_0\frac{2}{4k}\sin 2kR_0\right)\right\}$$

$$\simeq g\frac{\Theta_z}{\Theta}\frac{h_0^3}{24}\cdot 3a^2\left\{R_0-\frac{1}{4k}\sin 2kR_0\right\} \tag{A.5}$$

A.2 Land-Land

In this case we have a periodic horizontal distribution of CBL heights with asymptotic values h_{0_1} and h_{0_2}, which could arise because of differential surface heating (as is shown for instance in Fig. 2.7):

$$h = \frac{1}{2}h_{0_1}(1+a\sin kx)+\frac{1}{2}h_{0_2}(1+a\cos kx) \tag{A.6}$$

$$h_{0_1}=\frac{2Q_{0_1}}{\lambda N_0^2}\ ;\ h_{0_2}=\frac{2Q_{02}}{\lambda N_0^2}$$

$$\delta\theta = \Theta_z(h_1-z)He(h_1-z)-\Theta_z(h_2-z)He(h_2-z)$$

From the integral relations illustrated in the previous sections we get:

$$MAPE = g\frac{\Theta_z}{\Theta}\frac{h_{0_1}^3}{24}3a^2\left[R_0 - \frac{1}{4k}\sin(2kR_0)\right] - g\frac{\Theta_z}{\Theta}\frac{h_{0_2}^3}{24}\left\{3a^2\left[R_0 + \frac{1}{4k}\sin(2kR_0)\right.\right. \\ \left.\left. +3a\sin\frac{(kR_0)}{k}a^3\left[\frac{\sin(kR_0)}{k} - \frac{1}{3k}\sin^3(kR_0)\right]\right\}\right. \tag{A.7}$$

Valid in the interval $k_0 < k < l$, where k_0 is the inertial wavenumber and l is the Scorer parameter, $1/k_0$ representing a horizontal characteristic scale and $1/l$ representing a vertical characteristic scale of the mesoscale circulations.

$$k_0 = \frac{f}{U} \quad l = \frac{N_0}{U}$$

A.3 Mountain-Valley

In this case, instead of differential CBL height due to heating, we impose a differential terrain height due to a periodic horizontal distribution of mountains, with maximum height of 200m (H).

$h_m = H\sin kx$ is the mountain distribution in x.

$w_m = kUH\cos(kx + \mu z)$ is the induced vertical velocity, where μ is the vertical wavenumber.

$$\mu = k\sqrt{\frac{l^2 - k^2}{k^2 + k_0^2}} \tag{A.8}$$

$$k_0 = \frac{f}{U} \quad l = \frac{N_0}{U}$$

For $k_0 < k < l$

$$\frac{\partial MAPE}{\partial t} = \int dx \int dz \left(gw \frac{\delta\theta}{\Theta} \right) \tag{A.9}$$

$$MAPE = g\frac{\Theta_z}{\lambda\Theta}(KUH) \int_{-R_0}^{R_0} dx \left\{ \cos kx \int_0^h dz(h-z)\cos\mu z - \right.$$

$$\left. - \sin(kx) \int_0^h dz(h-z)\sin\mu z \right\} =$$

$$\frac{g\Theta}{\lambda\Theta}(kUH) \int_{-R_0}^{R_0} dx \left\{ \cos kx \left[\frac{1}{\mu^2}(1-\cos\mu h) \right] - \right.$$

$$- \sin kx \left[\frac{h}{\mu} - \frac{1}{\mu^2}\sin kh \right] =$$

$$= g\frac{\Theta_z}{\lambda\Theta}(kUH) \left\{ \int_{-R_0}^{R_0} dx \cos kx \left[\frac{1}{\mu^2}(1-\cos\mu h) \right] - \right.$$

$$\left. - \int_{-R_0}^{R_0} dx \sin kx \left[\frac{h}{\mu} - \frac{1}{\mu^2}\sin kh \right] \right\} =$$

$$= g\frac{\Theta_z}{\lambda\Theta}(kUH) \int_{-R_0}^{R_0} dx \left[\frac{\cos kx}{\mu^2} - \frac{h}{\mu}\sin kx \right] -$$

$$- \int_{-R_0}^{R_0} \cos\frac{(kx+\mu h)}{\mu^2} dx$$

As $\mu h = \frac{\mu}{2} h_0(1 + a\sin kx)$

$$MAPE = g\frac{\Theta_z}{\lambda\Theta}(kUH) \left[\frac{2}{k}\sin kR_0 \frac{1}{\mu^2} \left(1 - \cos\mu\frac{h_0}{2} \right) - \frac{ah_0}{\mu} \left[R_0 - \frac{1}{4k}\sin(2kR_0) \right] \right] \tag{A.10}$$

Appendix B

B.1 Biophysical parameters used for BOREAS

Table B.1: Table of biophysical parameters by AVHRR class used for the RAMS simulations.

AVHRR Class	June LAI	July LAI	Albedo	Fractional coverage (%)	Roughness Length (m)
1 wet conifer, low density	1	1.5	0.11	0.46	0.5
2 wet conifer, medium dens	2.5	3.0	0.11	0.66	1.0
3 wet conifer, high density	3.0	3.5	0.11	0.86	2.0
4 upland dense conifer	2.0	2.5	0.12	0.86	2.0
5 rock outcrop/bare ground sparse veg.	0.5	0.5	0.25	0.25	0.1
6 fen (NONE)	NA	NA	NA	NA	NA
7 water	0	0	0.04	0	0.024
8 regeneration young (NONE)	0.5	0.7	0.08	0.06	0.4
9 regeneration medium (old burns)	1.3	1.8	0.09	0.4	1.0
10 recent burn	0	0.2	0.07	0.1	0.25
11 mixed agric.	0.8	2.1	0.2	0.5	0.15
12 mixed agric./predom. grains	0.5	2.1	0.18	0.5	0.1
13 mixed agric./pasture/hay	0.5	1.8	0.16	0.3	0.1
14 grassland marshes	1.5	2.7	0.09	0.55	0.1
15 mixed: 80% conifer 20% deciduos	2.5	2.5	0.12	0.6	2.0
16 mixed: 50% conifer 50% deciduos	2.0	3.0	0.15	0.6	2.0
17 mixed: 20% conifer 80% deciduos	1.5	3.5	0.18	0.63	2.0
18 regeneration/deciduos in the south	1.5	1.8	0.12	0.5	1.0